6.

INJECTION SYSTEM

THE basic method proposed to fill the PEP-II rings with electrons and positrons is to use the first two-thirds of the SLC linac, including its damping rings and positron source. Given that the PEP-II luminosity lifetime will be about two hours, our goal will be to top off both rings about once per hour, and to complete the top-off injection cycle for both electrons and positrons in about 3 minutes. As will be shown below, the SLC linac (with a few modifications and simplifications) is very well suited for this function.

By the time PEP-II is operational, it is envisioned that the SLC will have completed its Z^0 experimental program and thus will no longer be operated in its e^+e^- collider mode. It is probable that the linac will still be used for physics to supply 50-GeV e^- beams for fixed-target experiments in End Station A and/or for accelerator R&D for the Next Linear Collider (NLC), which involves the Final Focus Test Beam (FFTB) as well as other projects now in the planning stages. It is thus worth noting that the modifications discussed here for the PEP-II injection system do not preclude such uses. Furthermore, the so-called Nuclear Physics Injector (NPI), located at the beginning of linac Sector 25 and capable of producing 2- to 10-GeV e^- beams at the end of the linac, will be operable simultaneously with the PEP-II injection system on a noninterfering basis.

6.1 OVERALL APPROACH AND SPECIFICATIONS

The basic approach adopted for the PEP-II injection system is illustrated schematically in Fig. 6-1, and the overall injection specifications and relevant parameters are given in Table 6-1.

A fundamental simplification in operation compared with the SLC results from the use of two bypass lines—one for nominally 3.1-GeV positrons, the other for nominally 9-GeV electrons. These positron and electron bypass lines start at linac Sectors 4 and 8, respectively, and run to the end of the linac at Sector 30, where they connect to the existing South Injection Transport (SIT) and North Injection Transport (NIT) injection lines leading to the PEP-II tunnel. Because the beams are extracted at their correct energies from early points along the linac and never reenter it, problems of emittance

6.

INJECTION SYSTEM

THE basic method proposed to fill the PEP-II rings with electrons and positrons is to use the first two-thirds of the SLC linac, including its damping rings and positron source. Given that the PEP-II luminosity lifetime will be about two hours, our goal will be to top off both rings about once per hour, and to complete the top-off injection cycle for both electrons and positrons in about 3 minutes. As will be shown below, the SLC linac (with a few modifications and simplifications) is very well suited for this function.

By the time PEP-II is operational, it is envisioned that the SLC will have completed its Z^0 experimental program and thus will no longer be operated in its e^+e^- collider mode. It is probable that the linac will still be used for physics to supply 50-GeV e^- beams for fixed-target experiments in End Station A and/or for accelerator R&D for the Next Linear Collider (NLC), which involves the Final Focus Test Beam (FFTB) as well as other projects now in the planning stages. It is thus worth noting that the modifications discussed here for the PEP-II injection system do not preclude such uses. Furthermore, the so-called Nuclear Physics Injector (NPI), located at the beginning of linac Sector 25 and capable of producing 2- to 10-GeV e^- beams at the end of the linac, will be operable simultaneously with the PEP-II injection system on a noninterfering basis.

6.1 OVERALL APPROACH AND SPECIFICATIONS

The basic approach adopted for the PEP-II injection system is illustrated schematically in Fig. 6-1, and the overall injection specifications and relevant parameters are given in Table 6-1.

A fundamental simplification in operation compared with the SLC results from the use of two bypass lines—one for nominally 3.1-GeV positrons, the other for nominally 9-GeV electrons. These positron and electron bypass lines start at linac Sectors 4 and 8, respectively, and run to the end of the linac at Sector 30, where they connect to the existing South Injection Transport (SIT) and North Injection Transport (NIT) injection lines leading to the PEP-II tunnel. Because the beams are extracted at their correct energies from early points along the linac and never reenter it, problems of emittance

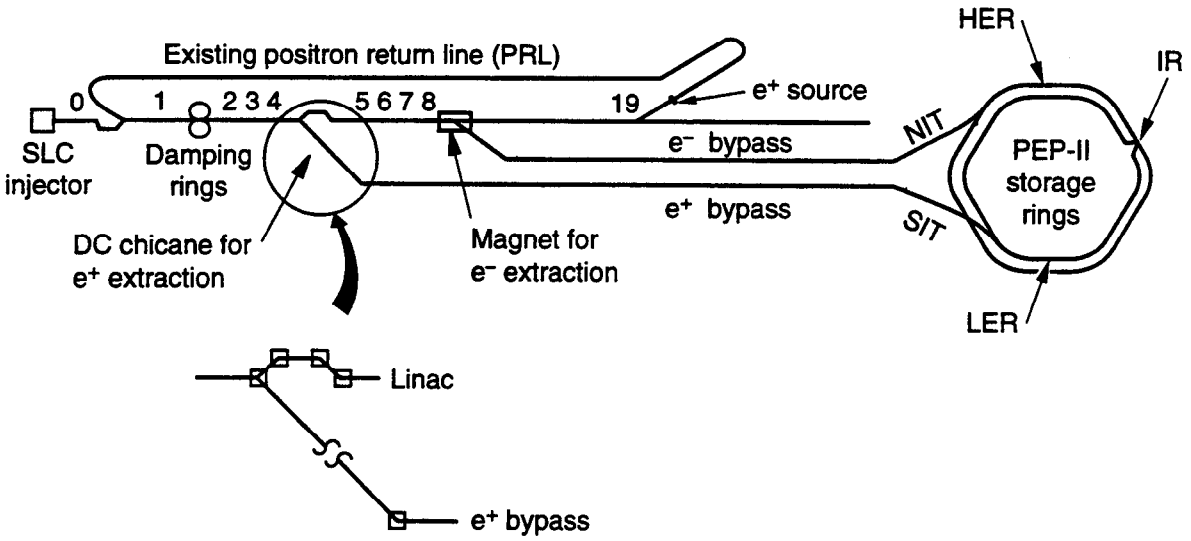

Fig. 6-1. Schematic of the PEP-II $e^{\pm}$ injection system, based on use of the SLC linac with bypass lines. The numbers along the linac indicate the location (not to scale) of each sector. Each of the 30 sectors is 100 m long.

growth and instabilities from wakefields in the disk-loaded waveguide structure are minimized and will not be an issue. An additional advantage of our approach is that it eliminates the need for a compromised transport lattice and for beam deceleration, unattractive features of the PEP injection process in the late 1980's, when PEP and SLC operations were interleaved. (The compromised lattice and beam deceleration were necessary in that scheme to maintain positron production with a 30-GeV beam at Sector 19.) In the PEP-II design, the linac is still used up to Sector 19 for positron production. That portion of the linac downstream of Sector 19 would still be available to provide high-energy beams for other uses, but will be turned off for normal PEP-II operation.

As discussed in Section 6.2, the two bypass lines (consisting of parallel and independent FODO arrays) are located above the existing linac, suspended in the tunnel just below the ceiling (much like the existing Positron Return Line, PRL, from Sector 19). The existing NIT and SIT lines will undergo only minor modifications (see Section 6.3). Injection into the high- and low-energy rings (HER and LER, respectively) will take place in the long straight sections (see Section 4.1) of IR-10 (e^-) and IR-8 (e^+). For both the HER and LER, injection will take place in the vertical plane, utilizing a combination of DC bumps and pulsed kickers. The decision to adopt vertical injection was a complex one; as discussed in Section 4.4, it was based on avoiding the increase in beam size that horizontal injection would produce due to the parasitic beam crossings near the IP. Because of the constraint from the parasitic crossings, there is more room for vertical injection than for horizontal. We note, however, that it is the low emittance of the damped SLC beam that is key to taking advantage of the vertical injection option.

The linac configuration proposed here was selected after considering other alternatives, including (i) using only the last one-third of the linac and building a new in-line positron source, (ii) using the NPI for electrons only, while using the SLC for positrons, and (iii) keeping a system very similar to the one previously used to fill PEP

Table 6-1. PEP-II injection specifications and parameters.

Beam energy	
High-energy ring (e^-) [GeV]	9 [range: 8–10][a]
Low-energy ring (e^+) [GeV]	3.1 [range: 2.8–4]
Beam current	
High-energy ring[A/10^{10} e^-]	0.99/4518
Low-energy ring [A/10^{10} e^+]	2.14/9799
Particles per bunch	
High-energy ring [10^{10} e^-]	2.7
Low-energy ring [10^{10} e^+]	5.9
Linac repetition rate [pps]	60 or 120
Linac current [10^{10} $e^\pm$ per pulse][b]	0.1–3
Invariant linac emittance [m·rad]	
Horizontal	4×10^{-5}
Vertical	0.5×10^{-5}
Normal filling time[c]	
Topping-off (80–100%) [min]	3
Filling time (0–100%) [min]	6
Ring circumference [m]	2199.318
Revolution period [μs]	7.336
Revolution frequency [kHz]	136.311
Bunch frequency [MHz]	476/2 = 238
Time between bunches [ns]	4.20
Harmonic number	3492
Number of bunches[d]	1746 – 5% = 1658
Vertical damping time	
High-energy ring [ms]	38
Low-energy ring, with wigglers [ms]	40
Low-energy ring, without wigglers [ms]	68
Nominal beam emittance [nm·rad][e]	
High-energy ring, horizontal/vertical	48/1.9
Low-energy ring, horizontal/vertical	64/2.6

[a]The present e^- extraction location has sufficient klystrons to provide a beam energy in excess of 12 GeV.

[b]The SLC routinely delivers 3×10^{10} e^+ and 3×10^{10} e^- per bunch on each linac pulse.

[c]Electron and positron bunches are injected on alternate pulses at 60 pps, in which case both rings can be topped-off in 3 minutes.

[d]For filling purposes, the rings will be divided into nine zones of equal length. The 5% gap leaves one zone partially unfilled.

[e]Storage ring emittances are quoted here, and elsewhere in this document, as unnormalized, or geometrical, values.

when its operation was interleaved with that of the SLC, where the low-energy $e^{\pm}$ beams (2.8–10 GeV) are obtained by deceleration downstream of Sector 19. Some of the reasons for ultimately rejecting these alternatives include:

- A new positron source would be very costly and would complicate the transmission of SLC-type beams to the Final Focus Test Beam or End Station A.
- NPI-type beams downstream of Sector 19 (electrons only) would either have bunch currents lower by two orders of magnitude (that is, about 10^8 electrons per bunch) or would require upgrading the NPI to SLC standards—a costly operation that would not, in any case, yield an SLC-quality beam emittance due to the absence of the damping rings in this scenario.
- Multibunch electron injection, that is, with a train of bunches 4.2 ns apart, would only pay off if the linac were not operated with SLED, so that a long pulse train of at least 200 bunches (about 840 ns) could be accelerated and stored. This would require a costly move of the NPI to about Sector 20 to obtain the required electron energy and would mean tying up that entire part of the linac solely for this purpose. Furthermore, this approach would not permit single-bunch electron filling and would make the electron injection scheme very different from, and less flexible than, positron filling—an undesirable feature per se. Finally, this filling method is less desirable for the storage ring feedback systems, which benefit from a scheme in which the injected beam comes in small increments, as discussed in Section 5.6.
- Using the SLC in the interleaved "PEP-SLC" filling mode would have all the disadvantages of backphasing the latter part of the linac and simultaneously having to handle beams of 3.1 and 9 GeV of opposite charges. Such a scheme would not work for 3.1-GeV beams and is likely to be very marginal even at 9 GeV.

A slightly less costly implementation for the proposed bypass scheme might be to use a single, common line for both positrons and electrons beyond Sector 8. Such a scheme could be made to work with a weaker focusing system for the electrons but with twice as many correctors and beam position monitor (BPM) electronic processing systems. Moreover, it would require a second chicane at the Sector 9 junction point, larger aperture quadrupoles and BPMs, and a method of separating the unequal-energy beams at the end of the linac into the NIT and SIT lines. These complications would likely lead to operational difficulties arising from steering and instrumentation problems. The resulting compromises would almost inevitably lead to inefficiencies and an overall decrease in the robustness of the injection system.

After considering the various scenarios, we adopted the more flexible and reliable scheme described here, with independent bypass lines. As outlined in Section 6.7, the optimum injection pattern involves "topping-off" the rings approximately once every hour, so the operational benefits of having a robust injection scheme are extremely important for maintaining the high integrated luminosity required of PEP-II.

As shown in Table 6-1, the bypass lines are presently optimized for an energy range of 2.8–4 GeV for positrons and 8–10 GeV for electrons. When filled to the nominal operating point (corresponding to the design luminosity of 3×10^{33} cm^{-2} s^{-1}), the LER will have a current of 2.14 A, or roughly 6×10^{10} positrons per bunch, and the HER will have a current of 0.99 A, or about 3×10^{10} electrons per bunch. The normal topping-off

operation will consist of delivering roughly 10^{10} particles to each of the 1658 bunches in each ring. For each bunch, this will be accomplished in five (nonconsecutive) linac pulses, at a rate of 60 pps. At present, the SLC routinely delivers 3×10^{10} electrons and 3×10^{10} positrons per pulse to the arcs. It will be straightforward to deliver less than one-fifth of this charge per pulse to the PEP-II rings. At 60 pps (interleaved) and an overall 75% filling efficiency for both e^- and e^+, the filling operation should take $(1658/60) \times 5 \times (1/0.75) = 184$ seconds, or about 3 minutes.

When filling from zero current (empty rings), the linac will deliver roughly 10^{10} $e^{\pm}$ per pulse, and all of the 1658 bunches will be filled to about 80% of their final charge. This operation will also take about four or five linac pulses, or about 3 minutes, to fill both storage rings to 80% of design current; an additional 3 minutes will then be needed to top-off, giving a total filling time of about 6 minutes.

Another great simplification in the injection process results from choosing a storage ring RF frequency of 476 MHz (that is, exactly one-sixth of the 2856-MHz linac frequency). The drive system along the 3-km linac already operates at 476 MHz, and extending it to PEP-II (or vice versa) will be straightforward. With this choice, all the key RF frequencies (the damping rings at 714 MHz, the linac at 2856 MHz, and the two collider rings at 476 MHz) will be harmonically related. For proper spacing around the rings, every second RF bucket is filled, giving a bunch repetition frequency of 238 MHz (i.e., a 4.2-ns bunch separation). With a harmonic number of 3492 ($= 2^2 \times 3^2 \times 97$) and a 5% gap for ion control, there will be 1658 filled buckets. As explained later, for filling purposes each ring will be divided into nine equal "zones" (194 buckets per zone), one of which will be left half empty to avoid ion trapping in the HER. By filling the bunches in sequential zones, the time that elapses between each individual bucket fill will be 27.6 seconds. More importantly, with this scheme no injected bunch would again experience the full kick from the injection kickers for about 150 ms, allowing ample time for coherent injection oscillations to damp (see Section 6.6).

6.1.1 Injection Energy Spread and Beam Size

The momentum spectrum of the linac 3.1-GeV positron beam or 9.0-GeV electron beam depends on a number of factors:

- The charge distribution in the bunch extracted from the damping ring, including the effect of intensity-dependent bunch lengthening (due to longitudinal wakefields)
- The momentum spectrum of the beam extracted from the damping ring, including effects of longitudinal wakefields
- The adjustment of the bunch compressor, which reduces the bunch length and increases the uncorrelated energy spread by the same factor
- The average phase of the bunch relative to the RF in all linac sections in which the bunch is accelerated
- The short-range longitudinal wakefields in all the structures through which the beam passes (dominated by the wakefields in the accelerator structures)

- The phase and momentum jitter of the beams extracted from the damping rings
- The phase jitter of the compressor klystron and all of the klystrons used to accelerate the beam, which determines the pulse-to-pulse momentum jitter of the beams injected into the PEP-II storage rings

We have developed a program at SLAC for analyzing the longitudinal phase-space distributions of the SLC beams that simulates all of these contributions except for the phase jitters listed in the last two points above. This program has been used to simulate the spectra expected for PEP-II beams. We find that the spectrum of the positron beam is broader than that of the (higher-energy) electron beam, because the uncorrelated energy spread coming out of the bunch compressor is a larger fraction of the full energy spread. In order to minimize the energy spread of the e^+ beam, we have considered two possible adjustments of the phase of the positrons relative to the phase of the RF in the linac for the high-intensity case of 2×10^{10} particles per pulse.

Figure 6.2a shows the results of the first approach, which attempts to optimize the charge within a 1% full-width momentum spectrum. The result is a quite rectangular momentum spectrum that is about 1% wide (FWHM) and has 92% of the charge in ±1%. The trouble with this choice of optimization is that the transmitted charge will be quite sensitive to energy jitter. From SLC experience, we know that the energy jitter will be about 0.1%, dominated by the phase jitter of the compressor klystron. For this strategy, which optimizes the charge transmitted, a 0.1% energy jitter gives almost 10% intensity jitter.

This unpleasant result led to another optimization strategy. Figure 6-2b shows the result of moving the bunch closer to the accelerating crest. We find a more Gaussian-shaped momentum spectrum, for which 88% would be transmitted through a 1% momentum slit. Compared with the first approach, the intensity fluctuations due to energy jitter are reduced by about a factor of three.

Figure 6-3 shows the momentum spectrum for the electron beam. The 9-GeV electron beam shows only a minor intensity variation problem. This is because the adjustment for nearly maximum transmission through a 1% slit produces a double-spiked momentum spectrum having 0.7% FWHM and with 97% of the charge within a 1% full width.

To define the energy spread of the beam and the beam size from the linac, sets of energy and beam-size collimators will be installed in each of the transport lines. These collimators will shadow the ring acceptance apertures, thus preventing unnecessary beam loss in the rings themselves. A set of two energy-defining slits will be located 90° apart in phase in the dispersive region of the extraction lines, downstream of the BPMs that are used to measure, and control with feedback, the beam energy and initial trajectory launch into the extraction lines. A pair of *x-y* collimator jaws, again separated by 90° in phase, will be located in each transport line for the purpose of defining the transverse acceptance aperture of the ring injection system. A second pair of *x-y* collimators will be located downstream of the first set for the purpose of secondary collimation, that is, to clean up the halo generated by the primary energy and transverse collimators. The separation of these cleanup sets of collimators is again nominally 90° in phase. The existing energy-defining slits, located in the NIT and SIT lines, will be preserved and used for redundant

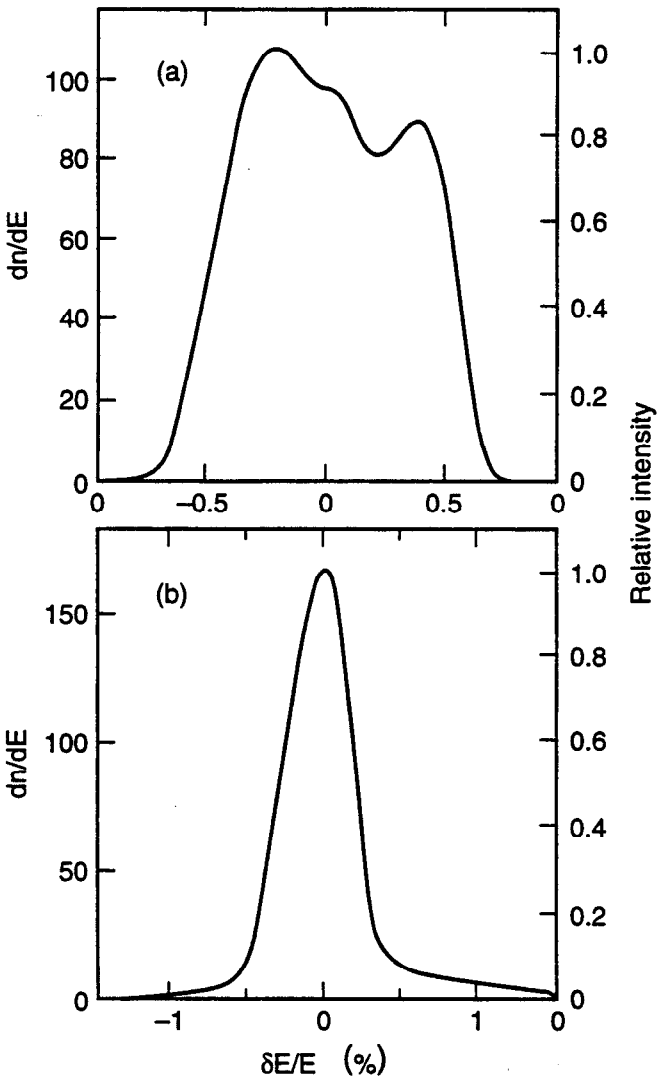

Fig. 6-2. (a) Momentum spectrum for the 3.1-GeV positron beam with $N_{e^+} = 2 \times 10^{10}$ per pulse, resulting from an attempt to optimize the charge within a 1% full-width momentum spectrum. This spectrum is 1% wide (FWHM) and has 92% of the charge in ±1% in momentum. For this spectrum, a 0.1% energy jitter gives almost 10% intensity jitter. (b) Momentum spectrum for the 3.1-GeV positron beam with $N_{e^+} = 2 \times 10^{10}$ per pulse, resulting from an approach that moves the bunch closer to the linac RF accelerating crest. A more Gaussian-shaped momentum spectrum results, for which 88% would be transmitted through a 1% slit. The intensity variation due to energy jitter is reduced by about a factor of three (to 3–4%) compared with the result in (a).

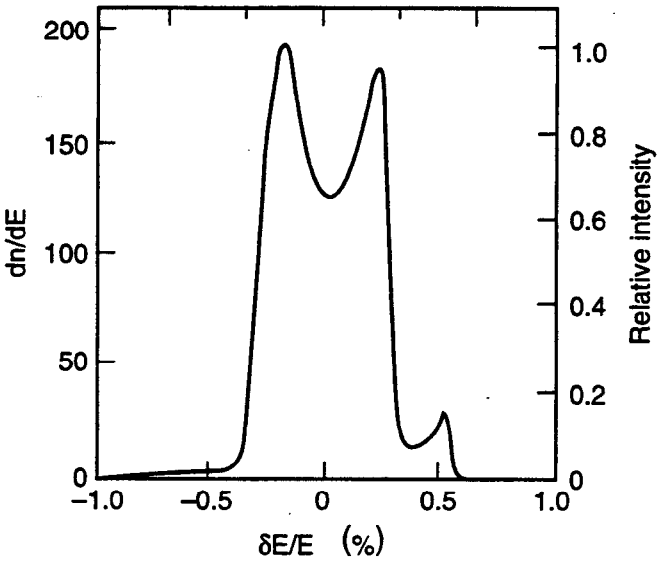

Fig. 6-3. Momentum spectrum for the 9.0-GeV e^- beam with $N_e - = 2 \times 10^{10}$ per pulse, resulting from the adjustment of phase for almost maximum transmission through a 1% slit. This produces a double-spiked spectrum having 0.7% FWHM that contains 97% of the charge within a ±1% momentum aperture. The intensity variation due to energy jitter is a minor problem in this configuration.

energy collimation. In addition, this collimation is envisioned to be used in defining a so-called "pencil beam." The pencil-beam concept will be useful during the commissioning stages to aid in the diagnosis of potential ring acceptance issues.

All of the collimator jaws will be remotely adjustable with a repeatability of about 30 μm. The design of the adjustable SLC linac collimators is more than adequate for this job in terms of power-handling capability and adjustability/setability. An engineering study will be made to see if a simpler set of collimators could be adapted from the existing design. BPMs and steering dipoles will be incorporated into a standard launch-control feedback to stabilize the beam trajectory through the collimators.

6.1.2 Beam Dump

A pulsed beam dumper (kicker magnet and water-cooled dump) will be located near the end of each transport line. The availability of such a system allows suppression of beam injection into the rings while preserving the steady-state operation of the injection complex. This feature is required during tuneup and diagnosis of the injection beams and is also needed for the selective dumping of bunches during top-off mode. The system will also be used during automated filling to generate the ion-clearing gap in the stored bunch pattern and will be incorporated into the machine protection system. The present design calls for a 120-Hz pulsed magnet capable of deflecting a 10-GeV beam by about 40 mrad. The installations in both the electron and positron lines will be identical, even though the beam energies and beam power requirements are different, to reduce

engineering and fabrication costs and to ensure that required spare components will be suitable for either system.

In the following sections, we describe in more detail the elements of the proposed injection system.

6.2 LINAC EXTRACTION AND TRANSPORT TO NIT AND SIT

As illustrated in Fig. 6-1, positrons will be extracted from the linac near the beginning of Sector 4 and electrons near the beginning of Sector 8. These choices provide considerable latitude in obtaining the desired energies, as the linac can provide roughly 1.8 GeV per sector with SLED. When operating at the nominal PEP-II design energy, there will be eight spare klystrons in Sectors 2 and 3, and another eight spare klystrons in Sectors 4 through 8. At each extraction point, some accelerator waveguide sections will have to be removed to provide space for extraction magnets. The existing linac quadrupoles, which are spaced 6.4 and 12.7 m apart in Sectors 4 and 8, respectively, will not be disturbed. After extraction, the beam will traverse the length of either the positron or electron bypass line (2.6 and 2.2 km, respectively). The bypass lines will be connected at their downstream ends to the existing NIT and SIT lines, which transport the beams to the injection points of their respective rings.

6.2.1 Sequence of Operation and Extraction Methods

The method used to extract the desired beam from the linac will be different for positrons and electrons. In the positron case, the extraction method takes advantage of the opposite charges of the beams to provide differing transverse deflections in DC magnets, whereas, in the electron case, separation of the like-charge beams requires transverse deflection by means of a pulsed magnet (having a relatively slow rise time of several milliseconds).

To understand how these extraction methods fit in with the operation of the linac for PEP-II injection, it is helpful to understand how the linac currently operates for SLC and then how this operation will be modified for PEP-II.

The pulse sequence for the present SLC operation is shown in Fig. 6-4a. Two electron bunches and one positron bunch are accelerated during each linac macropulse. The first two bunches are used for the electron-positron collisions in the SLC arcs, while the trailing "scavenger" electron bunch is used to create the positron bunch for the next pulse. To accomplish this, at 60 or 120 pps, Sectors 2 through 30 are pulsed essentially simultaneously (with just enough delay to synchronize them with the 10-μs overall particle transit time) and Sectors 0 and 1, upstream of the damping rings, are pulsed roughly 12 μs later to receive the positrons generated at Sector 19, which return to the injector via the PRL.

At Sector 1, these returning positrons, along with two new electron bunches out of the gun, are accelerated up to 1.2 GeV, after which each bunch is injected into its appropriate damping ring (electrons to the north and positrons to the south). After a few milliseconds (the exact time depending upon the pulse rate), the bunches for the next pulse are extracted from the damping rings. Although there is only one positron bunch to be

engineering and fabrication costs and to ensure that required spare components will be suitable for either system.

In the following sections, we describe in more detail the elements of the proposed injection system.

6.2 LINAC EXTRACTION AND TRANSPORT TO NIT AND SIT

As illustrated in Fig. 6-1, positrons will be extracted from the linac near the beginning of Sector 4 and electrons near the beginning of Sector 8. These choices provide considerable latitude in obtaining the desired energies, as the linac can provide roughly 1.8 GeV per sector with SLED. When operating at the nominal PEP-II design energy, there will be eight spare klystrons in Sectors 2 and 3, and another eight spare klystrons in Sectors 4 through 8. At each extraction point, some accelerator waveguide sections will have to be removed to provide space for extraction magnets. The existing linac quadrupoles, which are spaced 6.4 and 12.7 m apart in Sectors 4 and 8, respectively, will not be disturbed. After extraction, the beam will traverse the length of either the positron or electron bypass line (2.6 and 2.2 km, respectively). The bypass lines will be connected at their downstream ends to the existing NIT and SIT lines, which transport the beams to the injection points of their respective rings.

6.2.1 Sequence of Operation and Extraction Methods

The method used to extract the desired beam from the linac will be different for positrons and electrons. In the positron case, the extraction method takes advantage of the opposite charges of the beams to provide differing transverse deflections in DC magnets, whereas, in the electron case, separation of the like-charge beams requires transverse deflection by means of a pulsed magnet (having a relatively slow rise time of several milliseconds).

To understand how these extraction methods fit in with the operation of the linac for PEP-II injection, it is helpful to understand how the linac currently operates for SLC and then how this operation will be modified for PEP-II.

The pulse sequence for the present SLC operation is shown in Fig. 6-4a. Two electron bunches and one positron bunch are accelerated during each linac macropulse. The first two bunches are used for the electron-positron collisions in the SLC arcs, while the trailing "scavenger" electron bunch is used to create the positron bunch for the next pulse. To accomplish this, at 60 or 120 pps, Sectors 2 through 30 are pulsed essentially simultaneously (with just enough delay to synchronize them with the 10-μs overall particle transit time) and Sectors 0 and 1, upstream of the damping rings, are pulsed roughly 12 μs later to receive the positrons generated at Sector 19, which return to the injector via the PRL.

At Sector 1, these returning positrons, along with two new electron bunches out of the gun, are accelerated up to 1.2 GeV, after which each bunch is injected into its appropriate damping ring (electrons to the north and positrons to the south). After a few milliseconds (the exact time depending upon the pulse rate), the bunches for the next pulse are extracted from the damping rings. Although there is only one positron bunch to be

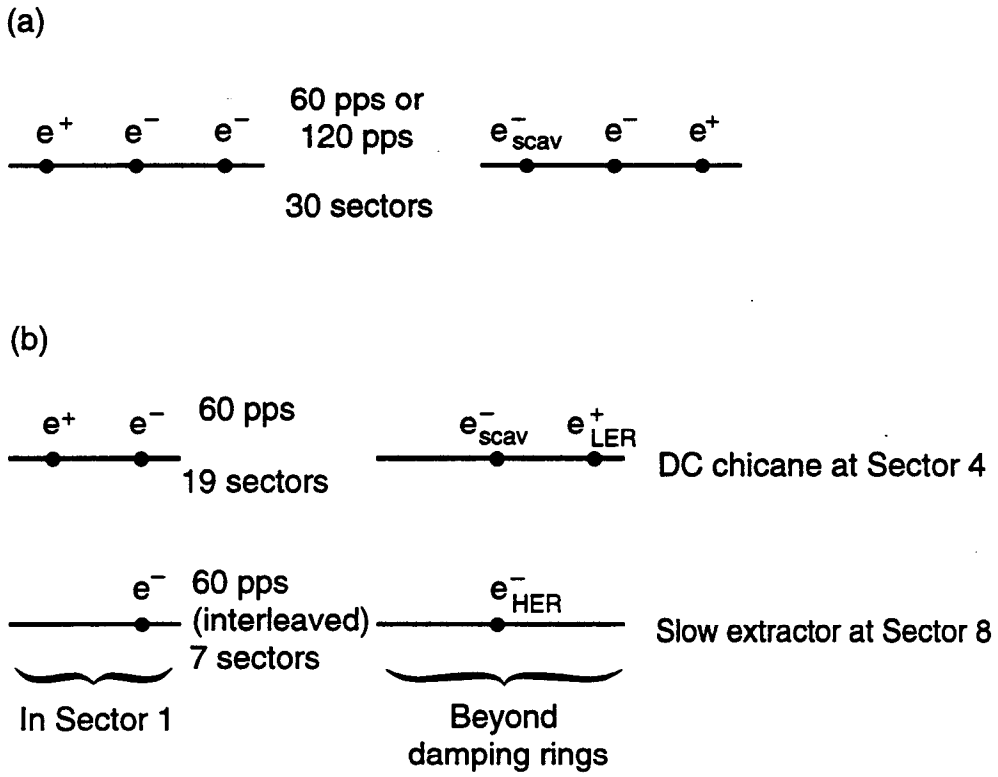

Fig. 6-4. Linac pulse and bunch sequence for (a) typical SLC operation and (b) injection into PEP-II.

extracted from the south damping ring, two bunches of electrons need to be extracted from the north damping ring; this leads to difficult kicker requirements—a fast rise time of a few nanoseconds coupled with a long flat-top. In Sectors 2 through 19, the positron bunch comes first, followed approximately 60 ns later by the first electron bunch and another 60 ns later by the second electron bunch. At Sector 19, the second electron bunch is redirected by a pulsed magnet (again having a very fast rise time of a few nanoseconds) and a Lambertson septum to the positron alcove, while the first electron bunch continues to be accelerated in the linac and eventually goes on to the SLC north arc.

In Sectors 0 and 1, the order of the bunches is inverted (for beam-loading reasons) and the newly generated electron bunches from the injector gun are placed ahead of the positron bunch returning from the positron source. The spacing between the three bunches is dictated by the almost diametrically opposite positions that they occupy in the damping rings and by the maximum appropriate distances at which they can ride on the SLED wave to acquire the proper energies in the linac.

The pulse sequence for filling PEP-II, shown in Fig. 6-4b, has been simplified vis-à-vis SLC operation. For PEP-II, a magnetic chicane at Sector 4 (see Fig. 6-1, and description below), set for a nominal energy of 3.1 GeV, extracts the positrons and reinjects the electrons into the linac. On one 60-pps time slot, the positron bunch comes first and the second bunch is the scavenger electron bunch, subsequently used to make new positrons. (We define a 60-pps "time slot" as a set of 60 pulses synchronized with one phase of the 60-Hz AC power line. When the accelerator runs at 120 pps, it uses two

such time slots, equally spaced in time.) Only one electron bunch is in the north damping ring at a time, and this considerably eases the difficulty of extraction compared with present SLC operation. To let the scavenger electron bunch reach Sector 19, the pulsed magnet at Sector 8 is turned off during this time slot. When the positron bunch returns via the PRL, only one new electron bunch is generated at the gun and stored in the north damping ring, while the positron bunch is stored in the south damping ring.

On the other time slot (8.3 ms, or 1/120 of a second, later), the electron bunch is ejected from the north damping ring and accelerated to Sector 8. This time, the extractor magnet is turned on and the electron bunch is launched into the electron bypass line. After 12 μs, the injector gun generates a new electron bunch that is stored in the north damping ring to become the next scavenger bunch (for the positron time slot 8.3 ms later). Subsequently, the entire pattern is repeated. Note that in this mode of injection there is no need for any new fast-pulsed magnet. The chicane has DC magnets and the magnet at Sector 8 need only be cycled on and off during successive pulses. Sectors 9 through 19 run at 60 pps, and Sectors 1 through 8 run at 120 pps.

6.2.2 Positron Extraction and the Chicane

The 3.1-GeV positron bunch is extracted at Sector 4 using DC magnets. These extraction magnets have a roll angle about the linac axis such that the plane of extraction for positrons is 59° from the vertical, as shown in Fig. 6-5. Also indicated in Fig. 6-5 are the orientation of the electron extraction plane (downstream at Sector 8, see below), which will be at 45° from the vertical, and the locations in the linac housing of the two new bypass lines (each more than 2 km in length) and the existing PRL.

Returning to the description of positron extraction, the electron bunches will undergo a local orbit excursion but will immediately be restored to their trajectories along the linac axis. This will be accomplished by a configuration of four dipole magnets (see Table 6-2), commonly referred to as a "chicane," that results in the bending sequence θ, $-\theta$, $-\theta$, θ. Note that the chicane consists entirely of DC magnets—an important feature when considering the stability of the extraction process. In the first magnet, both electrons and positrons enter coaxially and are deflected in opposite directions by 2.5°. This magnet will be less than 1 m long, with an integrated field of about 0.45 T·m. After drifting about 1 m, the electrons enter a second, C-type dipole that deflects them by 2.5° in the opposite direction, to a trajectory parallel to, but displaced from, the linac axis. A third dipole, identical to the second dipole then deflects the beam 2.5° (in the same sense as the second dipole) back towards the linac axis. When the electrons again cross the linac axis, a fourth dipole deflects them by 2.5° (in the opposite sense to dipoles 2 and 3) to make their trajectory again coaxial with the linac. For the electrons, the overall action of this chicane is independent of beam energy (except for slight flight-time variations), because it only affects the magnitude of the internal deflections and hence the orbit excursions. By utilizing a C-type dipole with a good-field region of reasonable size, and by fabricating a vacuum chamber with no obstructions between the linac axis and the maximum possible deflection (corresponding to the lowest energy accepted), the energy bandpass of the chicane can be made at least as large as 20%, and thus the chicane will be easy to operate. Aside from small edge-focusing effects, this region will be optically equivalent to a drift for the electrons.

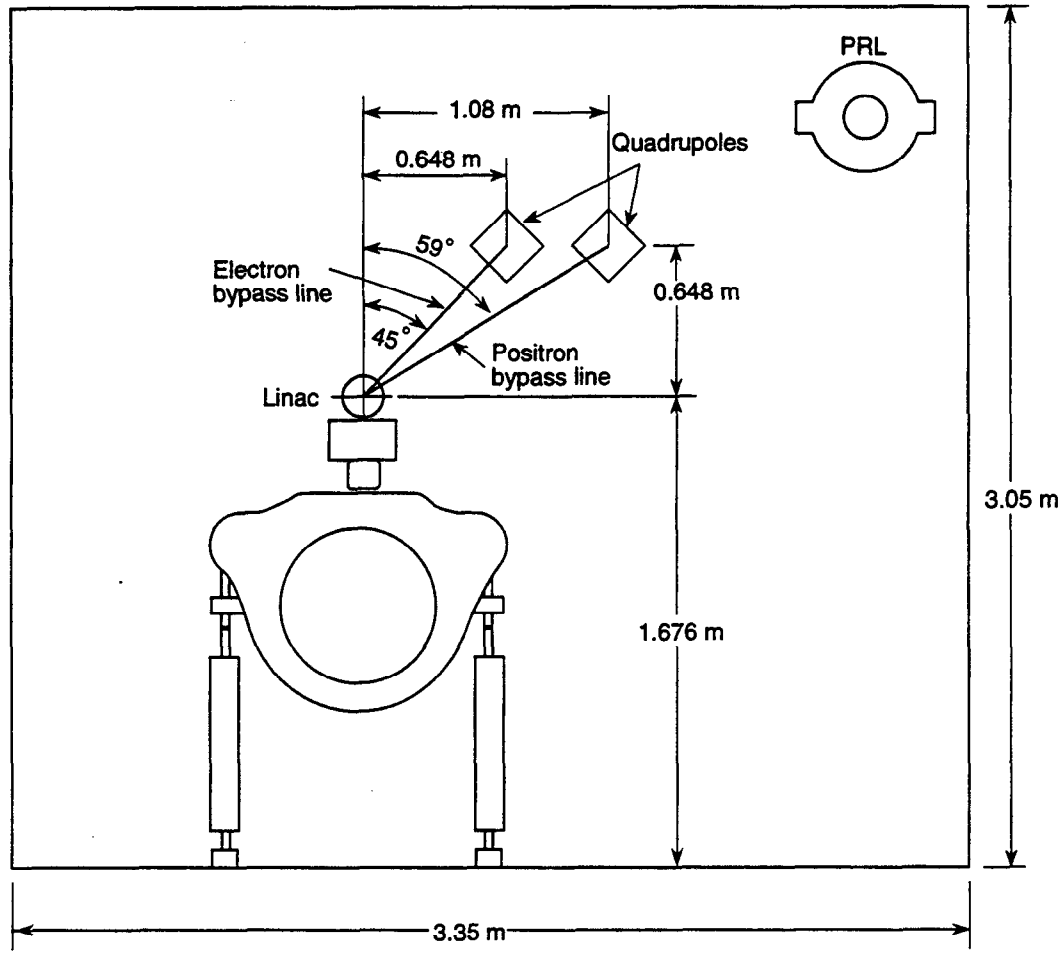

Fig. 6-5. Cross section of linac housing showing the locations of the electron and positron FODO array quadrupoles. Note the tilts of the extraction planes.

We now return our attention to the positron beam, which, after being deflected by the first dipole, will separate from the electron beam at a nominal angle of 5.0°. Because the strength of this first chicane magnet is always set by the requirement to deflect the positrons by a fixed angle of 2.5° for any energy selected for injection into the LER, the separation angle between positrons and electrons can vary. The nominal separation between the two beams at the entrance to the C-dipole (dipole 2) that deflects the electrons back towards the linac will be approximately 10 cm—a distance sufficient to allow good isolation of the positron beam from any adverse optical effects stemming from magnetic fringing fields. The positron bunch continues past this magnet for almost 6 m, at which point it will pass near the next quadrupole in the optical lattice of the linac. By the time the positron beam reaches this next linac quadrupole, it is offset transversely from the linac axis by nearly 25 cm and easily clears the quadrupole yoke. This is

Table 6-2a. Positron extraction line dipole parameters at 3.1 GeV. Coil material is copper for all magnets.

Magnet designation	2H24	2C24	2H24	2H24	2H24
Bending angle [deg]	2.5	2.5	2.5	2.5	1.122
Lattice designation	BS	Bchic.	BR	B1	B2
Number of magnets	1	2	1	2	2
Field @ 3.1 GeV [T]	0.752	0.752	0.752	0.752	0.338
Integrated field @ 3.1 GeV [T·m]	0.451	0.451	0.451	0.451	0.203
Pole width [in.]	8	8	8	8	8
Gap height [in.]	1	1	1	2	1
Core length [in.]	22.62	22.62	22.62	21.62	22.62
Magnetic length [in.]	23.62	23.62	23.62	23.62	23.62
Width of useful field, 0.1% [in.]	4.00	4.00	4.00	4.00	4.00
Lamination height [in.]	6.75	6.75	6.75	6.75	6.75
Lamination width [in.]	23	23	23	23	23
Packing factor, minimum [%]	96	96	96	96	96
Core weight [lb]	2,000	1,500	2,000	2,000	2,000
Amp·turns @ 3.1 GeV	7,598	7,598	7,598	15,197	9,548
Turns	36	36	36	36	36
Pancakes per pole	1	1	1	1	1
Conductor dimensions [in.]	0.34 × 0.34	0.34 × 0.34	0.34 × 0.34	0.34 × 0.34	0.34 × 0.34
Cooling hole diameter [in.]	0.1875	0.1875	0.1875	0.1875	0.1875
Conductor cross-sectional area [in.^{2}]	0.10	0.10	0.10	0.10	0.10
Conductor length/pole [ft]	211	211	211	205	211
Current @ 3.1 GeV [A]	211.06	211.06	211.06	422.13	265.23
Resistance @ 40°C [mΩ]	36.1	36.1	36.1	35.1	36.1
Power @ 3.1 GeV [kW]	1.61	1.61	1.61	6.25	2.54
Voltage drop @ 3.1 GeV [V]	7.6	7.6	7.6	14.8	9.6
Coil weight [lb]	154	154	154	149	154
Number of water circuits	2	2	2	2	2
Water flow rate, total [gpm]	1.3	1.3	1.3	1.3	1.3
Water pressure drop [psi]	150	150	150	150	150
Temperature rise [°C]	4.8	4.8	4.8	18.6	7.7
Total power (magnets and bus) [kW]	4.3	3.2	1.6	12.5	5.1
Total voltage (magnets and bus) [V]	49.2	25.2	17.6	39.6	26.7
Total system water requirements [gpm]	1.26	2.52	1.26	2.56	2.52

Table 6-2a. Positron extraction line dipole parameters at 3.1 GeV. Coil material is copper for all magnets (continued).

Magnet designation	2H60	2H80	2H60	2H60	2H60
Bending angle [deg]	0.162	0.824	3.731	0.646	0.162
Lattice designation	BH1	BV+	B02	B01	BH1
Number of magnets	2	1	2	2	1
Field @ 3.1 GeV [T]	0.019	0.074	0.449	0.078	0.019
Integrated field @ 3.1 GeV [T·m]	0.029	0.149	0.674	0.117	0.029
Pole width [in.]	8	8	8	8	8
Gap height [in.]	1	1	1	1	1
Core length [in.]	58.06	77.74	58.06	58.06	58.06
Magnetic length [in.]	59.06	78.74	59.06	59.06	59.06
Width of useful field, 0.1% [in.]	4.00	4.00	4.00	4.00	4.00
Lamination height [in.]	6.75	6.75	6.75	6.75	6.75
Lamination width [in.]	23	23	23	23	23
Packing factor, minimum [%]	96	96	96	96	96
Core weight [lb]	2,000	2,000	2,000	2,000	2,000
Amp·turns @ 3.1 GeV	197	751	4,536	785	197
Turns	36	36	36	36	36
Pancakes per pole	1	1	1	1	1
Conductor dimensions [in.]	0.34 × 0.34	0.34 × 0.34	0.34 × 0.34	0.34 × 0.34	0.34 × 0.34
Cooling hole diameter [in.]	0.1875	0.1875	0.1875	0.1875	0.1875
Conductor cross-sectional area [in.^{2}]	0.10	0.10	0.10	0.10	0.10
Conductor length/pole [ft]	424	542	424	424	424
Current @ 3.1 GeV [A]	5.47	20.87	126.00	21.82	5.47
Resistance @ 40°C [mΩ]	72.5	92.7	72.5	72.5	72.5
Power @ 3.1 GeV [kW]	0.00	0.04	1.15	0.03	0.00
Voltage drop @ 3.1 GeV [V]	0.4	1.9	9.1	1.6	0.4
Coil weight [lb]	308	394	308	308	308
Number of water circuits	2	2	2	2	2
Water flow rate, total [gpm]	0.9	0.8	0.9	0.9	0.9
Water pressure drop [psi]	150	150	150	150	150
Temperature rise [°C]	0.0	0.2	5.1	0.2	0.0
Total power (magnets and bus) [kW]	0.0	0.1	3.3	0.1	0.0
Total voltage (magnets and bus) [V]	1.9	6.0	43.1	7.5	1.5
Total system water requirements [gpm]	1.73	0.76	1.73	1.73	0.87

Table 6-2b. Electron extraction line dipole parameters at 9 GeV. Coil material is copper for all magnets.

Magnet designation	B2	B3	BP1	B2
Bending angle [deg]	2.511	1.031	0.25	2.511
Location	Extr./Septum	Extr.	Extr.	Extr.
Number of magnets	1	4	2	1
Field @ 9 GeV [T]	0.658	0.540	0.155	0.658
Integrated field @ 9 GeV [T·m]	1.3161	0.540	0.131	1.316
Pole width [in.]	8	8	8	8
Gap height [in.]	1	1.375	1.375	1.375
Core length [in.]	77.74	38.00	31.81	77.37
Magnetic length [in.]	78.74	39.37	33.19	78.74
Width of useful field, 0.1% [in.]	4.00	4.00	4.00	4.00
Lamination height [in.]	6.75	6.75	6.75	6.75
Lamination width [in.]	23	23	23	23
Packing factor, minimum [%]	98	98	98	98
Core weight [lb]	6,841	3,344	2,800	6,808
Amp·turns @ 9 GeV	6,646	15,282	4,396	9,138
Turns	36	48	36	36
Pancakes per pole	1	1	1	1
Conductor dimensions [in.]	0.34 × 0.34	0.34 × 0.34	0.34 × 0.34	0.34 × 0.34
Cooling hole diameter [in.]	0.1875	0.1875	0.1875	0.1875
Conductor cross-sectional area [in.^{2}]	0.08	0.08	0.08	0.08
Conductor length/pole [ft]	580	455	304	577
Current @ 9 GeV [A]	184.62	318.37	122.10	253.85
Resistance @ 40°C [mΩ]	116.1	91.1	60.9	115.6
Power @ 9 GeV [kW]	1.98	4.62	0.45	3.73
Voltage drop @ 9 GeV [V]	10.7	14.5	3.7	14.7
Coil weight [lb]	341.2	267.8	179.0	339.9
Number of water circuits	2	2	2	2
Water flow rate, total [gpm]	0.7	1.7	2.1	1.5
Water pressure drop [psi]	150	150	150	150
Temperature rise [°C]	10.3	10.5	0.8	9.7
Total power (magnets and bus) [kW]	2.0	18.5	0.9	3.7
Total voltage (magnets and bus) [V]	10.7	58.0	7.4	14.7
Total system water requirements [gpm]	1	7	4	1

Table 6-2b. Electron extraction line dipole parameters at 9 GeV. Coil material is copper for all magnets (continued).

Magnet designation	BHR3	BV+	BV–	BHL2
Bending angle [deg]	2.134	0.362	2.381	1.194
Location	Match	Match	Match	Match
Number of magnets	1	2	1	1
Field @ 9 GeV [T]	0.746	0.095	0.832	0.313
Integrated field @ 9 GeV [T·m]	1.1185	0.1897	1.2479	0.6258
Pole width [in.]	8	8	8	8
Gap height [in.]	1	1.375	1.375	1.375
Core length [in.]	58.06	77.37	57.68	77.37
Magnetic length [in.]	59.06	78.74	59.06	78.74
Width of useful field, 0.1% [in.]	4.00	4.00	4.00	4.00
Lamination height [in.]	6.75	6.75	6.75	6.75
Lamination width [in.]	23	23	23	23
Packing factor, minimum [%]	98	98	98	98
Core weight [lb]	5,109	6,808	5,076	6,808
Amp·turns @ 9 GeV	7,531	2,683	23,528	4,345
Turns	36	48	36	36
Pancakes per pole	1	1	1	1
Conductor dimensions [in.]	0.34 × 0.34	0.34 × 0.34	0.34 × 0.34	0.34 × 0.34
Cooling hole diameter [in.]	0.1875	0.1875	0.1875	0.1875
Conductor cross-sectional area [in.^{2}]	0.08	0.08	0.08	0.08
Conductor length/pole [ft]	461	770	459	577
Current @ 9 GeV [A]	209.20	55.89	653.55	120.71
Resistance @ 40°C [mΩ]	92.4	154.2	92.0	115.6
Power @ 9 GeV [kW]	2.02	0.24	19.64	0.84
Voltage drop @ 9 GeV [V]	9.7	4.3	30.1	7.0
Coil weight [lb]	271.7	453.2	270.4	339.9
Number of water circuits	2	2	2	2
Water flow rate, total [gpm]	0.8	1.3	1.7	1.5
Water pressure drop [psi]	150	150	150	150
Temperature rise [°C]	9.3	0.7	45.0	2.2
Total power (magnets and bus) [kW]	2.0	0.5	19.6	0.8
Total voltage (magnets and bus) [V]	9.7	8.6	30.1	7.0
Total system water requirements [gpm]	1	3	2	1

Table 6-2b. Electron extraction line dipole parameters at 9 GeV. Coil material is copper for all magnets (continued).

Magnet designation	BHR1	B2	B3
Bending angle [deg]	0.246	5.842	9.000
Location	Match	Extr.	Extr.
Number of magnets	1	1	1
Field @ 9 GeV [T]	0.086	1.177	0.898
Integrated field @ 9 GeV [T·m]	0.1289	3.0619	4.7171
Pole width [in.]	8	8	8
Gap height [in.]	1	1.375	1.375
Core length [in.]	58.06	101.00	205.43
Magnetic length [in.]	59.06	102.38	206.80
Width of useful field, 0.1% [in.]	4.00	4.00	4.00
Lamination height [in.]	6.75	6.75	6.75
Lamination width [in.]	23	23	23
Packing factor, minimum [%]	98	98	98
Core weight [lb]	5,109	8,888	18,078
Amp·turns @ 9 GeV	868	33,299	25,396
Turns	36	48	36
Pancakes per pole	1	1	1
Conductor dimensions [in.]	0.34 × 0.34	0.34 × 0.34	0.34 × 0.34
Cooling hole diameter [in.]	0.1875	0.1875	0.1875
Conductor cross-sectional area [in.^{2}]	0.08	0.08	0.08
Conductor length/pole [ft]	461	959	1346
Current @ 9 GeV [A]	24.12	693.73	705.44
Resistance @ 40°C [mΩ]	92.4	192.0	269.5
Power @ 9 GeV [kW]	0.03	46.21	67.06
Voltage drop @ 9 GeV [V]	1.1	66.6	95.1
Coil weight [lb]	271.7	564.5	792.3
Number of water circuits	2	2	2
Water flow rate, total [gpm]	0.8	1.1	0.9
Water pressure drop [psi]	150	150	150
Temperature rise [°C]	0.1	157.7	274.8
Total power (magnets and bus) [kW]	0.0	46.2	67.1
Total voltage (magnets and bus) [V]	1.1	66.6	95.1
Total system water requirements [gpm]	1	1	1

demonstrated in Fig. 6-6, where the quadrupoles for the linac and the bypass line are shown together with the S-band waveguide that feeds RF power to the linac.

While a large separation angle is desirable in order to clear the downstream components, it must be kept in mind that there are limits. If this angle becomes too large, then the rapid separation of the beams within the first magnet itself would require an excessively large good-field region. This, in turn, could lead to problems with available space and support structures due to excessive bulk of the magnet. Shortening the length and increasing the field strength of the first separation magnet is also not a good option, as this would increase the synchrotron-radiation-induced emittance growth. Estimates based upon these considerations indicate that there is a large range of comfortable design parameters and that a reasonable compromise can easily be found.

As mentioned earlier, for the present extraction design we have selected a separation dipole magnet with a bend angle of 2.5°. This angle gives sufficient separation of the two beams, leads to a reasonable design for the C-type dipoles required for the chicane, and provides adequate clearance for the required quadrupoles in both the linac and the extraction line. As described below, however, this choice also generated a geometrical problem for which a solution had to be found.

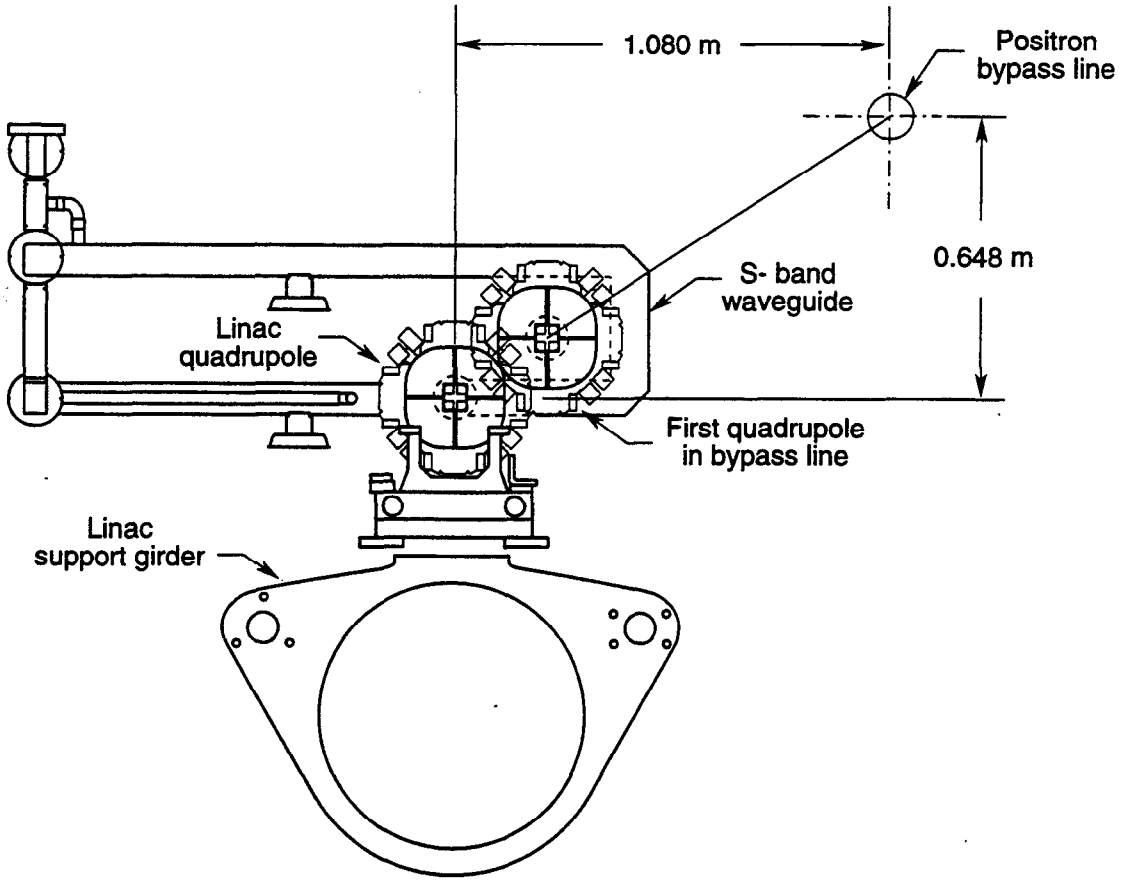

Fig. 6-6. Positron extraction line from linac, showing clearance at first downstream linac quadrupole.

6.2.3 Design of the Positron Extraction Line

The optical design of the positron extraction system is intended to satisfy the following requirements:

- Providing a good match to the beta functions of the linac lattice in both transverse planes
- Removing dispersion caused by the extraction dipoles
- Providing a region for monitoring and implementing feedback control of the positron energy
- Providing a region for optically matching to the bypass line
- Providing sufficient flexibility to match geometrically to the location of the bypass line, as required by engineering constraints

At the same time, it is advantageous to minimize disturbing the present linac structures. This strategy gives the option of early installation of some of the PEP-II injection hardware and the possibility of running beam tests prior to the cessation of the SLC experimental program.

Matching the beta functions and controlling dispersion are most easily managed by the simple expedient of using a FODO lattice with parameters closely matching those of the linac lattice. Our extraction line design is essentially an optical continuation of the linac lattice, and its cell length is very nearly that of the linac lattice (it has been slightly increased to longitudinally offset the first linac and extraction line quadrupoles downstream of the chicane for clearance purposes). For the extraction line, the phase advance per cell has been adjusted to be exactly 90° in both planes. In the linac lattice, the phase advance is kept near its optimum value of 76.5°, which maximizes the acceptance, though in practice the value of the phase advance is generally not carefully controlled and can vary.

The phase advance per cell of exactly 90° in the extraction line is necessary to provide an easy method for both controlling dispersion and matching to the desired geometry. The simplicity of matching results from the fact that four cells of such a lattice (phase advance of 2π) give an optical transfer matrix equal to the identity matrix. Thus, dispersion introduced by the 2.5° extraction magnet can be exactly canceled by a bend of equal strength, but in the opposite direction, placed four cells downstream. This use of equal but opposite bends, separated by a long drift, is ideal for the purpose of connecting two parallel beamlines. However, the desired large initial bend, coupled with the cell length of 12.7 m (50.8 m for four cells) as in the linac (needed for the beta function matching), would imply a transverse offset of more than 2 m from the linac; this would put the bypass at an awkward location in the linac tunnel. The obvious solution of simply decreasing the extraction angle is not acceptable, as it increases the difficulty of obtaining clearance for other components. Fortunately, the additional flexibility to match the geometry is easily provided by introducing two more dipoles (again of equal strength but of opposite sign and separated optically by the identity matrix). The first of these additional dipoles will bend in a direction opposite to that of the extraction dipole, but with less strength. We have determined that, with this scheme of using four magnets for

positron extraction, obstacles can be avoided and the design can be easily modified to optimize desired parameters or accommodate requested engineering changes.

The geometry of this extraction configuration is shown in Fig. 6-7, which indicates the location of key elements in elevation and in plan views (with the longitudinal scale

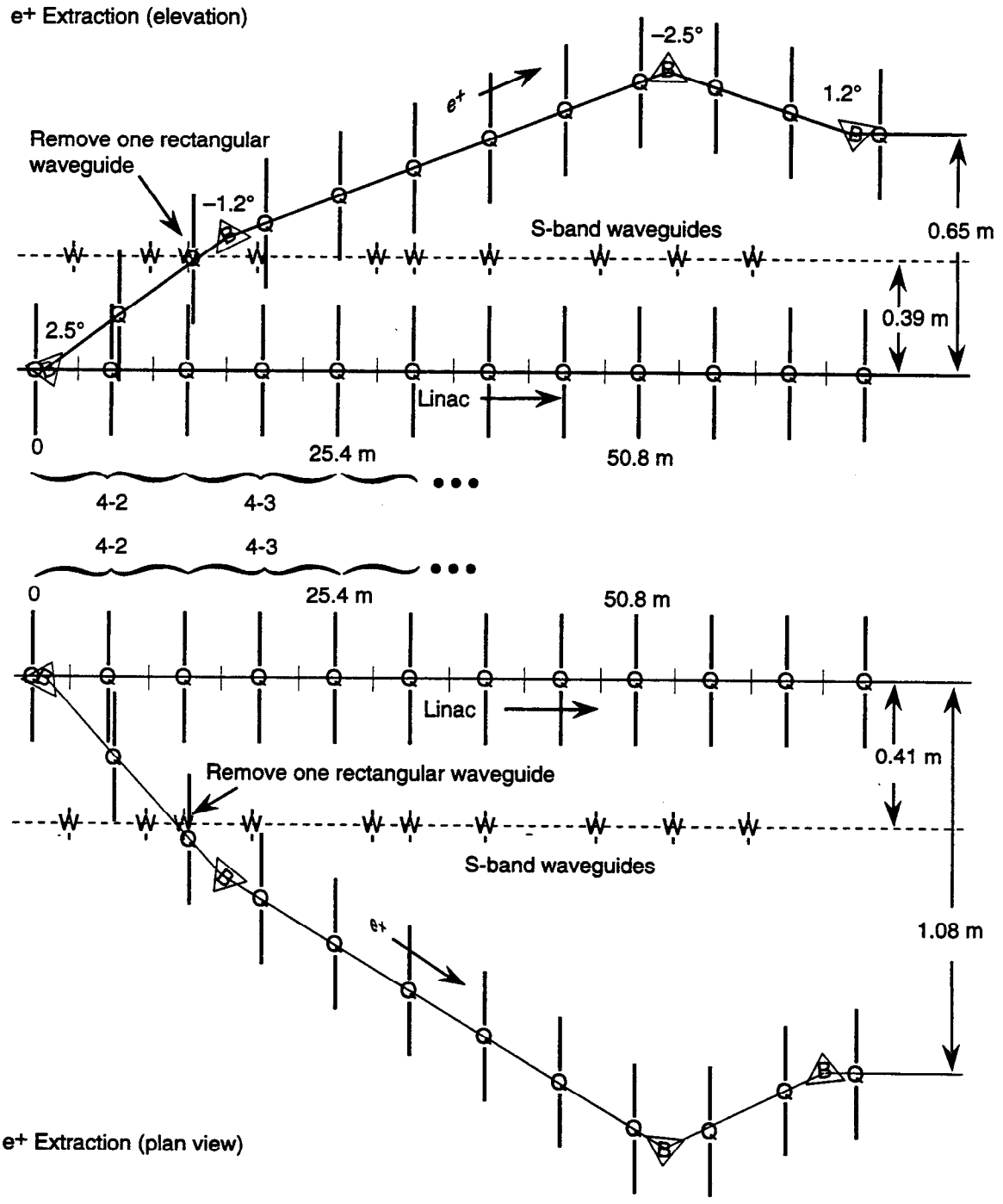

Fig. 6-7. Elevation and plan views of the positron extraction line. Linac quadrupole locations are marked Q, and the locations of S-band waveguides feeding power to the linac are marked W.

compressed). Also shown in this figure are the linac quadrupoles (indicated with Q) and the rectangular S-band waveguides (indicated with W), which we attempted to avoid. As can be seen, one such waveguide will have to be removed or rerouted.

The optical functions for this extraction configuration are shown in Fig. 6-8. The beta functions are almost a continuation of those of the linac, so the matching between the

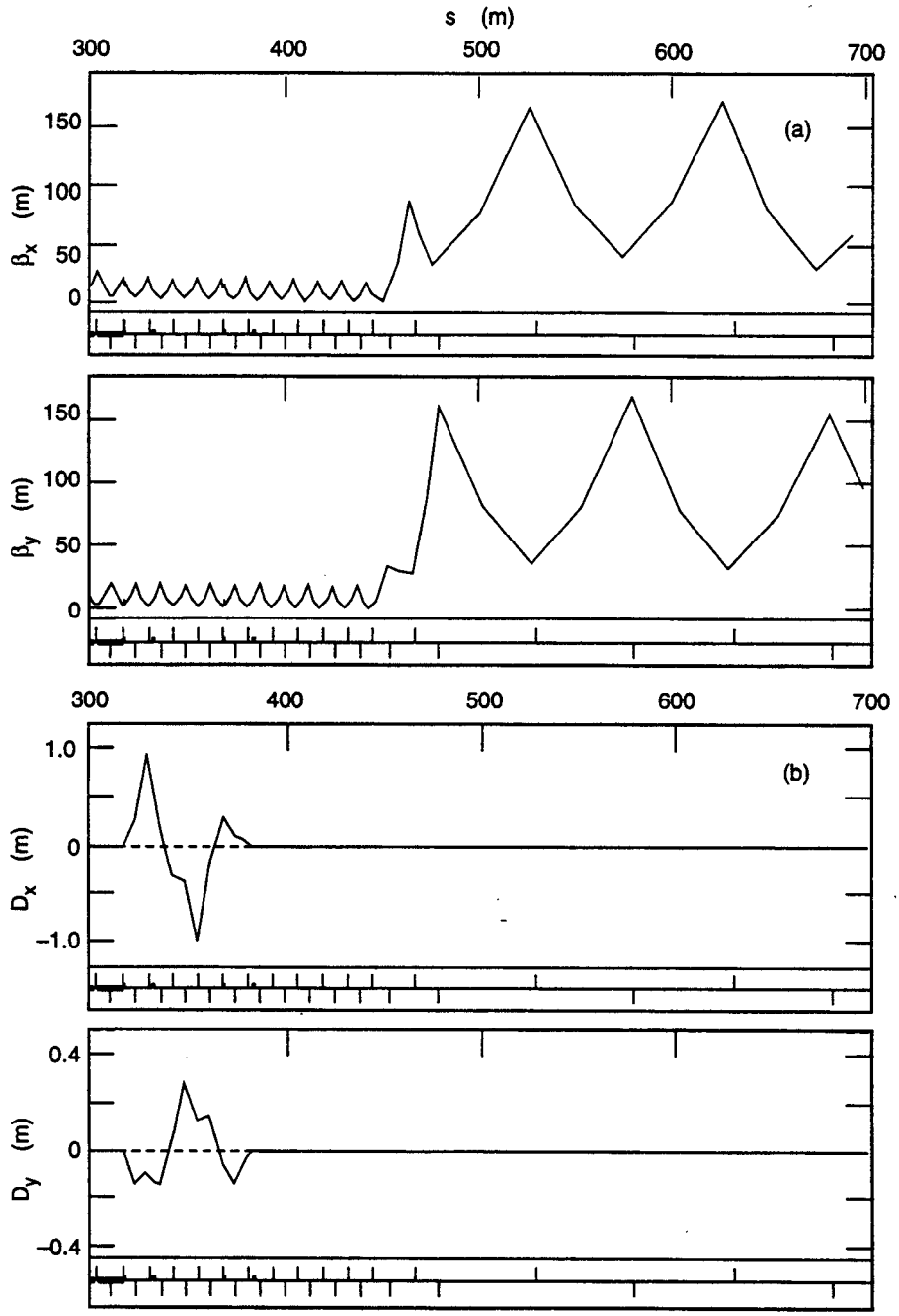

Fig. 6-8. Positron extraction line optical functions: (a) β_x and β_y; (b) D_x and D_y. The dispersion coupling results from not rolling the quadrupole axes to match the dipole roll angle.

lattices is easily achieved. In the optical configuration shown in Fig. 6-8, the quadrupoles are not rolled about the beam axis to match the roll angle of the dipoles. Although this preserves the matching of the beta functions, it means that the dispersion becomes coupled into both the vertical and horizontal planes. An alternative approach is possible, of course—to roll both quadrupoles and dipoles for uncoupled dispersion—but this would give both coupling and a large mismatch of the beta functions. Both options are under study and we will choose the one with the greatest tolerance for errors. In the example shown in Fig. 6-8, the energy resolution of the extraction line for an emittance-damped beam is approximately 1×10^{-3}, a value that matches the specification for the proposed energy feedback system.

Following the dispersive region is a dispersion-free region where the lattice continues with the same 90° phase advance per cell. This region will be used for beam diagnostics and for operational tuning of the optics to match into the bypass-line optics downstream. By maintaining an overall phase advance of 720°, this dispersion-free continuation also serves to preserve the option of rolling or not rolling the quadrupoles.

Following the continuation region is a short matching section, where four quadrupoles are used to match the beta functions to those of the bypass line optics.

6.2.4 Bypass Lines

Optical functions of the bypass lines are included in Fig. 6-8. The parameters of this FODO array have been adjusted such that there is exactly one cell per linac sector (L_{cell} = 101.6 m). A phase advance per cell of 76.5° has been chosen for this design, as that value maximizes the acceptance. Of course, the phase advance is not a fixed parameter and can be changed during operation. With the length L_{cell} and phase advance per cell μ determined, the values of the extrema for the matched beta function are given by the equation

$$\beta_{max,min} = \frac{L_{cell}}{\sin \mu}\left(1 \pm \sin \mu/2\right) \qquad (6\text{-}1)$$

which gives β_{max} = 169 m and β_{min} = 40 m, as we see in Fig. 6-8. The required focal length f is given by

$$f = \frac{L_{cell}}{4 \sin \mu/2} = 41 \text{ m} \qquad (6\text{-}2)$$

Achieving this value for the focal length will require only about 0.25 T of integrated gradient at 3.1 GeV.

These low-strength quadrupoles (two per sector, or 50.8 m apart) will be suspended from the ceiling of the linac housing, as suggested by Fig. 6-5. At each quadrupole, there is a BPM that measures either the horizontal or vertical position of the beam and one steering dipole that steers the beam in that same plane. Thus, each corrector is located at a point where the beta function in the plane in which it steers is a maximum, and there will be a phase advance between like correctors equal to that for one cell (76.5°).

As shown in Fig. 6-9, the bypass line vacuum chambers will be fabricated from 2-in.-diameter seamless stainless-steel tubing. This chamber aperture provides sufficient vacuum pumping conductance but, at each quadrupole (every 50.8 m), the chamber will be necked down to about 1-in. diameter to allow for small-bore quadrupoles and, more importantly, to reduce the cost of the line by the use of smaller flanges, bellows, and BPMs. For each line, there will be one 30-L/s pump every 101.6-m length (one FODO cell). Isolation valves are provided every third cell, and roughing connections are provided each cell, as indicated in Fig. 6-10.

Four independent power supplies will supply power to four strings of quadrupole magnets connected in series. All horizontally focusing quadrupoles will comprise one string, and all vertically focusing quadrupoles another string, in each of the two bypass lines. A parameter list for the injection system quadrupole magnets is given in Table 6-3.

Profile monitors and/or wire scanners will be used to check the beam emittance and beam shape at the launch point and before injection into the NIT and SIT lines. Intensity monitors will be placed near each end of the bypass lines and used to supplement the total charge information obtained from the BPM striplines.

The large maximum value of the beta function in the bypass line means that the transverse beam size will reach values as large as 0.5 mm rms for electrons and 0.75 mm rms for positrons. A series of four variable- (and overlapping-) jaw collimators in each beamline will serve to tailor the beam size and hence the emittance of the injected beam. These collimators will be placed 90° apart in phase advance in both the horizontal and vertical planes. In addition to these eight emittance-defining collimators, one or two collimators will be included in the dispersive region of the extraction line (downstream of the energy feedback devices) for the purpose of removing unwanted energy tails. Optimum locations for the variable-jaw collimators will be determined by further study. In addition to these controllable collimators, the existing energy-defining collimators in both the NIT and SIT beamlines will be used.

6.2.5 Electron Extraction

At Sector 8, the linac lattice has a cell length of 25.4 m (12.7-m spacing between quadrupoles). In order to provide the space for e^- extraction, it will be necessary to remove all of the disk-loaded accelerating structure corresponding to one klystron (a 12.7-m section).

As mentioned earlier, the electron extraction will take advantage of the temporal separation of about 8.3 ms between the scavenger bunch (used for positron production) and the electron bunch needed for injection into the HER. Because of this relatively large separation in time, the pair of pulsed magnets used at PEP to kick the electrons and positrons into the SIT and NIT lines are adequate for this purpose. These magnets (or perhaps newly designed equivalents) are each 0.843 m in length and have an integrated flux density of Bl = 0.14 T·m, sufficient to provide a total kick of 0.5° to the 9-GeV electron beam.

After a drift of 3 m following this kick, the beam will be sufficiently separated from the on-axis beam to be captured by a Lambertson septum magnet that will deflect the beam (by about 2.5°, orthogonal to the original deflection) sufficiently to avoid the first linac quadrupole. As was done in the positron extraction scheme (see Section 6.2.3),

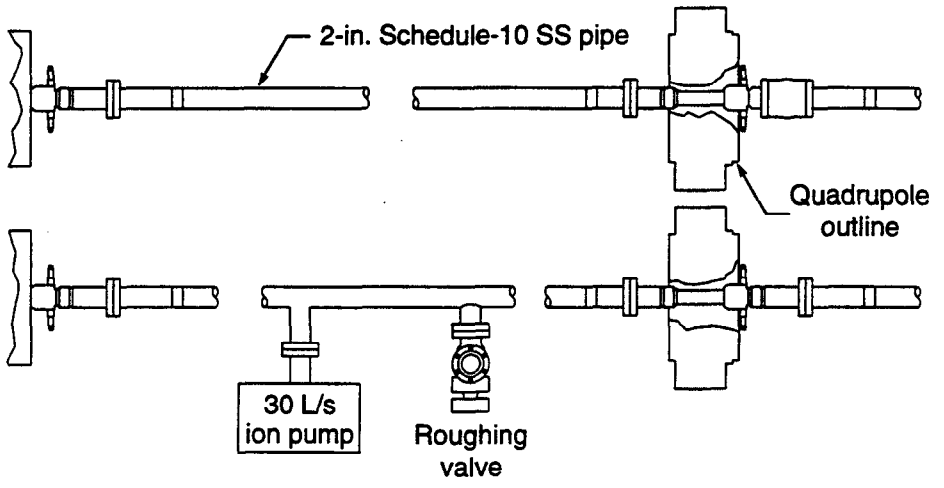

Fig. 6-9. Schematic layout of bypass lines.

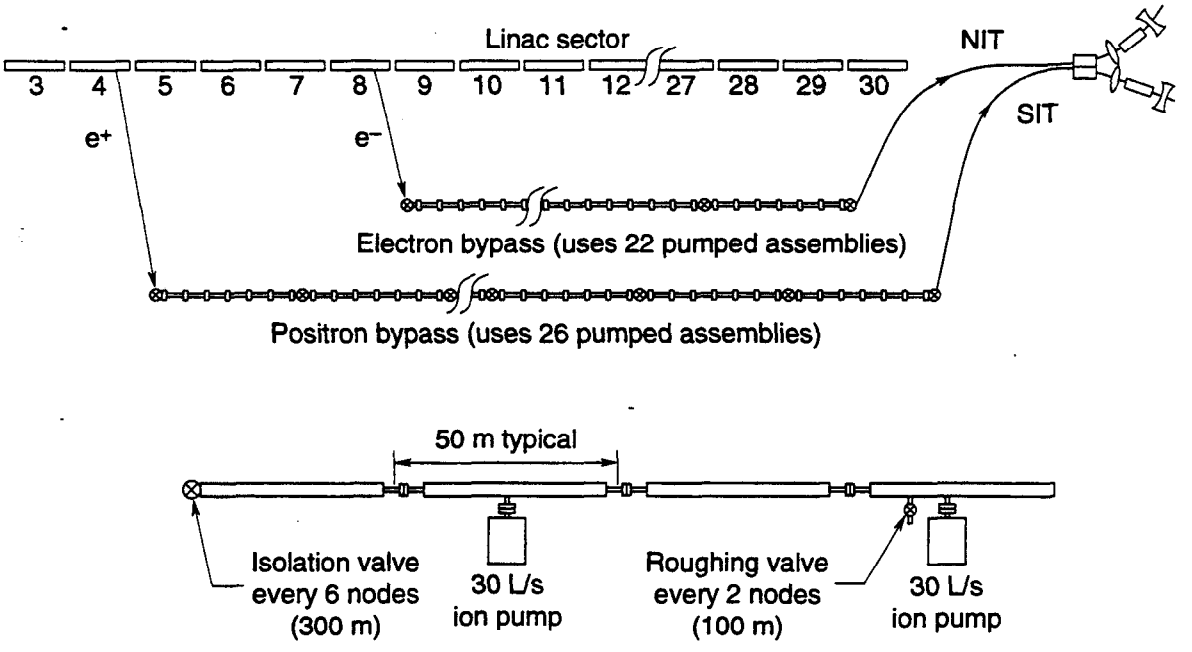

Fig. 6-10. Vacuum layout for bypass lines.

Table 6-3a. Positron injection line quadrupole parameters at 3.1 GeV. Coil material is copper for all magnets.

Magnet designation	2Q10	2Q10	2Q10	2Q10	2Q10	2Q10
Location	Extr.	Extr.	Extr.	Extr.	Extr.	Extr.
Lattice designation	QD	QF	QDI	QFI	QFM	QDM
Number of magnets	5	5	4	4	2	2
Operating gradient @ 3.1 GeV [T/m]	9.008	9.008	9.008	9.008	4.041	4.041
Pole-tip field @ operating gradient [T]	0.232	0.232	0.232	0.232	0.104	0.104
Gradient-length product [T]	2.25	2.25	2.25	2.25	1.01	1.01
Inscribed radius [in.]	1.015	1.015	1.015	1.015	1.015	1.015
Core length [in.]	9.34	9.34	9.34	9.34	9.34	9.34
Magnetic length [in.]	9.84	9.84	9.84	9.84	9.84	9.84
Lamination height [in.]	6.75	6.75	6.75	6.75	6.75	6.75
Lamination width [in.]	6.75	6.75	6.75	6.75	6.75	6.75
Packing factor, minimum [%]	98	98	98	98	98	98
Core weight [lb]	420	420	420	420	420	420
Amp·turns per pole @ 3.1 GeV	2381	2381	2381	2381	1068	1068
Turns per pole	34	34	34	34	34	34
Pancakes per pole	1	1	1	1	1	1
Conductor dimensions [in.]	0.2×0.2	0.2×0.2	0.2×0.2	0.2×0.2	0.2×0.2	0.2×0.2
Cooling hole diameter [in.]	0.11	0.11	0.11	0.11	0.11	0.11
Conductor cross-sectional area [in.^{2}]	0.022	0.022	0.022	0.022	0.022	0.022
Conductor length/pole [ft]	124	124	124	124	124	124
Current @ 3.1 GeV [A]	70	70	70	70	31	31
Resistance @ 40°C [mΩ]	198.5	198.5	198.5	198.5	198.5	198.5
Power @ 3.1 GeV [kW]	0.97	0.97	0.97	0.97	0.20	0.20
Voltage drop @ 3.1 GeV [V]	14	14	14	14	6	6
Coil weight [lb]	50	50	50	50	50	50
Number of water circuits	4	4	4	4	4	4
Water flow rate [gpm]	0.8	0.8	0.8	0.8	0.8	0.8
Water pressure drop [psi]	150	150	150	150	150	150
Temperature rise [°C]	4.5	4.5	4.5	4.5	0.9	0.9
Total power (magnets and bus) [kW]	4.9	4.9	3.9	3.9	0.4	0.4
Total voltage (magnets and bus) [V]	70	70	56	56	12	12
Total magnet water requirements [gpm]	4.9	4.9	3.9	3.9	0.4	0.4

Table 6-3a. Positron injection line quadrupole parameters at 3.1 GeV. Coil material is copper for all magnets (continued).

Magnet designation	2Q10	1Q4	1Q4	1Q4	1Q4	1Q4
Location	Extr.	Bypass	Bypass	Match	Match	Match
Lattice designation	QA2	QFBY	QDBY	QA2	QDSL	QFSL
Number of magnets	1	22	21	1	2	2
Operating gradient @ 3.1 GeV [T/m]	2.370	2.387	2.387	5.585	5.585	5.585
Pole-tip field @ operating gradient [T]	0.061	0.031	0.031	0.072	0.072	0.072
Gradient-length product [T]	0.59	0.25	0.25	0.59	0.59	0.59
Inscribed radius [in.]	1.015	0.5075	0.5075	0.5075	0.5075	0.5075
Core length [in.]	9.34	3.92	3.92	3.92	3.92	3.92
Magnetic length [in.]	9.84	4.17	4.17	4.17	4.17	4.17
Lamination height [in.]	6.75	6.75	6.75	6.75	6.75	6.75
Lamination width [in.]	6.75	6.75	6.75	6.75	6.75	6.75
Packing factor, minimum [%]	98	98	98	98	98	98
Core weight [lb]	420	176	176	176	176	176
Amp·turns per pole @ 3.1 GeV	626	158	158	369	369	369
Turns per pole	34	34	34	34	34	34
Pancakes per pole	1	1	1	1	1	1
Conductor dimensions [in.]	0.2×0.2	0.2×0.2	0.2×0.2	0.2×0.2	0.2×0.2	0.2×0.2
Cooling hole diameter [in.]	0.11	0.11	0.11	0.11	0.11	0.11
Conductor cross-sectional area [in.^{2}]	0.022	0.022	0.022	0.022	0.022	0.022
Conductor length/pole [ft]	93	93	47	47	47	93
Current @ 3.1 GeV [A]	18	5	5	11	11	11
Resistance @ 40°C [mΩ]	198.5	149.4	149.4	149.4	149.4	149.4
Power @ 3.1 GeV [kW]	0.07	0.00	0.00	0.02	0.02	0.02
Voltage drop @ 3.1 GeV [V]	4	1	1	2	2	2
Coil weight [lb]	50	37	37	37	37	37
Number of water circuits	4	4	4	4	4	4
Water flow rate [gpm]	0.8	1.0	1.0	1.0	1.0	1.0
Water pressure drop [psi]	150	150	150	150	150	150
Temperature rise [°C]	0.3	0.0	0.0	0.1	0.1	0.1
Total power (magnets and bus) [kW]	0.07	0.1	0.1	0.02	0.04	0.04
Total voltage (magnets and bus) [V]	4	22	21	2	4	4
Total magnet water requirements [gpm]	0.1	0.1	0.1	0.0	0.0	0.0

Table 6-3a. Positron injection line quadrupole parameters at 3.1 GeV. Coil material is copper for all magnets (continued).

Magnet designation	1Q4	1Q4	1Q4	1Q4	1Q4	1Q4
Location	Match	Match	Match	Match	Match	Match
Lattice designation	QA3	QMF	QMD	QEF	QED	QD
Number of magnets	1	2	2	4	4	1
Operating gradient @ 3.1 GeV [T/m]	4.115	8.182	8.182	0.818	0.818	0.818
Pole-tip field @ operating gradient [T]	0.053	0.105	0.105	0.011	0.011	0.011
Gradient-length product [T]	0.44	0.87	0.87	0.09	0.09	0.09
Inscribed radius [in.]	0.5075	0.5075	0.5075	0.5075	0.5075	0.5075
Core length [in.]	3.92	3.92	3.92	3.92	3.92	3.92
Magnetic length [in.]	4.17	4.17	4.17	4.17	4.17	4.17
Lamination height [in.]	6.75	6.75	6.75	6.75	6.75	6.75
Lamination width [in.]	6.75	6.75	6.75	6.75	6.75	6.75
Packing factor, minimum [%]	98	98	98	98	98	98
Core weight [lb]	176	176	176	176	176	176
Amp·turns per pole @ 3.1 GeV	272	541	541	54	54	54
Turns per pole	34	34	17	17	17	34
Pancakes per pole	1	1	1	1	1	1
Conductor dimensions [in.]	0.2×0.2	0.2×0.2	0.2×0.2	0.2×0.2	0.2×0.2	0.2×0.2
Cooling hole diameter [in.]	0.11	0.11	0.11	0.11	0.11	0.11
Conductor cross-sectional area [in.^{2}]	0.022	0.022	0.022	0.022	0.022	0.022
Conductor length/pole [ft]	93	93	47	47	47	93
Current @ 3.1 GeV [A]	8	16	32	3	3	2
Resistance @ 40°C [mΩ]	149.4	149.4	74.7	74.7	74.7	149.4
Power @ 3.1 GeV [kW]	0.01	0.04	0.08	0.00	0.00	0.00
Voltage drop @ 3.1 GeV [V]	1	2	2	0	0	0
Coil weight [lb]	37	37	19	19	19	37
Number of water circuits	4	4	0	0	4	4
Water flow rate [gpm]	1.0	1.0	0	0	1.4	1.0
Water pressure drop [psi]	150	150	0	0	150	150
Temperature rise [°C]	0.0	0.1	0	0	0.0	0.0
Total power (magnets and bus) [kW]	0.01	0.1	0.2	0.03	0.03	0.0
Total voltage (magnets and bus) [V]	1	4	4	0.01	0.01	0.0
Total magnet water requirements [gpm]	0.0	0.1	0	0	0.0	0.0

Table 6-3b. Electron injection line quadrupole parameters at 9 GeV. Coil material is copper for all magnets.

Magnet designation	1Q4	2Q9	2Q9	2Q9	2Q9
Location	Bypass	Extr.	Extr.	Extr.	Extr.
Lattice designation	QB	QD	QF1	QD2	QF3
Number of magnets	32	1	1	1	1
Operating gradient @ 9 GeV [T/m]	7.889	13.193	13.988	13.252	13.156
Pole-tip field @ operating gradient [T]	0.102	0.340	0.361	0.342	0.339
Gradient-length product [T]	0.84	3.30	3.50	3.31	3.29
Inscribed radius [in.]	0.5075	1.015	1.015	1.015	1.015
Core length [in.]	3.67	8.83	8.83	8.83	8.83
Magnetic length [in.]	4.17	9.84	9.84	9.84	9.84
Lamination height [in.]	6.75	6.75	6.75	6.75	6.75
Lamination width [in.]	6.75	6.75	6.75	6.75	6.75
Packing factor, minimum [%]	98	98	98	98	98
Core weight [lb]	93	222	222	222	222
Amp-turns per pole @ 9 GeV	521	3487	3697	3502	3477
Turns per pole	34	34	34	34	34
Pancakes per pole	1	1	1	1	1
Conductor dimensions [in.]	0.2×0.2	0.2×0.2	0.2×0.2	0.2×0.2	0.2×0.2
Cooling hole diameter [in.]	0.11	0.11	0.11	0.11	0.11
Conductor cross-sectional area [in.^{2}]	0.022	0.022	0.022	0.022	0.022
Conductor length/pole [ft]	92	121	121	121	121
Current @ 9 GeV [A]	15	103	109	103	102
Resistance @ 40°C [mΩ]	147.1	193.9	193.9	193.9	193.9
Power @ 9 GeV [kW]	0.03	2.04	2.29	2.06	2.03
Voltage drop @ 9 GeV [V]	2.3	19.9	21.1	20.0	19.8
Coil weight [lb]	36.78	48.48	48.48	48.48	48.48
Number of water circuits	0	4	4	4	4
Water flow rate [gpm]	0.0	0.2	0.2	0.2	0.2
Water pressure drop [psi]	0	150	150	150	150
Temperature rise [°C]	0.0	9.3	10.4	9.3	9.2
Total power (magnets and bus) [kW]	1.0	2.0	2.3	2.1	2.0
Total voltage (magnets and bus) [V]	73.6	19.9	21.1	20.0	19.8
Total magnet water requirements [gpm]	0	0.84	0.84	0.84	0.84

Table 6-3b. Electron injection line quadrupole parameters at 9 GeV. Coil material is copper for all magnets (continued).

Magnet designation	2Q9	2Q9	2Q9	2Q9	2Q9
Location	Extr.	Extr.	Extr.	Extr.	Extr.
Lattice designation	QD4	QF1	QD2	QF3	QD4
Number of magnets	1	1	1	1	1
Operating gradient @ 9 GeV [T/m]	13.304	12.396	13.132	13.228	13.080
Pole-tip field @ operating gradient [T]	0.343	0.320	0.339	0.341	0.337
Gradient-length product [T]	3.33	3.10	3.28	3.31	3.27
Inscribed radius [in.]	1.015	1.015	1.015	1.015	1.015
Core length [in.]	8.83	8.83	8.83	8.83	8.83
Magnetic length [in.]	9.84	9.84	9.84	9.84	9.84
Lamination height [in.]	6.75	6.75	6.75	6.75	6.75
Lamination width [in.]	6.75	6.75	6.75	6.75	6.75
Packing factor, minimum [%]	98	98	98	98	98
Core weight [lb]	222	222	222	222	222
Amp·turns per pole @ 9 GeV	3516	3276	3471	3496	3457
Turns per pole	34	34	34	34	34
Pancakes per pole	1	1	1	1	1
Conductor dimensions [in.]	0.2×0.2	0.2×0.2	0.2×0.2	0.2×0.2	0.2×0.2
Cooling hole diameter [in.]	0.11	0.11	0.11	0.11	0.11
Conductor cross-sectional area [in.^{2}]	0.022	0.022	0.022	0.022	0.022
Conductor length/pole [ft]	121	121	121	121	121
Current @ 9 GeV [A]	103	96	102	103	102
Resistance @ 40°C [mΩ]	193.9	193.9	193.9	193.9	193.9
Power @ 9 GeV [kW]	2.07	1.80	2.02	2.05	2.00
Voltage drop @ 9 GeV [V]	20.1	18.7	19.8	19.9	19.7
Coil weight [lb]	48.48	48.48	48.48	48.48.	48.48
Number of water circuits	4	4	4	4	4
Water flow rate [gpm]	0.2	0.2	0.2	0.2	0.2
Water pressure drop [psi]	150	150	150	150	150
Temperature rise [°C]	9.4	8.2	9.2	9.3	9.1
Total power (magnets and bus) [kW]	2.1	1.8	2.0	2.1	2.0
Total voltage (magnets and bus) [V]	20.1	18.7	19.8	19.9	19.7
Total magnet water requirements [gpm]	0.84	0.84	0.84	0.84	0.84

Table 6-3b. Electron injection line quadrupole parameters at 9 GeV. Coil material is copper for all magnets (continued).

Magnet designation	1Q6	1Q6	1Q6	1Q6	1Q6
Location	Extr.	Extr.	Extr.	Extr.	Extr.
Lattice designation	QF	QALF	QDM	QFM	QDYB
Number of magnets	1	1	3	2	1
Operating gradient @ 9 GeV [T/m]	19.631	21.798	5.648	5.648	7.888
Pole-tip field @ operating gradient [T]	0.253	0.281	0.073	0.073	0.102
Gradient-length product [T]	3.30	3.66	1.41	1.41	1.97
Inscribed radius [in.]	0.5075	0.5075	0.5075	0.5075	0.5075
Core length [in.]	6.11	6.11	9.34	9.34	9.34
Magnetic length [in.]	6.61	6.61	9.84	9.84	9.84
Lamination height [in.]	6.75	6.75	6.75	6.75	6.75
Lamination width [in.]	6.75	6.75	6.75	6.75	6.75
Packing factor, minimum [%]	98	98	98	98	98
Core weight [lb]	154	154	234	234	234
Amp-turns per pole @ 9 GeV	1297	1440	373	373	521
Turns per pole	34	34	34	34	34
Pancakes per pole	1	1	1	1	1
Conductor dimensions [in.]	0.2×0.2	0.2×0.2	0.2×0.2	0.2×0.2	0.2×0.2
Cooling hole diameter [in.]	0.11	0.11	0.11	0.11	0.11
Conductor cross-sectional area [in.^{2}]	0.022	0.022	0.022	0.022	0.022
Conductor length/pole [ft]	106	106	124	124	124
Current @ 9 GeV [A]	38	42	11	11	15
Resistance @ 40°C [mΩ]	169.2	169.2	198.5	198.5	198.5
Power @ 9 GeV [kW]	0.25	0.30	0.02	0.02	0.05
Voltage drop @ 9 GeV [V]	6.5	7.2	2.2	2.2	3.0
Coil weight [lb]	42.31	42.31	49.63	49.63	49.63
Number of water circuits	4	4	4	4	4
Water flow rate [gpm]	0.2	0.2	0.2	0.2	0.2
Water pressure drop [psi]	150	150	150	150	150
Temperature rise [°C]	1.0	1.3	0.1	0.1	0.2
Total power (magnets and bus) [kW]	0.25	0.30	0.06	0.04	0.05
Total voltage (magnets and bus) [V]	6.5	7.2	6.6	4.4	3.0
Total magnet water requirements [gpm]	0.90	0.90	0.83	0.83	0.83

Table 6-3b. Electron injection line quadrupole parameters at 9 GeV. Coil material is copper for all magnets (continued).

Magnet designation	1Q6	1Q6	1Q6	1Q6	1Q9
Location	Extr.	Match	Match	Match	Match
Lattice designation	QFB1	QDSL	QFSL	QA2	QFM
Number of magnets	1	2	2	1	1
Operating gradient @ 9 GeV [T/m]	12.232	11.862	11.862	80.437	105.215
Pole-tip field @ operating gradient [T]	0.158	0.153	0.153	1.037	1.356
Gradient-length product [T]	2.06	1.99	1.99	13.51	26.30
Inscribed radius [in.]	0.5075	0.5075	0.5075	0.5075	0.5075
Core length [in.]	6.11	6.11	6.11	6.11	9.34
Magnetic length [in.]	6.61	6.61	6.61	6.61	9.84
Lamination height [in.]	6.75	6.75	6.75	6.75	6.75
Lamination width [in.]	6.75	6.75	6.75	6.75	6.75
Packing factor, minimum [%]	98	98	98	98	98
Core weight [lb]	154	154	154	154	234
Amp·turns per pole @ 9 GeV	808	784	784	5315	6952
Turns per pole	34	34	34	34	34
Pancakes per pole	1	1	1	1	1
Conductor dimensions [in.]	0.2×0.2	0.2×0.2	0.2×0.2	0.2×0.2	0.2×0.2
Cooling hole diameter [in.]	0.11	0.11	0.11	0.11	0.11
Conductor cross-sectional area [in.^{2}]	0.022	0.022	0.022	0.022	0.022
Conductor length/pole [ft]	106	106	106	106	124
Current @ 9 GeV [A]	24	23	23	156	204
Resistance @ 40°C [mΩ]	169.2	169.2	169.2	169.2	198.5
Power @ 9 GeV [kW]	0.10	0.09	0.09	4.14	8.30
Voltage drop @ 9 GeV [V]	4.0	3.9	3.9	26.5	40.6
Coil weight [lb]	42.31	42.31	42.31	42.31	49.63
Number of water circuits	4	4	4	4	4
Water flow rate [gpm]	0.2	0.2	0.2	0.2	0.2
Water pressure drop [psi]	150	150	150	150	150
Temperature rise [°C]	0.4	0.4	0.4	17.4	38.2
Total power (magnets and bus) [kW]	0.1	0.2	0.2	4.1	8.3
Total voltage (magnets and bus) [V]	4.0	7.8	7.8	26.5	40.6
Total magnet water requirements [gpm]	0.90	0.90	0.90	0.90	0.83

Table 6-3b. Electron injection line quadrupole parameters at 9 GeV. Coil material is copper for all magnets (continued).

Magnet designation	1Q20	1Q20	1Q20	1Q20
Location	Match	Match	Match	Match
Lattice designation	DEF	QED	QD	Q1
Number of magnets	5	5	1	1
Operating gradient @ 9 GeV [T/m]	4.852	4.852	4.852	5.391
Pole-tip field @ operating gradient [T]	0.063	0.063	0.063	0.069
Gradient-length product [T]	2.51	2.51	2.51	2.79
Inscribed radius [in.]	0.5075	0.5075	0.5075	0.5075
Core length [in.]	19.85	19.85	19.85	19.85
Magnetic length [in.]	20.35	20.35	20.35	20.35
Lamination height [in.]	6.75	6.75	6.75	6.75
Lamination width [in.]	6.75	6.75	6.75	6.75
Packing factor, minimum [%]	98	98	98	98
Core weight [lb]	497	497	497	497
Amp·turns per pole @ 9 GeV	321	321	321	356
Turns per pole	34	34	34	34
Pancakes per pole	1	1	1	1
Conductor dimensions [in.]	0.2×0.2	0.2×0.2	0.2×0.2	0.2×0.2
Cooling hole diameter [in.]	0.11	0.11	0.11	0.11
Conductor cross-sectional area [in.^{2}]	0.022	0.022	0.022	0.022
Conductor length/pole [ft]	184	184	184	184
Current @ 9 GeV [A]	9	9	9	10
Resistance @ 40°C [mΩ]	294	294	294	294
Power @ 9 GeV [kW]	0.03	0.03	0.03	0.03
Voltage drop @ 9 GeV [V]	2.8	2.8	2.8	3.1
Coil weight [lb]	73.46	73.46	73.46	73.46
Number of water circuits	4	4	4	4
Water flow rate [gpm]	0.2	0.2	0.2	0.2
Water pressure drop [psi]	150	150	150	150
Temperature rise [°C]	0.1	0.1	0.1	0.2
Total power (magnets and bus) [kW]	0.15	0.15	0.03	0.03
Total voltage (magnets and bus) [V]	14.0	14.0	2.8	3.1
Total magnet water requirements [gpm]	0.67	0.67	0.67	0.67

additional dipoles are placed downstream to increase the flexibility to match the desired geometry. The dispersion and bending angle from each of these dipoles are exactly canceled by placing a corresponding dipole, bending in the opposite direction, at its image point (four cells downstream in the 90° lattice). This extraction line lattice continues for approximately two sectors (203 m), beyond which a matching region with four quadrupoles will match the optics into the electron bypass line.

The electron bypass is optically the same as that for positrons (see Section 6.2.4) but will operate at a higher energy (9 GeV). The connections of the bypass lines to the NIT and SIT lines will be accomplished by using a general and flexible method (see Section 6-3).

6.3 UPGRADE OF THE NIT AND SIT BEAMLINES

The NIT and SIT beamlines were used to transport electrons and positrons, respectively, between the linac and the PEP ring. A schematic layout of both lines, including currently available instrumentation, is shown in Fig. 6-11. Except for a few minor modifications at the entrance and exit, the optics and geometry of these lines will not be changed. Each line is made up of three achromats comprising four cells with a phase advance of 90° per cell. Thus, the optical transfer matrix between any two points separated by a path length difference equal to the length of two cells is the negative of the identity matrix. This attribute of the achromats has been used extensively in the design of these beamlines to locate magnets and to roll whole sections in order to provide needed vertical deflections while simultaneously controlling the dispersion.

As an example, the dispersion induced by the first group of bending magnets, B1, B2, and B3, is canceled by the two dipoles B4 and B5. More subtle is the fact that dispersion induced by the vertically bending pulsed magnets 40PM1 and 40PM2 and the vertical magnet BVA is canceled by rolling the two downstream magnets. Therefore, it would be difficult to change any one region in these beamlines without significantly affecting the geometry and optics elsewhere. Because of this close coupling of optical and geometric parameters, it was decided to establish a matching point early in the beamline, beyond which all optical and geometrical parameters would remain fixed (that is, only upstream modifications would be allowed).

There are 14 such parameters in all: 8 optical parameters (β_x, β_y, α_x, α_y, D_x, D_y, D'_x, and D'_y) and 6 geometric parameters (X, Y, Z coordinates, the polar and azimuthal direction angles, and the roll angle of the curvilinear beam coordinate system). A workable solution for matching the bypass lines to the NIT and SIT lines has been found using a general method with great flexibility. The procedure is as follows:

- Extend the NIT or SIT optical lattice upstream as far as necessary (at least four cells); this continuation ensures an easy matching of the beta functions, once the geometry and dispersion are controlled by other means
- Modify the bending arrangement to obtain the desired geometry
- Add bending magnet configurations (some similar to the chicane described in Section 6.2.2) that allow independent adjustment of the dispersion while maintaining a desirable geometry

additional dipoles are placed downstream to increase the flexibility to match the desired geometry. The dispersion and bending angle from each of these dipoles are exactly canceled by placing a corresponding dipole, bending in the opposite direction, at its image point (four cells downstream in the 90° lattice). This extraction line lattice continues for approximately two sectors (203 m), beyond which a matching region with four quadrupoles will match the optics into the electron bypass line.

The electron bypass is optically the same as that for positrons (see Section 6.2.4) but will operate at a higher energy (9 GeV). The connections of the bypass lines to the NIT and SIT lines will be accomplished by using a general and flexible method (see Section 6-3).

6.3 UPGRADE OF THE NIT AND SIT BEAMLINES

The NIT and SIT beamlines were used to transport electrons and positrons, respectively, between the linac and the PEP ring. A schematic layout of both lines, including currently available instrumentation, is shown in Fig. 6-11. Except for a few minor modifications at the entrance and exit, the optics and geometry of these lines will not be changed. Each line is made up of three achromats comprising four cells with a phase advance of 90° per cell. Thus, the optical transfer matrix between any two points separated by a path length difference equal to the length of two cells is the negative of the identity matrix. This attribute of the achromats has been used extensively in the design of these beamlines to locate magnets and to roll whole sections in order to provide needed vertical deflections while simultaneously controlling the dispersion.

As an example, the dispersion induced by the first group of bending magnets, B1, B2, and B3, is canceled by the two dipoles B4 and B5. More subtle is the fact that dispersion induced by the vertically bending pulsed magnets 40PM1 and 40PM2 and the vertical magnet BVA is canceled by rolling the two downstream magnets. Therefore, it would be difficult to change any one region in these beamlines without significantly affecting the geometry and optics elsewhere. Because of this close coupling of optical and geometric parameters, it was decided to establish a matching point early in the beamline, beyond which all optical and geometrical parameters would remain fixed (that is, only upstream modifications would be allowed).

There are 14 such parameters in all: 8 optical parameters (β_x, β_y, α_x, α_y, D_x, D_y, D'_x, and D'_y) and 6 geometric parameters (X, Y, Z coordinates, the polar and azimuthal direction angles, and the roll angle of the curvilinear beam coordinate system). A workable solution for matching the bypass lines to the NIT and SIT lines has been found using a general method with great flexibility. The procedure is as follows:

- Extend the NIT or SIT optical lattice upstream as far as necessary (at least four cells); this continuation ensures an easy matching of the beta functions, once the geometry and dispersion are controlled by other means
- Modify the bending arrangement to obtain the desired geometry
- Add bending magnet configurations (some similar to the chicane described in Section 6.2.2) that allow independent adjustment of the dispersion while maintaining a desirable geometry

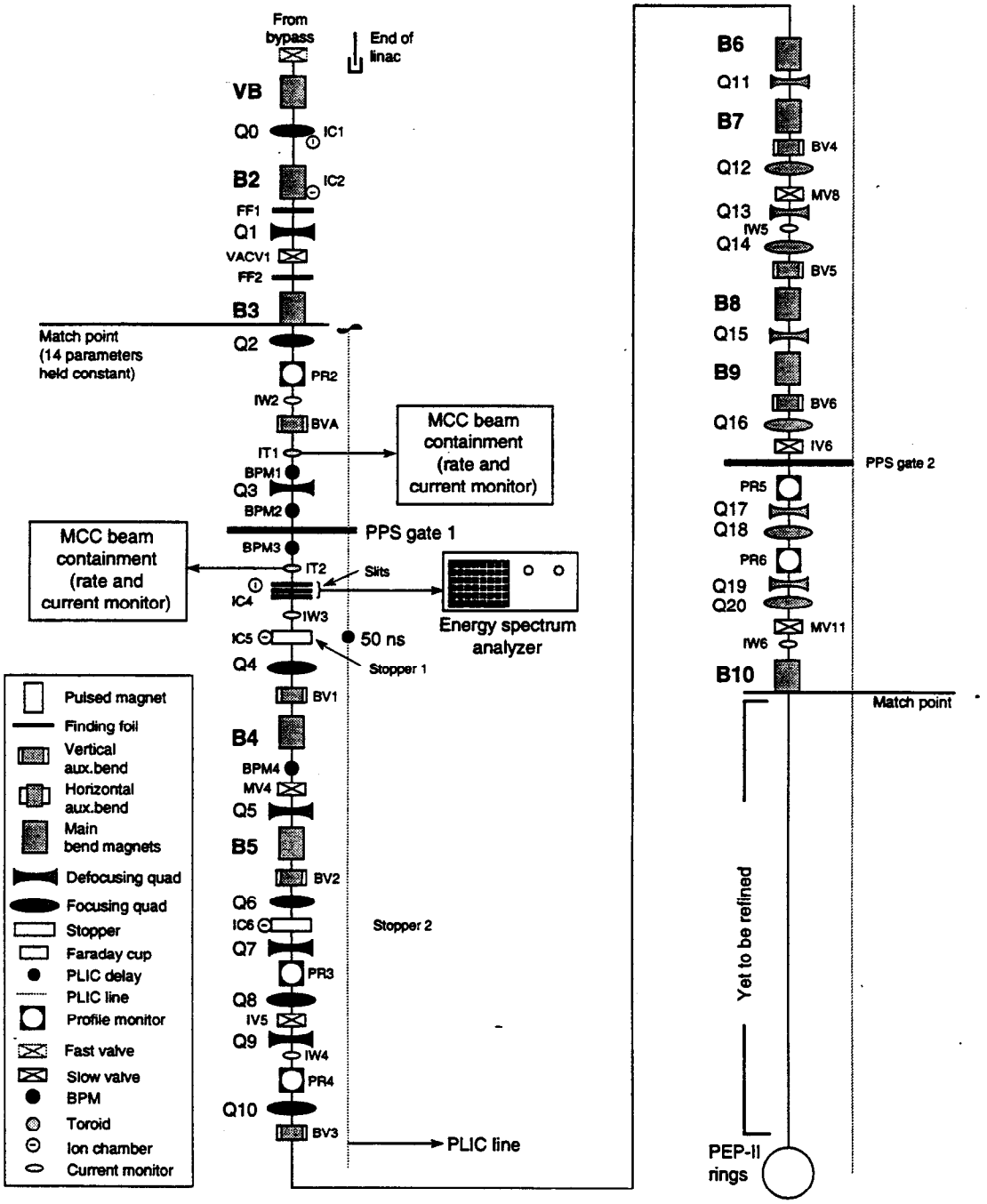

Fig. 6-11. Schematic layout of the identical NIT and SIT lines.

As described below, we have applied this method to optically connect the bypass lines to the NIT and SIT lines; the resulting solutions are shown in Fig. 6-12.

In the existing NIT and SIT beamlines, the separation of the electrons and positrons at the end of the linac is initiated by two vertically bending pulsed magnets that direct either beam into a downstream Lambertson septum dipole, B1. In this magnet, the beams are

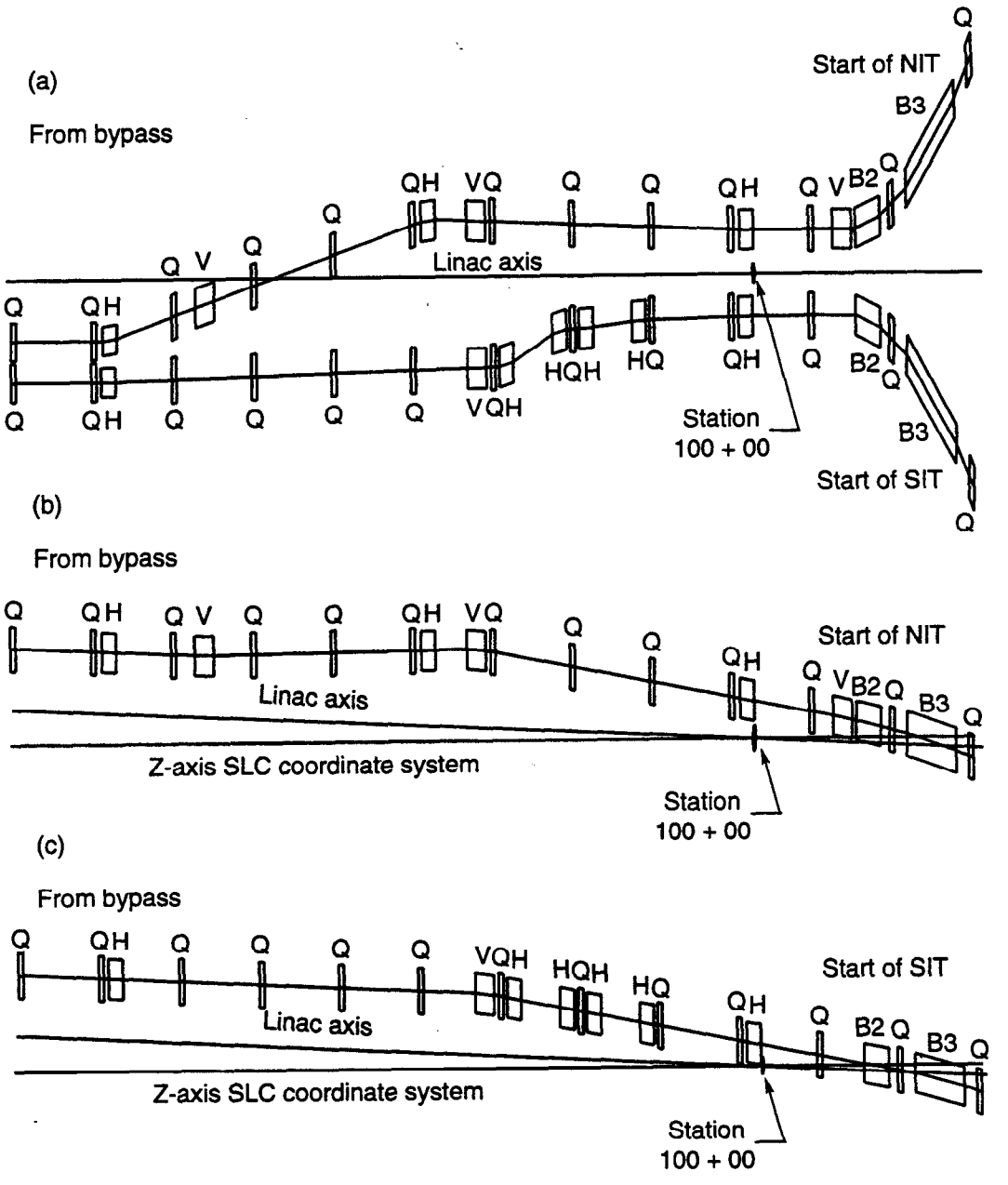

Fig. 6-12. Plan (a) and elevation (b, c) views of interfaces between the electron and positron bypass lines and the NIT and SIT lines, respectively. Vertically bending magnets are denoted with a V, and horizontally bending magnets are denoted with an H.

bent in opposite directions by 3.75° each. The two beamlines downstream of B1 are now independent; they are designed to be identical and are simply mirror images reflected about the linac axis. Two more bending magnets, B2 and B3, complete the horizontal deflection in this region, the first bending the beam by 3.75° and the second by 7.5°.

For the PEP-II injection optics, the downstream end of the B4 magnet was chosen as the matching point at which to hold fixed the 14 optical and geometric parameters while the geometry and optics upstream were changed (see Fig. 6-11). The first modifications were to increase the bend angle of B3 from 7.5° to 9° and to increase the bend angle of B2 from 3.75° to 6°. Thus, the total bend of 15° was maintained while eliminating magnet B1. These modifications resulted in a horizontal displacement of the input beam axis (still parallel to the linac axis) by 47 cm at the end of the linac; this is shown in Fig. 6-12.

Next, the matching of the geometry and dispersion in the vertical plane are accomplished by utilizing small vertical bending magnet pairs having opposite strengths and placed four cells apart (that is, imaged by the optical identity). The strength of these magnets is adjusted to match the vertical height and direction of the positron bypass, thus connecting the beamlines and completing the geometrical match in the vertical plane. The vertical dispersion caused by these magnets nearly cancels because of their optical placement, but there remains a residual vertical dispersion that must be controlled to obtain the correct values of D_y and D_y' (both nonzero) at the matching point. This was accomplished by simultaneously rolling the magnet B4 (which changes vertical geometry and couples horizontal and vertical dispersion) and adjusting the strength of one additional small magnet to complete the vertical geometry and dispersion matching.

The same approach is applied to the horizontal plane but with added flexibility to match dispersion and geometry beyond that provided simply by using matched pairs of magnets. When the geometrical match is completed using only paired magnets, there remains residual dispersion to correct. This is done utilizing several differing configurations that can either change dispersion without changing the overall geometry (that is, the input and output are made coaxial) or offset the beam (that is, the input and output are made parallel but not coaxial), allowing an additional freedom of choice in the optimization of dispersion and geometry. For example:

- Use of four bending magnets in a chicane, placed symmetrically about a quadrupole. This will introduce dispersion and will have coaxial input and output beams. Two such chicanes, placed 90° apart in phase advance, provide control over the dispersion and its derivative.
- Use of two bending magnets of equal and opposite strength, placed either in a drift or at any two points in the lattice that are not separated by the negative identity matrix. This will introduce dispersion and simultaneously introduce a parallel offset.

Either of these two schemes can be used to adjust the geometry and dispersion without affecting the beta function matching. An example of one such configuration, which connects the electron and positron bypass lines to the NIT and SIT beamlines, is shown in Fig. 6-12.

With the geometry and dispersion matching between the bypass lines and NIT and SIT completed, it becomes a simple task to introduce a short optical section (consisting only of quadrupoles) to match the beta functions of the two lines.

Figures 6-13 and 6-14 show the optics for the completed positron and electron transport lines (including SIT and NIT), respectively, starting at the point where the beam from the damping ring is injected into Sector 2 of the linac and terminating at a point in the PEP tunnel near where the beam will be injected into its appropriate ring. In this optics calculation, the positron beam starts with an energy of 1.21 GeV (the design energy for the damping ring), is accelerated to 3.1 GeV in Sector 2, coasts through Sector 3 at constant energy, and is extracted at Sector 4. The electron beam also starts at 1.21 GeV but is accelerated to 9 GeV in Sectors 2–7 and extracted at Sector 8. The positron (electron) bypass line has 22 (18) cells and has been matched to the SIT (NIT) beamline as described above. The final segments of these beamlines, which will match to the parameters required for injection into the rings, are under design and will be completed soon. Because our design approach is quite flexible, it will easily accommodate any required engineering changes.

6.3.1 Coordinate System for the Injection Transport Lines

Before building the PEP-II injection lines, it is necessary to establish their coordinates and dimensions in the real world. The injection lines are longer than 3 km and undergo many elevation changes along their lengths. Furthermore, the lines cross the boundaries of regions where local coordinate systems and fiducial monuments have been previously defined and surveyed. Thus, three differing coordinate systems are needed for defining the positions of beamline components for installation and alignment purposes. The transformations required to ensure continuity across the regional boundaries are already well understood, though they will continue to be refined in surveys by the SLAC alignment group.

All work on the optical design of the injection lines has included the coordinates of components in their appropriate coordinate system; these have been checked for consistency at regional boundaries, as well as being checked with previous specifications (as with the NIT and SIT beamlines). Before describing these coordinate systems in detail, we note here that they are defined (and used in the optical codes) as right-handed coordinate systems. These same coordinate systems are often converted to left-handed systems by the SLAC alignment group. Fortunately, this conversion requires only a sign change of the X coordinate so this should not be a cause for confusion.

The three coordinate systems are depicted in Fig. 6-15, along with sufficient information to define all of the required coordinate transformations. The first coordinate system, that used in the linac housing, has as its origin the linac injector. The Z-axis for the linac coordinate system is along the linac central axis. This axis and the local gravity vector at the injector define a plane that is used to define the other two orthogonal directions. The X-axis is perpendicular to this plane, pointing north, and the Y-axis lies within this plane pointing upward (note that since the linac is sloped, the Y-axis is *not* along the local gravity vector). In this coordinate system, the coordinates (in meters) of the end of Sector n is given by (0, 0, 101.6n), so that the end of the last sector (Sector 30)

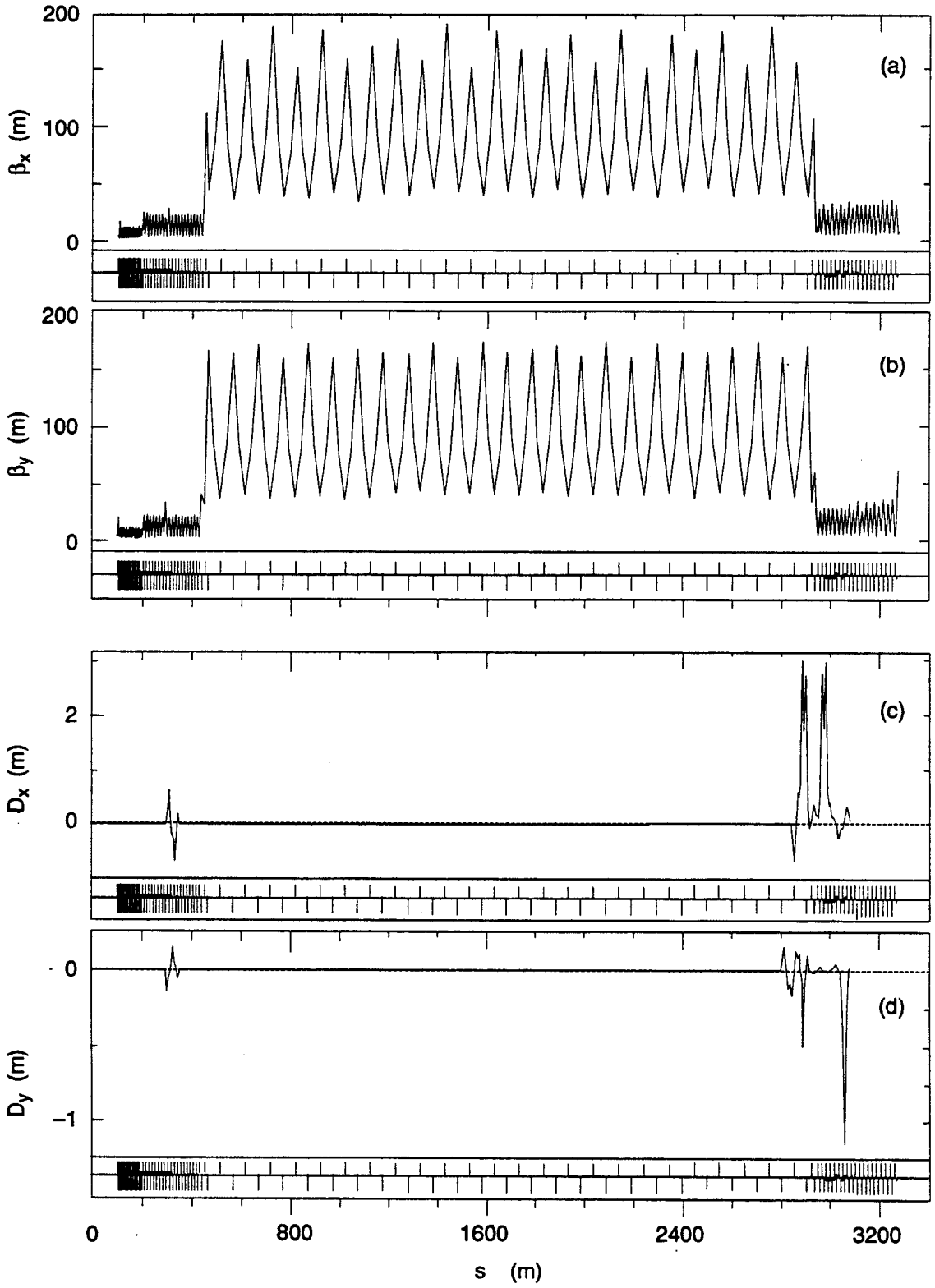

Fig. 6-13. Optics for the complete positron transport line.

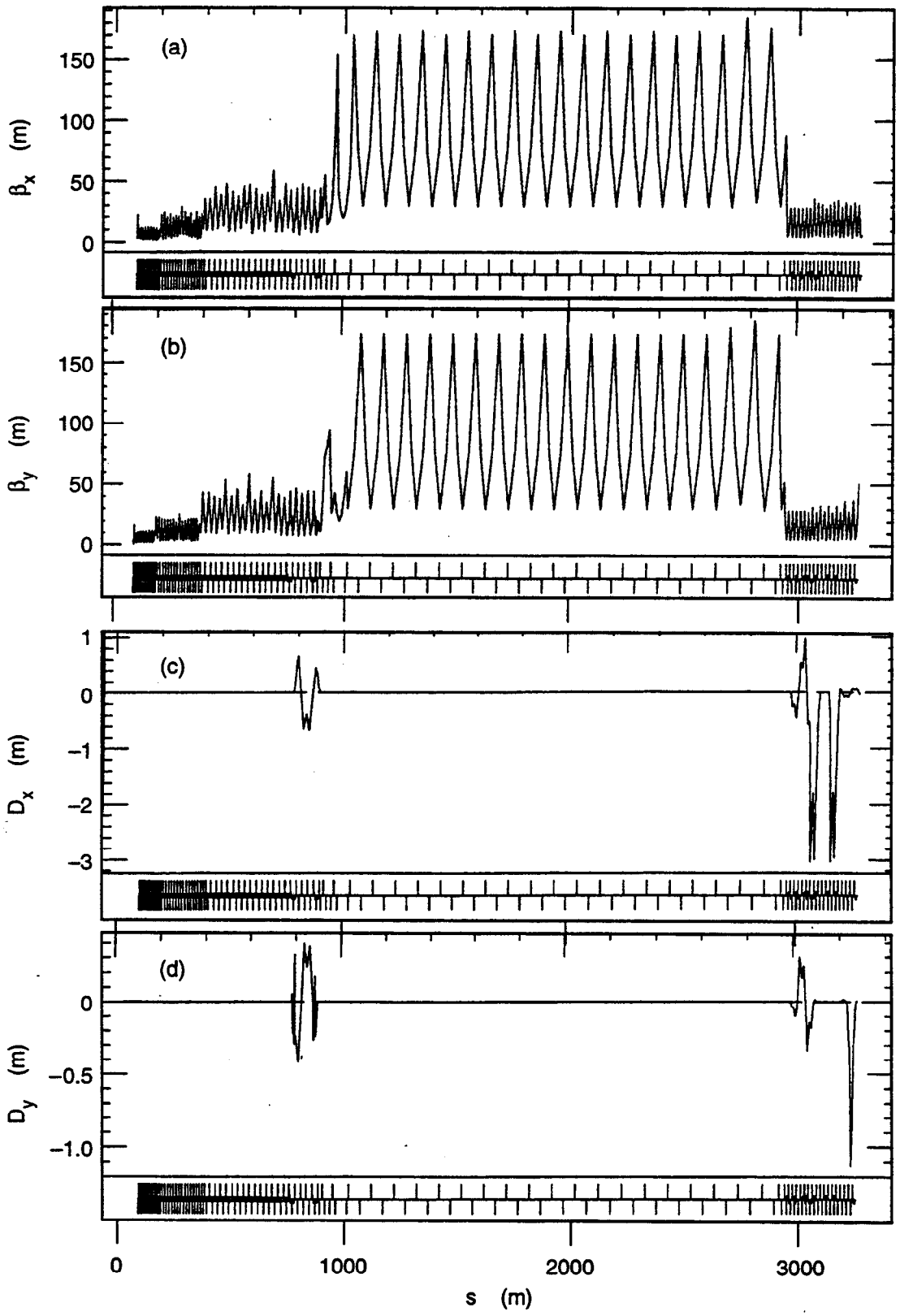

Fig. 6-14. Optics for the complete electron transport line.

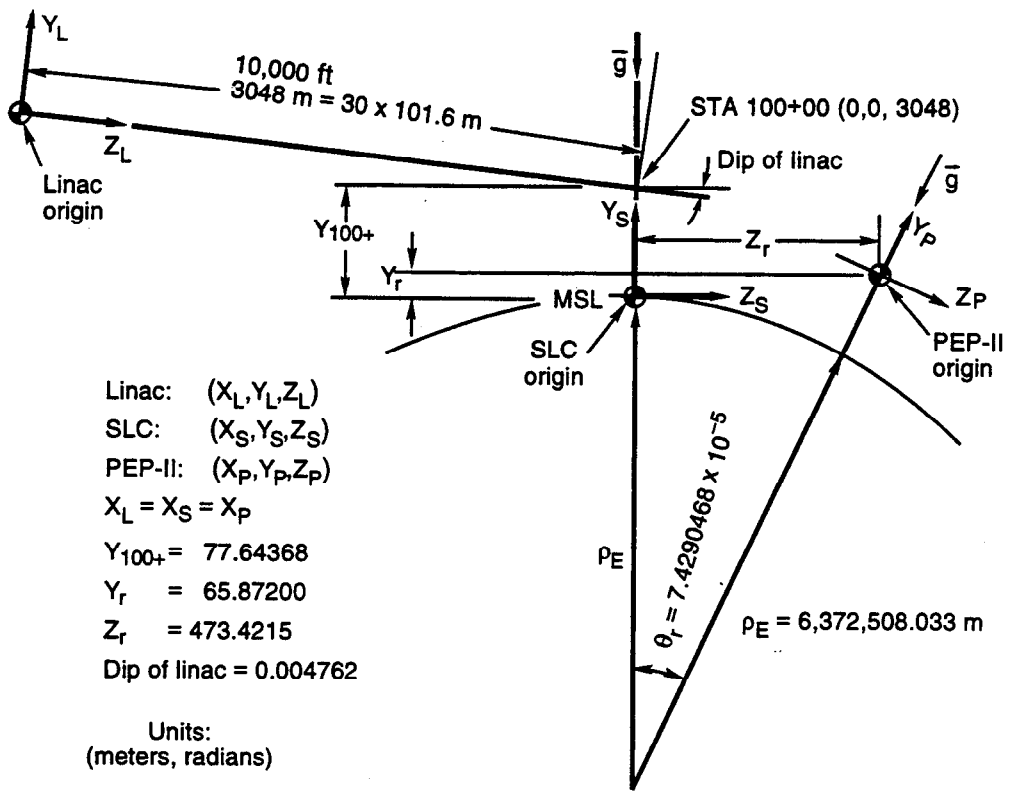

Fig. 6-15. Relationship among the various PEP-II coordinate systems. The coordinates Y_r, Z_r, and θ_r give the origin of the PEP-II coordinate system in the SLC coordinate system.

occurs at (0, 0, 3048), or exactly 10,000 feet from the origin. This point has been given a special name and is called "STA(tion) 100+ 00." We note it here because it leads us directly to the definition of the next coordinate system, which is the "SLC coordinate system."

The origin of the SLC coordinate system is at mean sea level (MSL), and its positive *Y*-axis is antiparallel to the local gravity vector and passes through the point on the linac axis denoted STA 100+ 00. The *Z*-axis of this coordinate system is perpendicular to the local gravity vector and is coplanar with this vector and those vectors defining the *Y*- and *Z*-axes for the linac coordinate system. Thus, we see that the *X* coordinate of a point in the SLC coordinate system has the same value as its *X* coordinate in the linac coordinate system. This turns out also to be true for the remaining coordinate system, the "PEP-II coordinate system," as the origins of all three of these systems are in a common vertical plane (that is, the plane of the paper in Fig. 6-15). The SLC coordinate system will be used for the alignment of the NIT and SIT beamlines.

The PEP-II coordinate system, which will be used for defining the locations of the ring components and the nearby components of the injection lines, has as its origin the center of the PEP-II HER. Its positive *Y*-axis is again antiparallel to the local gravity vector, and this vector, along with the orthogonal *Z*-axis, are coplanar with the linac axis

and the *Y*-axes of the other two coordinate systems. Information defining the translation and rotation transformation between this system and the other two is provided in Fig. 6-15. We note here that during alignment of the ring, it will be necessary to apply a correction to allow for the variation with ring azimuth of the difference between the *Y*-axis and the gravity vector at the ring perimeter. Furthermore, we note that the current computer model of the SIT beamline in this coordinate system has successfully reproduced alignment data for optical components that was last published in 1978.

6.4 FEEDBACK AND DIAGNOSTIC DEVICES

The PEP-II injection system must operate with very high reliability. To achieve this, diagnostic devices are needed to characterize and tune the beam so that filling of the rings can proceed efficiently. In addition, a fast feedback system is required to ensure that the injection system can be run in a routine fashion. Both the hardware and the software necessary to implement such a feedback system are therefore necessary.

Clearly, the injection transport lines will operate at maximum efficiency when the beams are of a specific energy for the rings, are of a specific size and shape, are injected at a specific location and angle, have the minimum possible energy spread, and do not suffer any unwanted losses. Hence, we must provide the hardware to measure the energy, phase-space distribution, trajectory, and energy spread, and to localize and measure beam losses. Considerable experience with the necessary devices has been gained during the operation of the SLC. That experience gives us high confidence that the PEP-II injection system is well matched to the hardware capability.

A generalized, database-driven fast feedback system has already been developed for the SLC [Rouse et al., 1991; Hendrickson et al., 1991; Rouse et al., 1992]. The system is designed to facilitate the implementation of new feedback loops. The hardware necessary to operate a particular fast feedback loop comprises only a distributed set of microprocessors and a communication link between them, as shown in Fig. 6-16. We intend to directly use the software and hardware already developed by the SLC in the PEP-II injection system. The following subsections will detail our specifications for the system. All of the comments should be interpreted to apply to both transverse planes of both the electron and positron transport lines.

6.4.1 Diagnostic Devices

In simplest terms, our diagnostic system must be able to measure beam positions, angles, and intensities, beam shape, beam energy and energy spread, and beam losses. We need the positions and angles to determine the beam trajectory. We must measure the trajectory reasonably precisely in order to steer the beam, determine its energy, and match it to the PEP-II rings. We need to determine the shape of the beam to ensure that we understand its phase-space area. (The transport lattice will operate at peak efficiency only over a limited range of beam energy and emittance values.) Finally, we must be able to localize beam losses to determine where we must resteer the beams.

and the *Y*-axes of the other two coordinate systems. Information defining the translation and rotation transformation between this system and the other two is provided in Fig. 6-15. We note here that during alignment of the ring, it will be necessary to apply a correction to allow for the variation with ring azimuth of the difference between the *Y*-axis and the gravity vector at the ring perimeter. Furthermore, we note that the current computer model of the SIT beamline in this coordinate system has successfully reproduced alignment data for optical components that was last published in 1978.

6.4 FEEDBACK AND DIAGNOSTIC DEVICES

The PEP-II injection system must operate with very high reliability. To achieve this, diagnostic devices are needed to characterize and tune the beam so that filling of the rings can proceed efficiently. In addition, a fast feedback system is required to ensure that the injection system can be run in a routine fashion. Both the hardware and the software necessary to implement such a feedback system are therefore necessary.

Clearly, the injection transport lines will operate at maximum efficiency when the beams are of a specific energy for the rings, are of a specific size and shape, are injected at a specific location and angle, have the minimum possible energy spread, and do not suffer any unwanted losses. Hence, we must provide the hardware to measure the energy, phase-space distribution, trajectory, and energy spread, and to localize and measure beam losses. Considerable experience with the necessary devices has been gained during the operation of the SLC. That experience gives us high confidence that the PEP-II injection system is well matched to the hardware capability.

A generalized, database-driven fast feedback system has already been developed for the SLC [Rouse et al., 1991; Hendrickson et al., 1991; Rouse et al., 1992]. The system is designed to facilitate the implementation of new feedback loops. The hardware necessary to operate a particular fast feedback loop comprises only a distributed set of microprocessors and a communication link between them, as shown in Fig. 6-16. We intend to directly use the software and hardware already developed by the SLC in the PEP-II injection system. The following subsections will detail our specifications for the system. All of the comments should be interpreted to apply to both transverse planes of both the electron and positron transport lines.

6.4.1 Diagnostic Devices

In simplest terms, our diagnostic system must be able to measure beam positions, angles, and intensities, beam shape, beam energy and energy spread, and beam losses. We need the positions and angles to determine the beam trajectory. We must measure the trajectory reasonably precisely in order to steer the beam, determine its energy, and match it to the PEP-II rings. We need to determine the shape of the beam to ensure that we understand its phase-space area. (The transport lattice will operate at peak efficiency only over a limited range of beam energy and emittance values.) Finally, we must be able to localize beam losses to determine where we must resteer the beams.

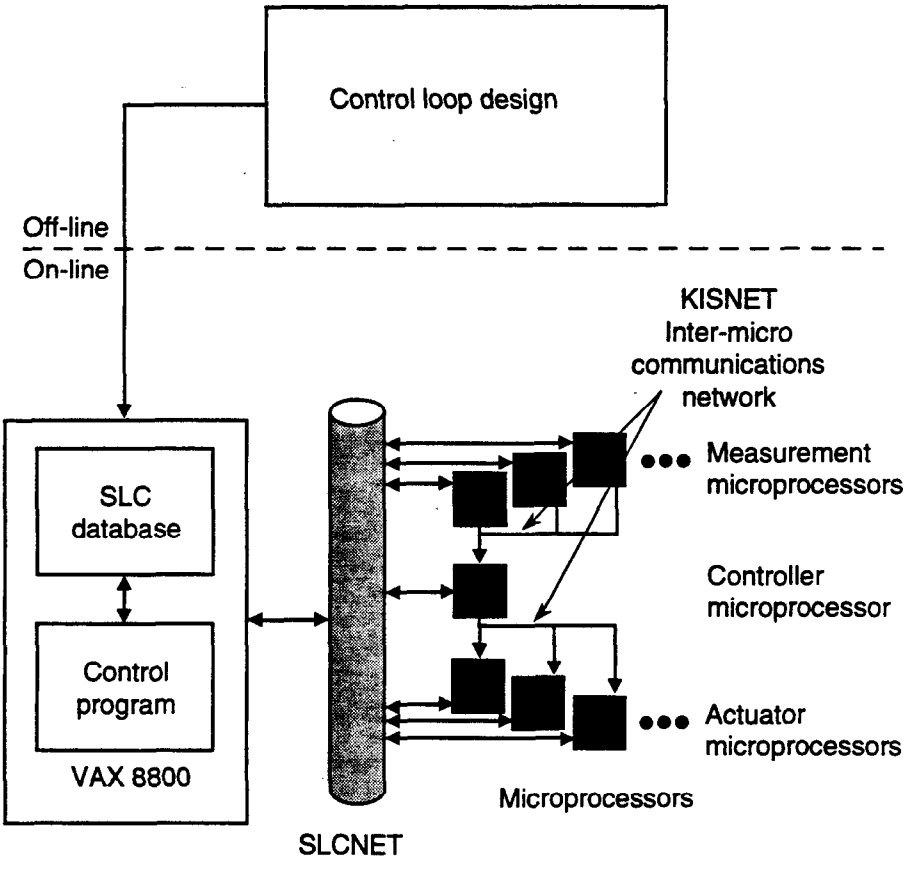

Fig. 6-16. Necessary hardware to implement a fast feedback loop for the injection system.

6.4.1.1 Injection Line BPMs. We will use BPMs to characterize the beam trajectory. Each quadrupole in the extraction, transport, and NIT/SIT parts of the injection line will have an x-y BPM (though only the two x strips or the two y strips will be connected to cables, depending on the quadrupole type—QFs having x readouts, QDs having y readouts). Near the ring injection point, we are dealing with devices (the kicker magnets and septum) that are best calibrated by use of the beam itself. Hence, we propose to add extra BPMs at this crucial location. A pair of BPMs will bracket each kicker magnet in the ring and three BPMs will be added in the region of the septum magnets. The BPMs may be either linac-style or FFTB-style devices. The electrodes will be slightly recessed in the beam pipe wall and will be rotated to be in the x and y directions, as only one plane will be read out for each quadrupole to reduce cabling and processing electronics costs.

BPM Electronics and Cabling. Where possible, a pair of cables will be run from each PEP-II injection line BPM to a nearby linac BPM. The cables will be coupled into the cables of the linac BPMs with 10-dB-loss couplers. To keep signals from the x and y plates the same relative size, four couplers must be installed together on any linac BPM. Thus, two injection BPMs can be connected to each linac BPM used. (This multiplexing

into existing cables and electronics has already been done successfully in the PRL.) An important restriction of this scheme is that, during one linac pulse, the BPM electronics module timing can only be set to look at one of the BPMs connected to its input. Care must also be taken to ensure that BPM pulses from the injection line positrons and linac scavenger electrons do not arrive too close together in time at the BPM electronics module. This time separation can be increased by always connecting the injection line BPMs to upstream linac BPMs.

In a similar fashion, the BPMs in the upstream NIT line will be multiplexed with those in the upstream SIT line, as the cables come back to the same service building. The downstream NIT BPMs, along with any used in the HER injection straight section, will come up in the IR-10 service building. It will not be possible to multiplex these with the downstream SIT and the LER injection BPMs, because these latter cables appear in the service building at IR-8.

For injection into the PEP-II rings, the smallest injected pulse is expected to contain 1/20 (~2×10^9 particles) of a full storage ring bunch (3–6×10^{10} particles). In the linac at present, the sum of the four strips in a 2.5-cm-diameter × 10-cm-long BPM can detect a minimum bunch intensity of 2×10^9 particles. We will design the BPMs to have an operating range of 0.1–3×10^{10} particles (that is, the modules will have a dynamic range of 30:1). This is a factor of two increase in sensitivity compared with the BPMs of the linac (for which a bunch with lower charge will not reliably trigger the linac BPM module to convert). Because the 10-dB-loss coupler will introduce a factor of 3.2 loss in pulse height for the injection BPMs, and an additional factor of two loss results from the fact that only two strips will be summed (either the x or the y strips), the signal height must be increased by a factor of 13 compared with the linac BPMs in order to make use of the linac BPM electronics. This will be accomplished by increasing the length of the injection line BPMs and by having the strips cover a greater fraction of the beam pipe circumference.

BPM Position Resolution. The position resolution required of the injection line BPMs is dictated by our need to steer through apertures and to reliably and routinely match the position, angular, and energy acceptance of the PEP-II rings. If the BPM resolution is better than the rms beam sizes, $\bar{\sigma}_x$ and σ_y, everywhere in the injection line, then the beam position will clearly be sufficiently well known compared with the $>10\sigma$ apertures of the injection line. The smallest β_x or β_y at the injection line quadrupoles (where the BPMs are located) is $\beta \approx 40$ m. For an injection line emittance of 0.28 nm·rad, this corresponds to $\sigma = 0.1$ mm. In terms of spatial distance, the closest object to the injected beam is the septum at 3.5 mm. The energy aperture of the ring is ±0.5%, which corresponds to ±2 mm of horizontal motion in the dispersive region ($D_x \approx$ 0.4 m) at the beginning of the injection line (where the beam energy will be stabilized by a feedback loop). An rms resolution of 100 μm for all injection line BPM position measurements would be comfortably within these requirements. This 100 μm specification is for a pulse of 1×10^9 electrons, or about 1/40 of a full ring bucket. This is about half the smallest quantum of charge we contemplate injecting.

6.4.1.2 Energy Measurement. To measure and control the beam energy, we use BPMs to determine the incoming and outgoing beam angles from a calibrated dipole magnet [Abrams et al., 1987] in a dispersive region of each extraction line. One wire scanner will also be placed in the dispersive region in each line to measure the energy profile of the beam.

6.4.1.3 Beam Size and Shape Measurement. A wire scanner will be placed in a dispersion-free region of each extraction line. By varying a quadrupole strength, this scanner can be used to measure the beam phase-space ellipse, and thus the beam emittance. It is expected that such an emittance measurement will be done infrequently. An additional four wire scanners will be placed near the end of each injection line, again to measure the beam phase-space ellipse and emittance. These latter devices are expected to see more frequent use. Therefore, they are located so that measurements can be made during injection without having to vary a quadrupole. The injection lines will have a total of 12 wire scanners.

We intend to augment the wire-scanner measurements with observations from beam profile monitors (phosphorescent screens that can be viewed remotely via a television camera). Operators can insert the screens and directly view the beam shape. This information is not the quantitative equivalent of the wire-scanner information, but it is very useful operationally. We envision at least four screens for each beam—one to augment the measurement of the energy spread in the extraction line, one at the entrance to the NIT or SIT line, one at the exit of the NIT or SIT line, and one near the ring injection point.

6.4.1.4 Beam Loss Measurement. Lastly, we need a system to localize beam loss so that the operators can quickly isolate and correct any badly steered portions of the transport line. BPMs can be used to get an overall view of beam loss, but since the quadrupoles are approximately 50 m apart, this must be viewed as crude. We intend to augment the BPMs with a so-called PLIC (Panofsky Long Ion Chamber) cable strung along the entire length of the bypass lines. The ring injection areas are once again the most crucial locations. Fast ion chambers may be installed here to distinguish between beam losses at injection and beam losses in the ring. (A PLIC cable is already in place in the existing NIT and SIT lines.)

6.4.1.5 NIT and SIT Diagnostics. For the NIT and SIT lines, most of the instruments shown in Fig. 6-11 are satisfactory and will be used in the PEP-II injection system. The beam position systems in the NIT and SIT lines will be enhanced. Originally, beam position and shape were measured at 10 locations along each injection line, using scintillation screens. In the late 1980's, six additional SLC-type stripline BPMs, four of which are indicated in Fig. 6-11, were installed in each line. For PEP-II, new BPMs will be built so that there will be one BPM per quadrupole. As is the case elsewhere in the injection lines, the horizontal plates will be read out at QF locations and the vertical plates at QD locations.

The beam current is now measured by toroids installed in the NIT and SIT lines. The operation of these devices is satisfactory and they will be retained, though located in different places along the lines. The region after B10 is still in the process of refinement

and is not detailed in Fig. 6-11. In particular, the instrumentation in the critical region of the injection septa is not yet finalized. Section 6.4.2 discusses some of these issues.

6.4.2 Energy, Position, and Angle Feedback

For a generalized fast feedback system, the action of any closed feedback loop can be cast into a single matrix equation that can easily be implemented on a microprocessor. For the SLC system, the required matrices are designed off-line and downloaded via a database. The system is designed to run on a distributed set of microprocessors, so all routing and communication information is downloaded at startup time. All feedback loops use the same code except for nonlinear loops, for which a few special modules are needed. Currently, 18 such loops run on the SLC, with several more planned. It took about three months to implement all 18 loops.

Figures 6-17 and 6-18 show how the present feedback loops work on the SLC. The action of the energy feedback loop is displayed in Fig. 6-17. This loop modifies the phase of one klystron and keeps the energy constant to within 0.1%. Figure 6-18 shows the action of a steering loop. In this case, the beam upstream of the loop was perturbed and the effect on the position and angle were observed. Steady-state response is sufficient to steer the beam to within 15–20 μm and 1–2 μrad. Steering loops will constitute the majority of the loops for the PEP-II injection lines.

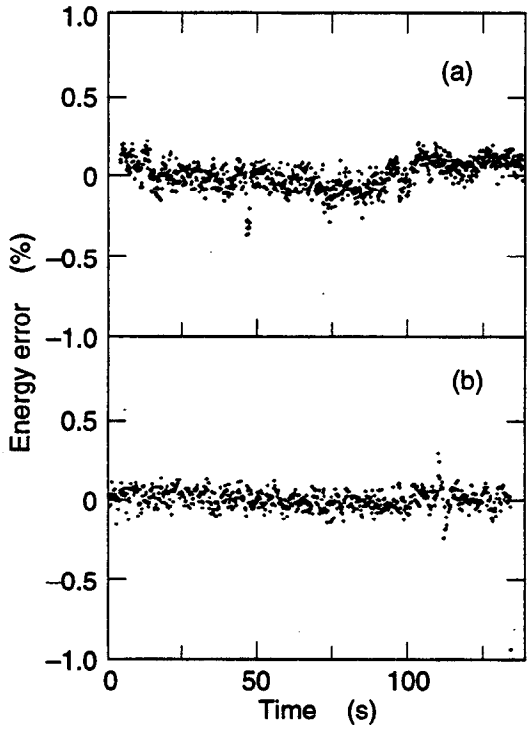

Fig. 6-17. SLC beam energy (a) without and (b) with energy feedback.

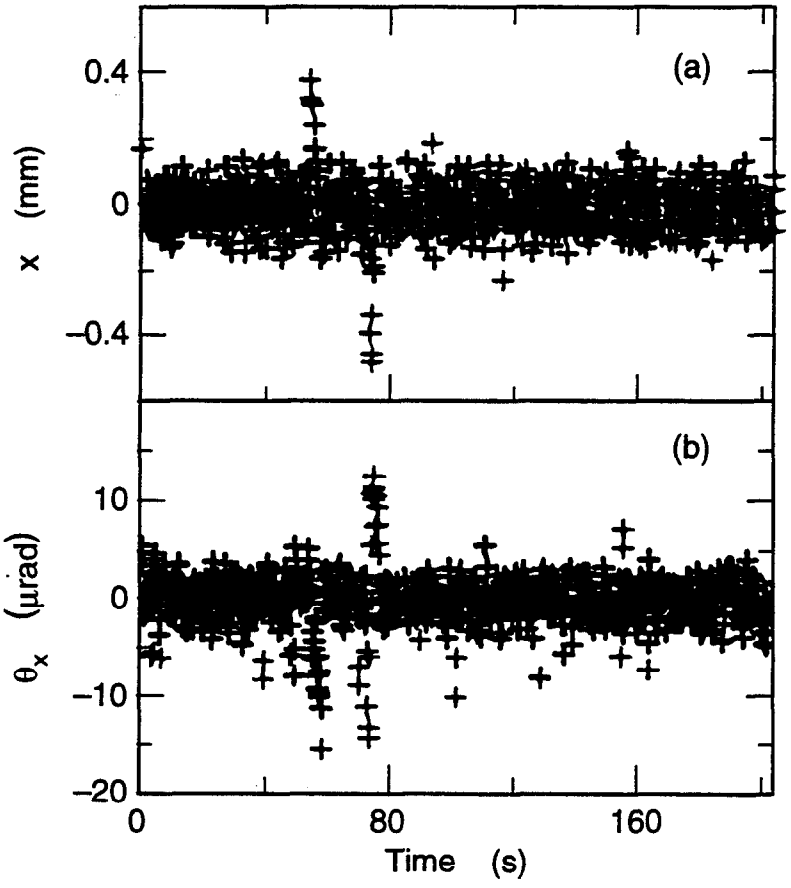

Fig. 6-18. Response of a typical steering feedback loop to an upstream beam perturbation.

Locations of the proposed steering and energy loops are indicated in Fig. 6-19. Steering loops will be placed at injection into the transport lines, at injection into the NIT and SIT tunnels, and at injection into the PEP-II rings. Instrumentation to measure the energy will be placed in the linac extraction area at the location with the highest precision for an energy measurement. The resultant information will then be sent to the microprocessor controlling a particular linac klystron assigned to adjust the energy. The magnets required to steer the beam for feedback will be located near the quadrupoles in the transport lines, as discussed earlier. The diagnostic devices listed above will perform the measurements. Phase shifters or drive amplitude control will be used on selected linac klystrons to change the energy of the beam.

Because we base the feedback and diagnostics for the PEP-II injection system entirely on the SLC, no new types of hardware or software need be developed; we use proven and reliable designs already built for the SLC. This gives us confidence that we can meet the goal of steering to within 15–20 μm and 2 μrad and can build a beam diagnostics system that can identify problems sufficiently to correct them in a timely manner. Our approach ensures that the injection system will always run at high efficiency.

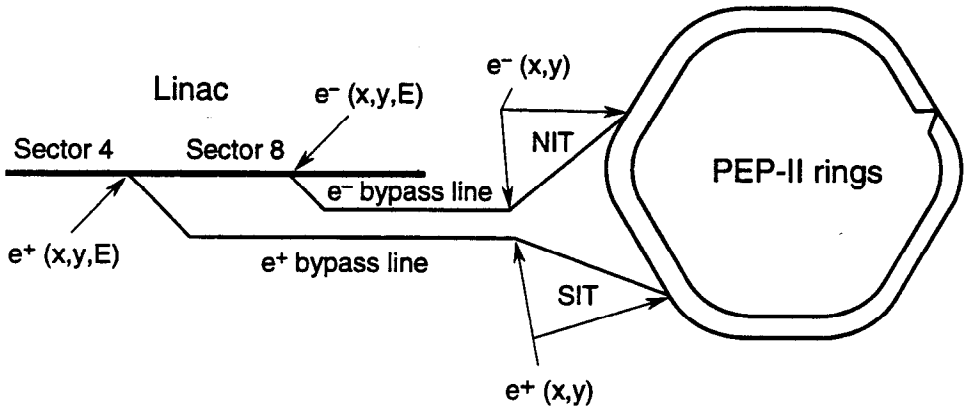

Fig. 6-19. Locations for steering and energy-correction feedback loops (schematic).

6.5 INJECTION INTO THE HER AND LER

Initially, we considered a horizontal injection scheme similar to that in PEP. Ultimately, however, we settled on a vertical injection scheme, which will be described below. The main potential advantage of horizontal over vertical injection is that the uncoupled horizontal emittance ε_x is twice the fully coupled vertical emittance ε_y. Thus, the rms horizontal beam size is at least 1.4 times the vertical beam size (for equal beta functions).

An injection septum in the horizontal case occupies a relatively smaller area in the available phase space, simply because the horizontal phase space is larger. In our case, however, a horizontally injected beam in one ring, which makes large oscillations before damping, will interact parasitically with the circulating beam in the other ring in the region where the two share the same pipe (i.e., near the IP). Beam-beam simulations (described in Section 4.4) show that significant blowup of the low-energy beam size is expected. Thus, in PEP-II, where the beams are separated horizontally, vertical injection is much more effective at reducing the parasitic beam-beam forces and leads to considerably less beam blowup. This was the strongest reason for choosing vertical injection.

There are also other considerations that favor vertical injection for PEP-II:

- Motion in the vertical plane is unaffected by synchrotron oscillations. This simplifies the problem of masking the detector from particles lost during injection. (If we injected in the horizontal plane, off-energy particles could miss the tight masking due to energy-related displacements in the arcs, where there is nonzero horizontal dispersion; vertical injection avoids this possibility.)
- Since there is essentially no bending in the vertical plane, vertical injection avoids the need to correct a nonlinear dispersion function. The nonlinear momentum dependence of the beta function (nonlinear chromaticity) will be slightly worse in the vertical than in the horizontal plane, but we have adopted a chromaticity correction scheme that provides adequate compensation for this.

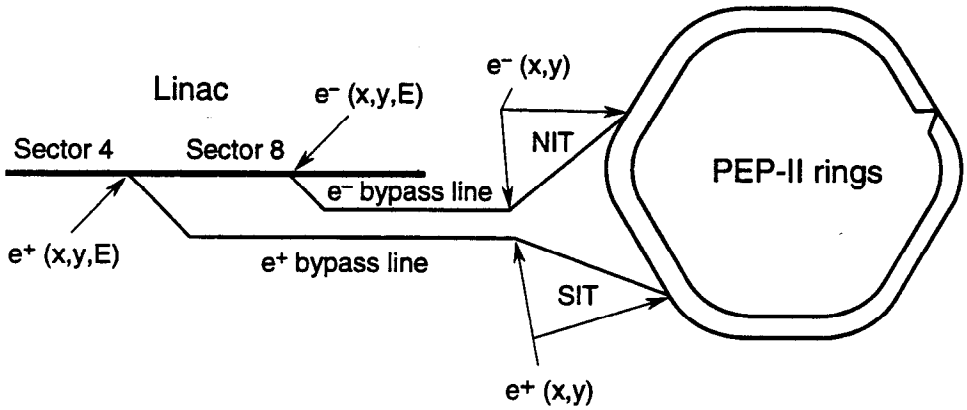

Fig. 6-19. Locations for steering and energy-correction feedback loops (schematic).

6.5 INJECTION INTO THE HER AND LER

Initially, we considered a horizontal injection scheme similar to that in PEP. Ultimately, however, we settled on a vertical injection scheme, which will be described below. The main potential advantage of horizontal over vertical injection is that the uncoupled horizontal emittance ε_x is twice the fully coupled vertical emittance ε_y. Thus, the rms horizontal beam size is at least 1.4 times the vertical beam size (for equal beta functions).

An injection septum in the horizontal case occupies a relatively smaller area in the available phase space, simply because the horizontal phase space is larger. In our case, however, a horizontally injected beam in one ring, which makes large oscillations before damping, will interact parasitically with the circulating beam in the other ring in the region where the two share the same pipe (i.e., near the IP). Beam-beam simulations (described in Section 4.4) show that significant blowup of the low-energy beam size is expected. Thus, in PEP-II, where the beams are separated horizontally, vertical injection is much more effective at reducing the parasitic beam-beam forces and leads to considerably less beam blowup. This was the strongest reason for choosing vertical injection.

There are also other considerations that favor vertical injection for PEP-II:

- Motion in the vertical plane is unaffected by synchrotron oscillations. This simplifies the problem of masking the detector from particles lost during injection. (If we injected in the horizontal plane, off-energy particles could miss the tight masking due to energy-related displacements in the arcs, where there is nonzero horizontal dispersion; vertical injection avoids this possibility.)
- Since there is essentially no bending in the vertical plane, vertical injection avoids the need to correct a nonlinear dispersion function. The nonlinear momentum dependence of the beta function (nonlinear chromaticity) will be slightly worse in the vertical than in the horizontal plane, but we have adopted a chromaticity correction scheme that provides adequate compensation for this.

The injection scheme envisioned for PEP-II is different from that used for PEP. In particular, the drift space constituting the injection straight in PEP-II is an optical section having three additional quadrupoles compared with PEP (for a total of five quadrupoles).

The scheme we have chosen has two significant advantages:

- The transport matrix element R_{12} between the first kicker, K1, and the injection point is large; the vertically defocusing second quadrupole adds to the total kick, thus reducing the burden on K1.
- It is possible to replace the septum kicker used in PEP—which kicked both the circulating and the injected beam and required a rather high voltage—with a DC septum that kicks only the injected beam. This avoids the jitter in the septum kicker that worsened the tracking between it and the other two injection kickers, and thus made it difficult to close the kicker bump in PEP.

The PEP-II injection optics is designed as a $-I$ transformer from the center of the first quadrupole to the center of the fifth quadrupole (180° phase shift). It has mirror symmetry around the central quadrupoles, QDI, with a 90° phase shift between the QDOI and QDI centers. Two slightly different implementations of the PEP-II injection straight section were considered. In the first, the central quadrupole, QDI, is a single element; two possible locations of the injection septum, S0, were investigated. In the second, QDI is split into two elements, with the injection septum centered between them. On comparing the three injection points, we noted two advantages of the split-quadrupole arrangement: (i) somewhat more phase space is available for injection, and (ii) a significantly smaller angular deflection is required from the current-sheet septum, S0, which reduces the current density needed. For these reasons, we selected the split-quadrupole solution.

Apart from the quadrupoles, the chosen injection optics uses two kickers driven in parallel for best tracking. The two kicks are identical and the resulting beam bump is always closed. Also required for the present injection scheme are two pairs of DC magnets, arranged in mirror symmetry with respect to the center of the QDI pair. Their function is to produce part of the bump required for injection and to give additional flexibility in tuning. The fields are always chosen so that the total DC bump is also closed. Finally, there are two septa, S0 and S1. The first of these, S0, is a current-sheet septum at the injection point. It is located inside the storage ring vacuum chamber to avoid the reduction in injected-beam acceptance that would result from providing an additional beam pipe wall. The second septum, S1, is a Lambertson septum designed such that the injected beam approaching its center horizontally from the outside (in the x-z plane) is kicked into the vertical plane for injection. Details of the injection optics are given in Section 6.5.1 below.

The criteria used in designing the injection region were as follows:

- The beam-stay-clear aperture of the circulating *unbumped* beam must be at least $12\sigma + 5$ mm.
- The beam-stay-clear aperture with the DC bump only must be at least 10σ.
- The fully bumped beam-stay-clear aperture must be at least 6σ.

- The vertical emittance used in calculating the beam size must be based on a fully coupled beam; it is $\varepsilon_y = 25$ nm·rad in the HER and $\varepsilon_y = 33$ nm·rad in the LER. (To accommodate a higher than normal β_y^* value in the HER, a larger vertical emittance value of $\varepsilon_y = 50$ nm·rad was used to define the beam-stay-clear aperture for the LER injection hardware.)

Figures 6-20 and 6-21 illustrate the injection straights, showing the paths of both the injected beam and the bumped circulating beam around the injection point of the HER and LER, respectively. Relevant angles and distances are noted. The local stored-beam orbits during the injection process are shown in Fig. 6-22.

The injected beam passes through a double window (two 0.5-mil stainless-steel foils), which isolates the ultrahigh vacuum needed in the storage ring from the poorer vacuum adequate for the injected-beam transport line. A small amount of helium gas is contained between the two windows to permit the detection of any leaks. The double window is placed at a point upstream of the thin septum where β_y of the injected beam is minimum and the phase ellipse is upright. This location minimizes the emittance growth due to multiple scattering in the window. Given the very small vertical emittance of the linac

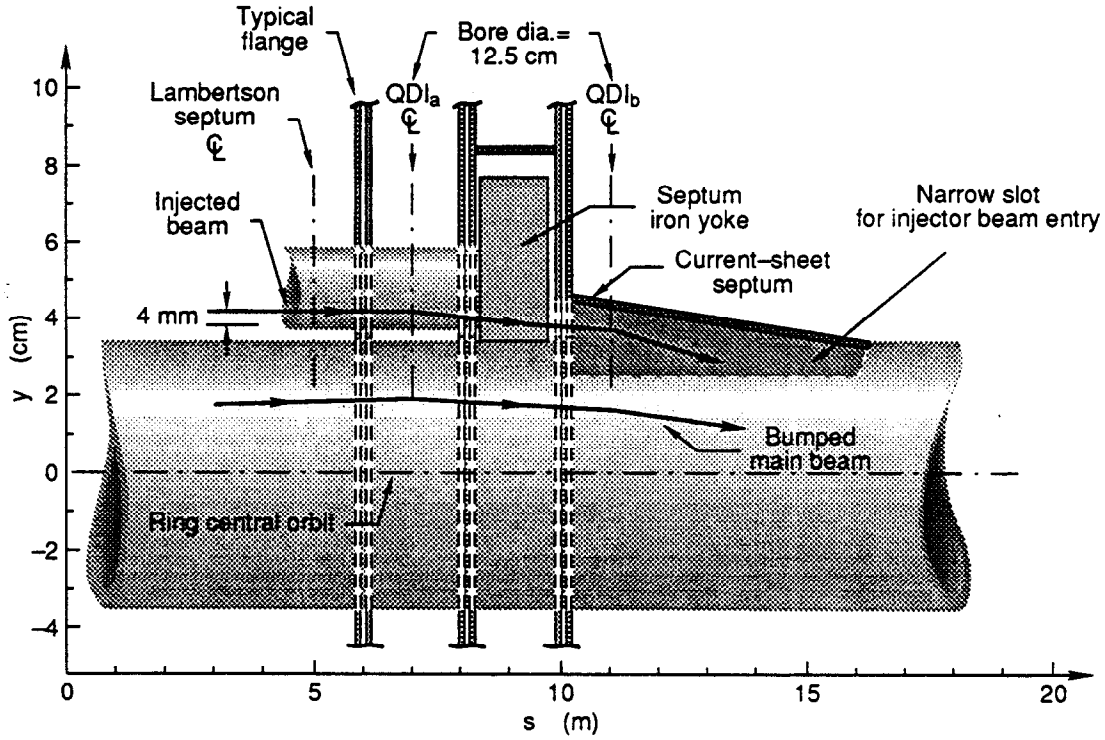

Fig. 6-20. Paths of injected beam and bumped circulating beam in the HER.

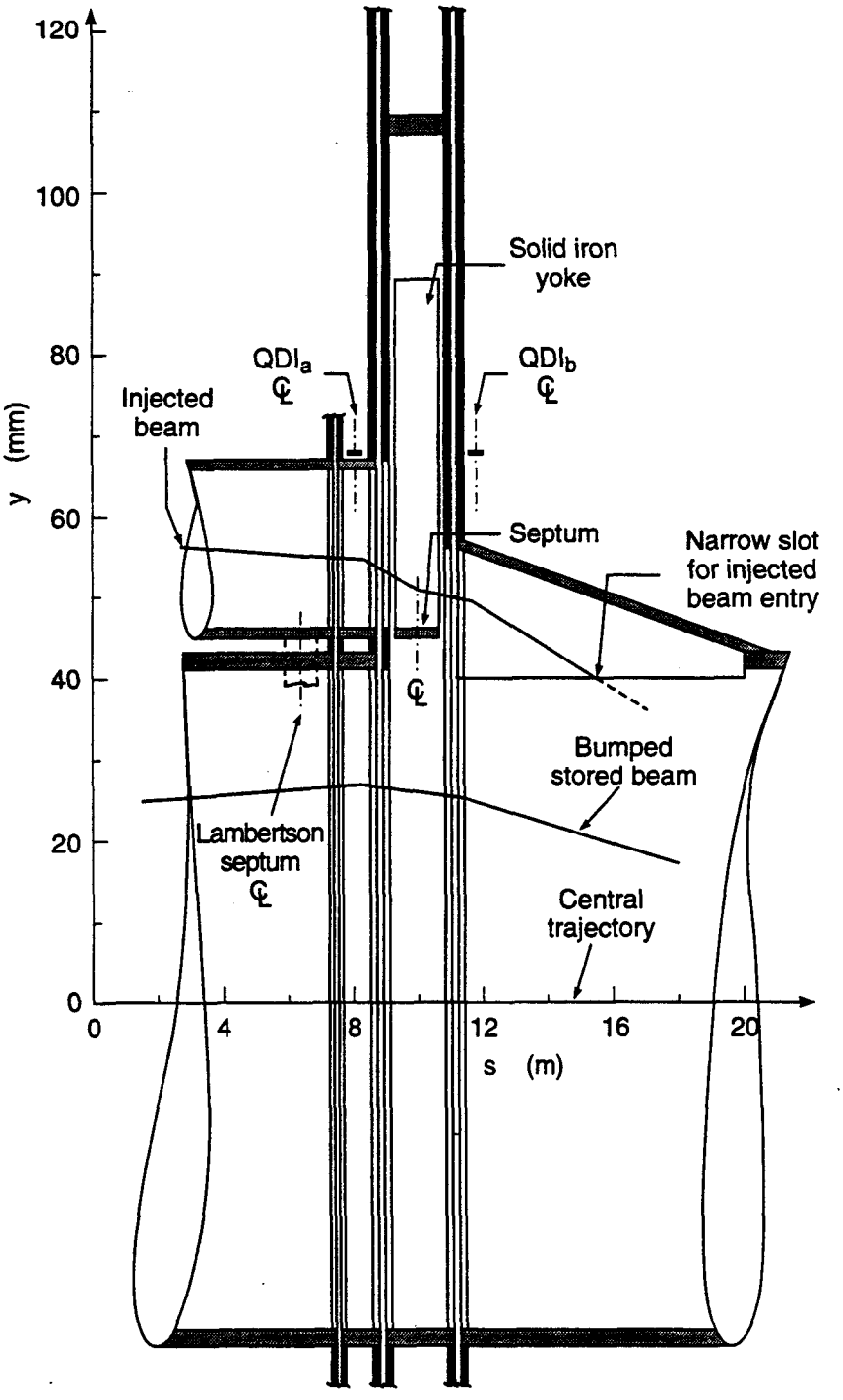

Fig. 6-21. Paths of injected beam and bumped circulating beam in the LER.

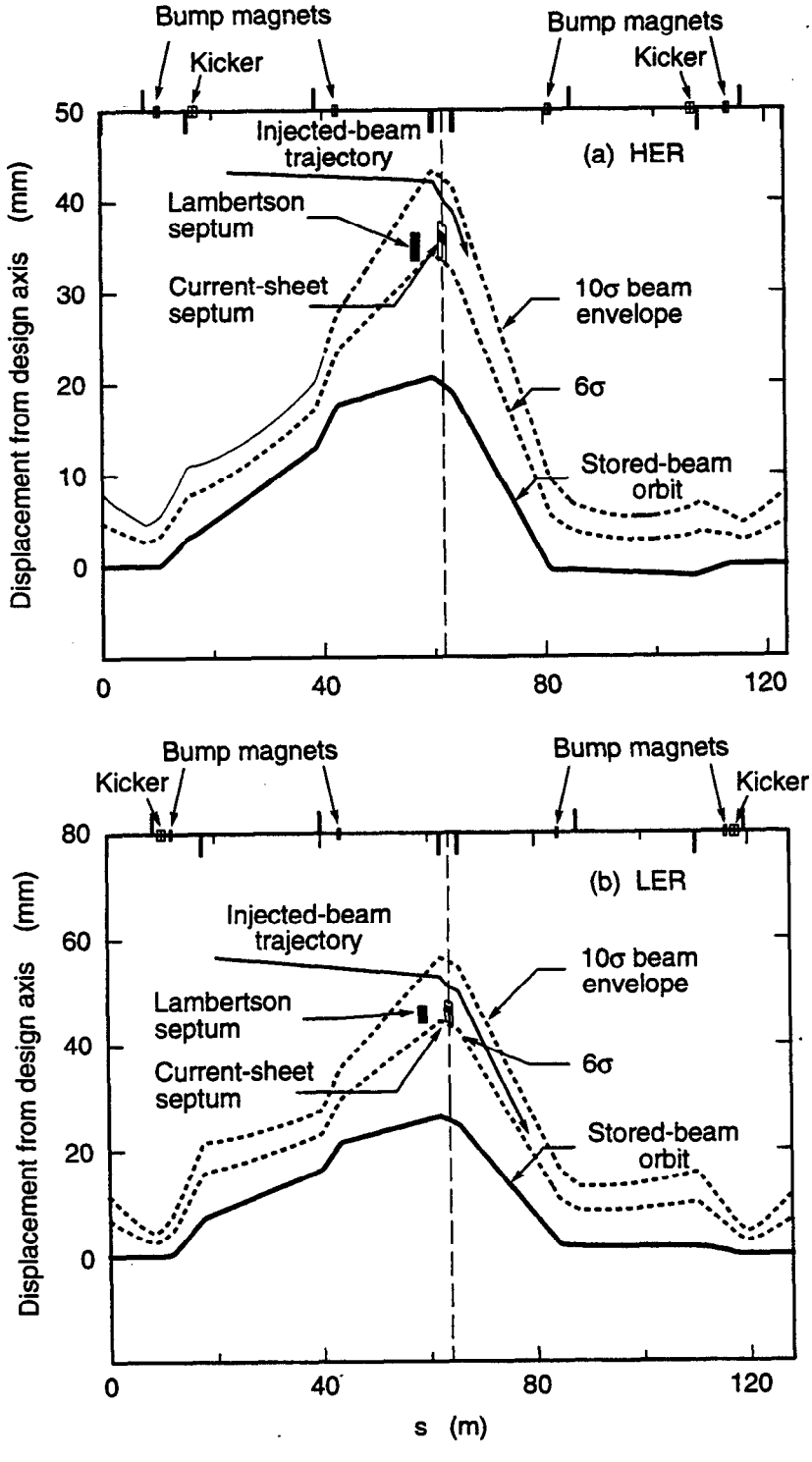

Fig. 6-22. Stored-beam orbit during the injection process, (a) HER and (b) LER.

beams, the actual emittance of the beam injected into the rings is dominated by multiple scattering in the windows. To control the beta functions in this region and to produce an upright phase ellipse at the injection point, two quadrupoles have been added to the injection line in the region between the window and the ring. Figure 6-23 shows the

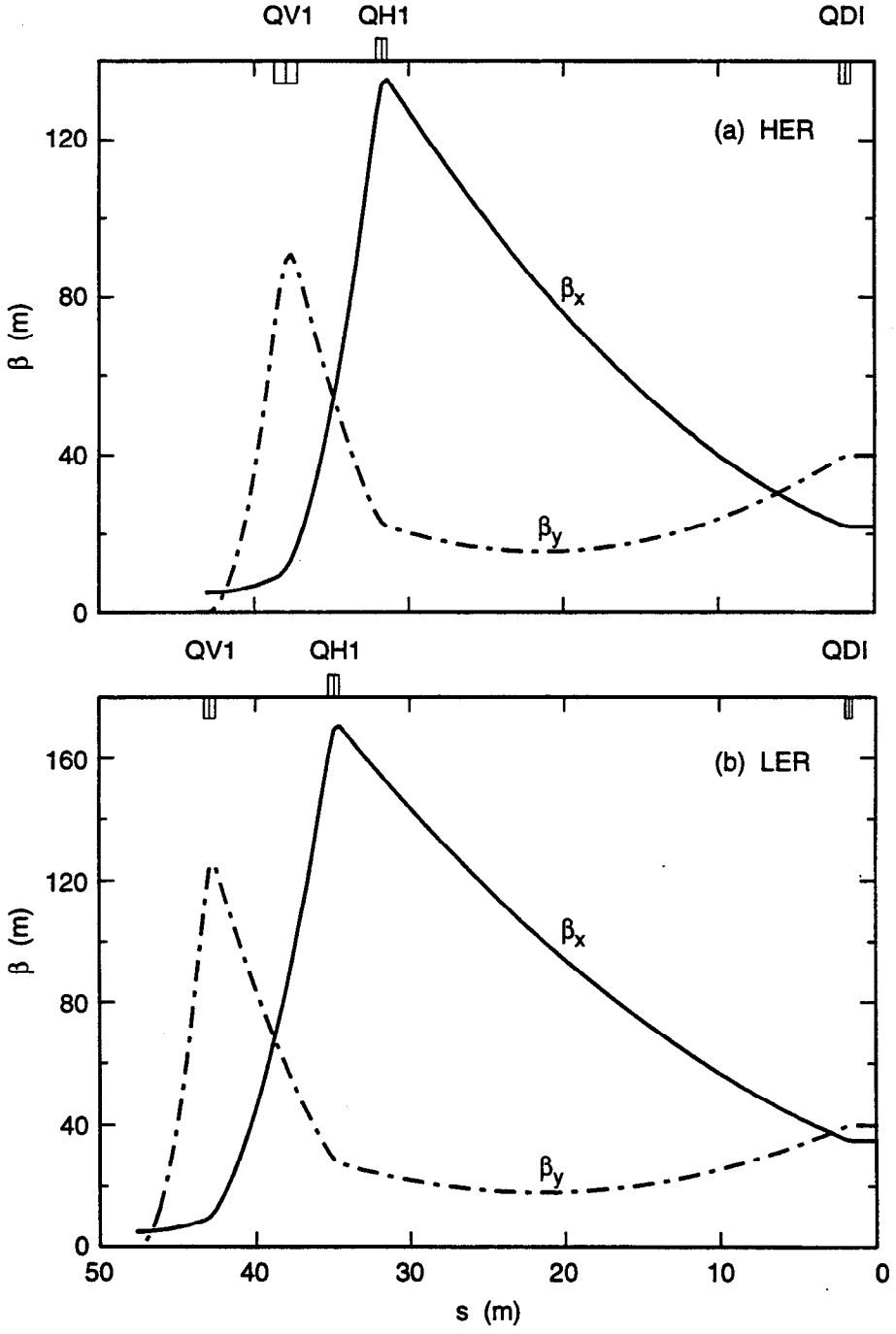

Fig. 6-23. Matching optics from vacuum isolation window to injection point, (a) HER and (b) LER.

resultant matching optics for each ring. The beta functions at the window locations will serve as an additional matching point for the upstream optics, as discussed in Section 6.3.

Figure 6-24 shows the 10σ phase-space ellipses of the HER and LER, indicating the septum (S0) location and the position and size of the injected beam. In both rings, the

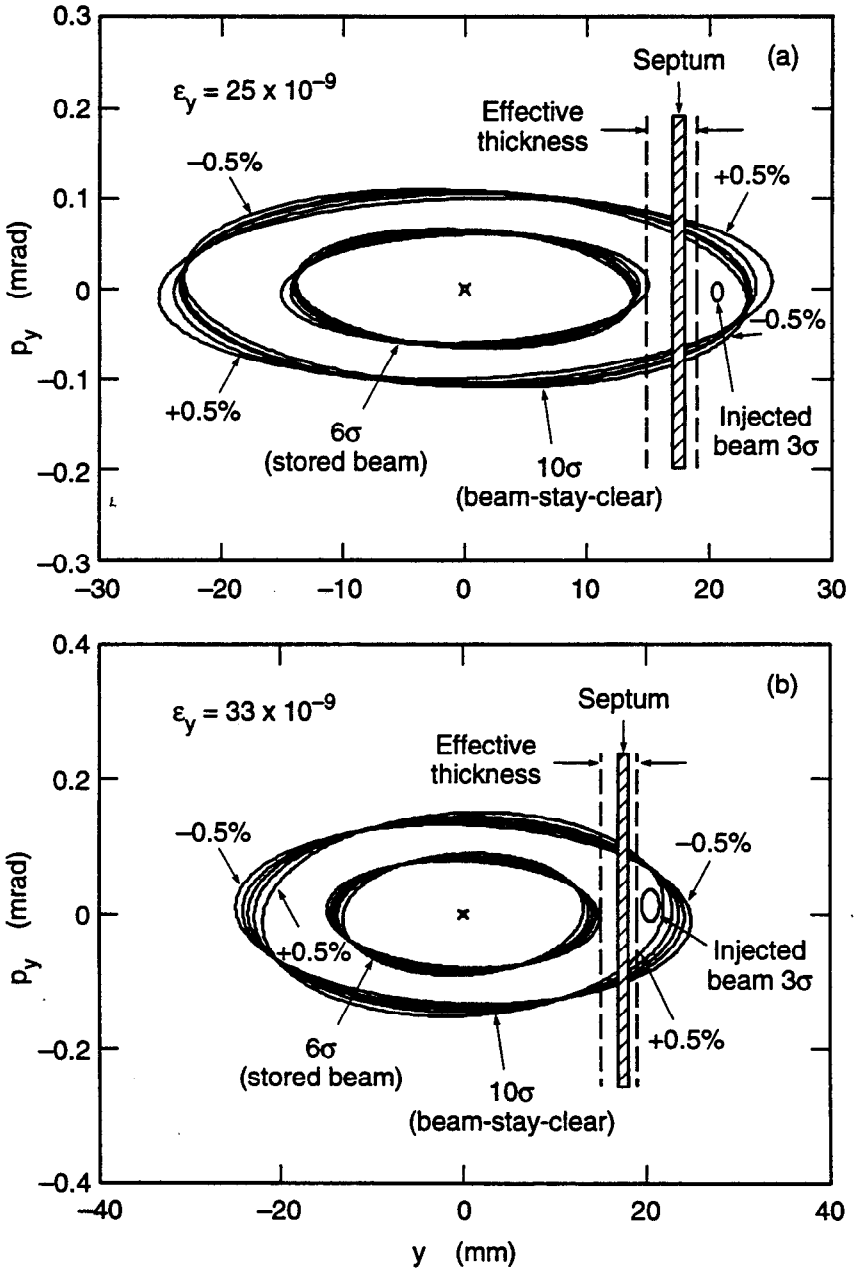

Fig. 6-24. Phase-space diagram of injection acceptance, (a) HER and (b) LER. The dashed lines indicate the effective thickness of the 1-mm septum. Injected beam sizes shown include the effects of multiple scattering in the isolation windows.

distance of S0 from the central orbit is 2 mm beyond that required to satisfy the beam-stay-clear criterion mentioned above, in order to allow for leakage field from the septum. This eliminates the possibility that the septum field might adversely influence the bumped circulating beam.

6.5.1 Ring Optics for Injection

A reasonably large value of the beta function in the plane of injection is needed at the injection septum. In essence, the requirement is that the septum appear to be thin relative to the sum of the injected and stored beam sizes at that point. The value of β at the injection point should not, however, be so large as to give rise to significant extra chromaticity.

Another important factor in the injection straight section design is to have the kickers very well matched to each other. This is especially important for PEP-II, because the bunch spacing is very small and many bunches will be affected by each firing of the kickers. As the filling proceeds, bunches already stored will see the rising and falling edges of the kicker waveform. To ensure well-matched kickers over their entire waveform, we select a system of two identical kickers, spaced 180° apart in betatron phase.

As discussed above, we chose to inject in the vertical plane and to make the optics almost identical for the HER and LER. Transverse dimensions of the LER orbit manipulations are simply scaled up from those of the HER due to the larger emittance of the LER beam.

The actual implementation of the injection scheme in both rings is shown in Fig. 6-25. At the center of the injection straight are two 90° cells. The injection kickers are placed toward the outside of these cells so as to have 180° of betatron phase between them. At each end of the injection straight, one straight-section cell (of length 15.419 m) is added, making the two center cells each 44.391 m in length. (The actual straight section length is somewhat greater than that given by the sum of these cell lengths, to accommodate the septum hardware.) These cells operate as quarter-wave transformers (from the normal cell beta functions to the beta functions at the center of the injection straight) that amplify the normal cell beta functions by a factor of $(44.391/15.419)^2 = 8.3$. Thus, we obtain a beta function of 215 m at the injection septum. In the LER, the quadrupoles must be shifted slightly to avoid interference with particular HER RF cavities in the same section of the tunnel. This changes the value of β_y at the injection point to 170 m for the LER, and requires the relocation of the LER kickers.

As mentioned earlier, the central quadrupole is split into two sections so that injection can occur at the center of the straight where $\alpha_x = \alpha_y = 0$. Four variable parameters (the strengths of quadrupoles QFI, QDI, QFOI, QDOI) ensure the ability to match to the lattice (i.e., to achieve $\alpha_x = \alpha_y = 0$ at the center of the straight section), to obtain 180° of betatron phase advance between the kickers, and to have fine control of the vertical beta function.

The vertical injection process occurs as shown schematically in configuration space and phase space in Figs. 6-26 and 6-27, respectively. The closed orbit of the stored beam is distorted by means of four DC bump magnets and two kickers. The stored beam is first

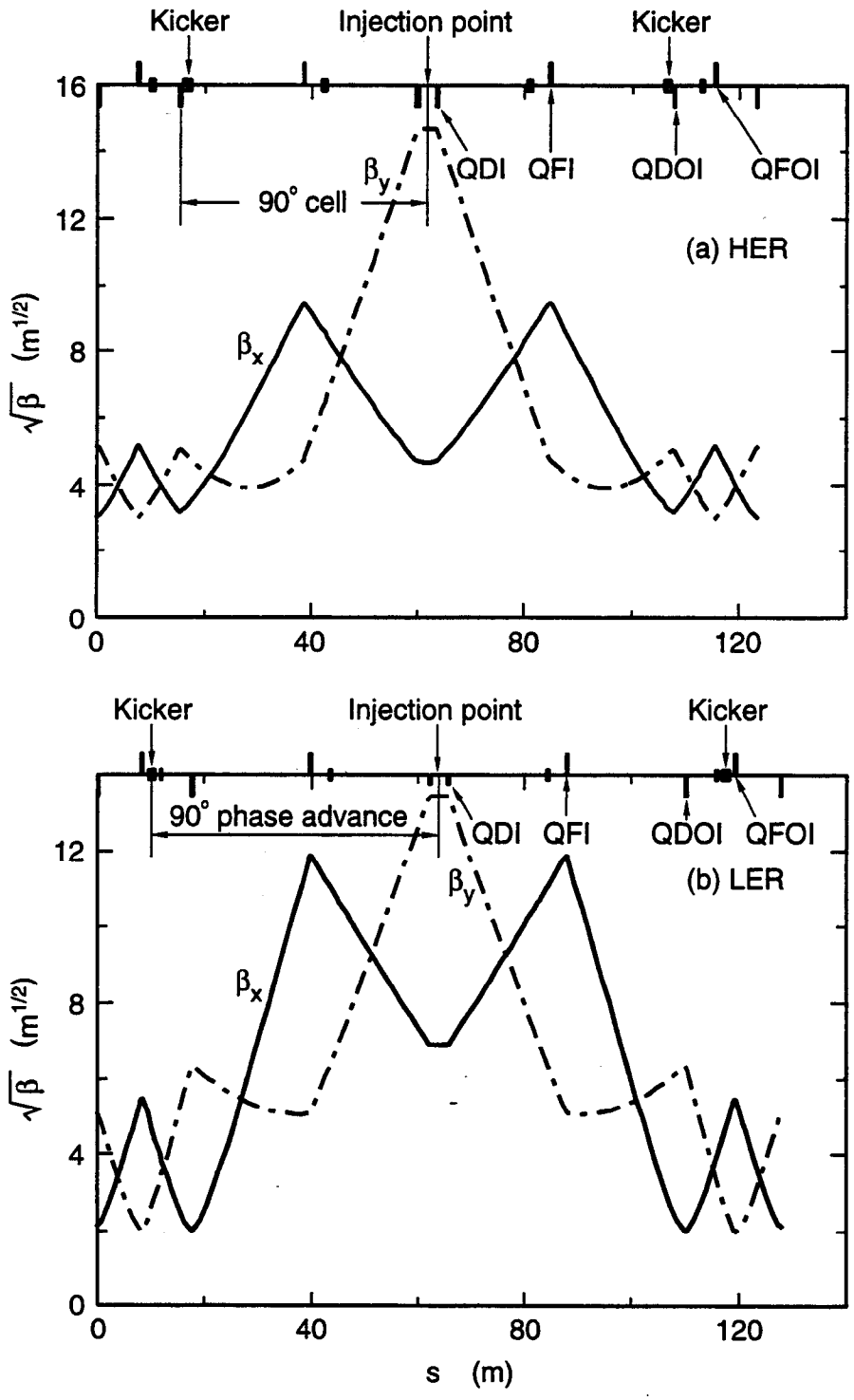

Fig. 6-25. Twiss parameters β_x and β_y in the injection straight section, (a) HER and (b) LER.

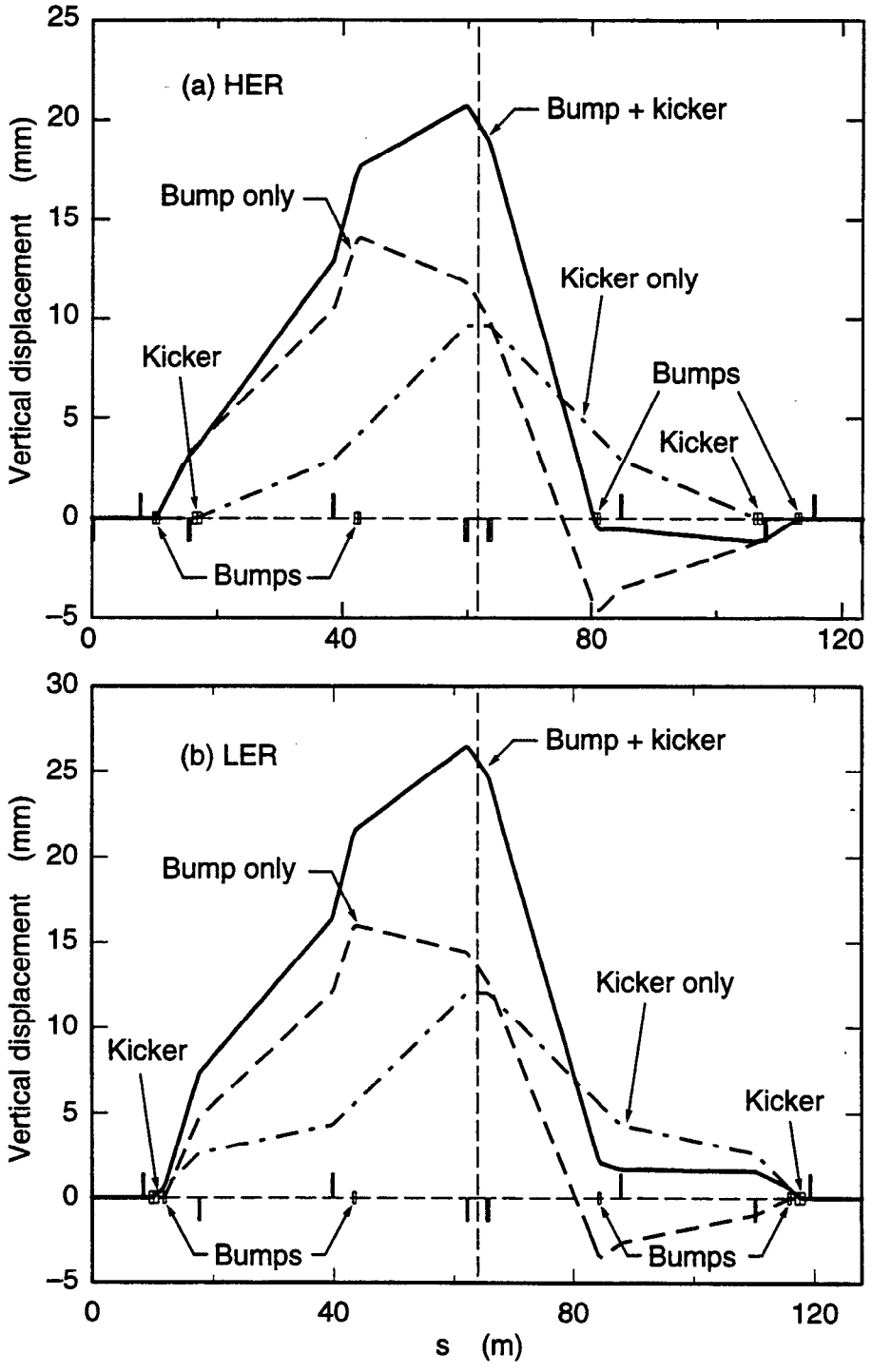

Fig. 6-26. Schematic of the vertical injection scheme, showing displaced orbits, (a) HER and (b) LER.

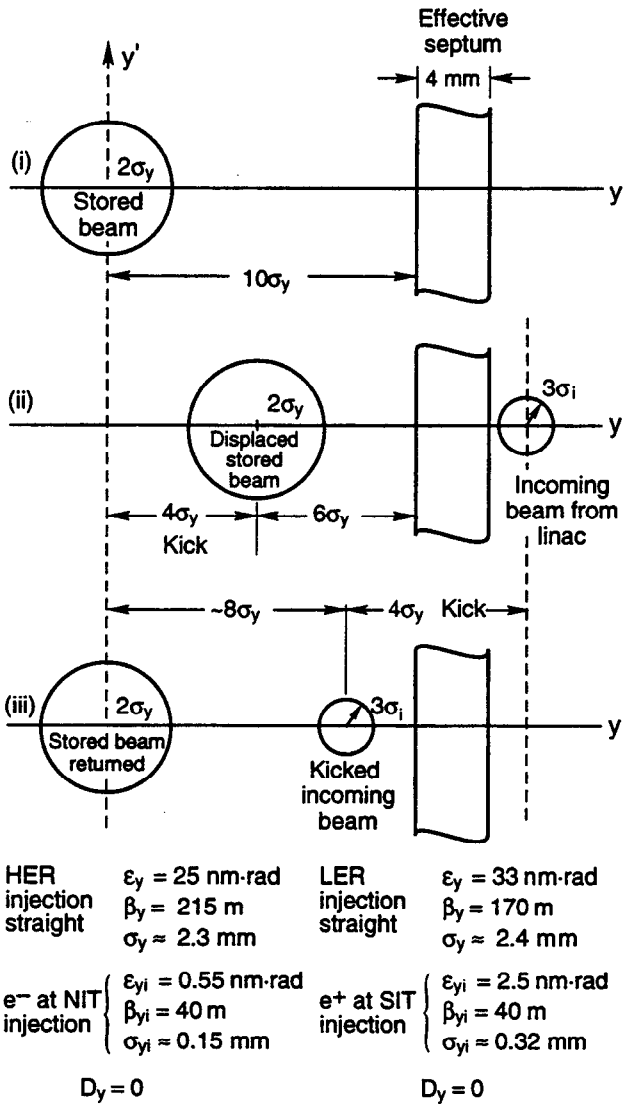

Fig. 6-27. Phase-space diagram of the vertical injection process.

moved to the DC bumped position, $10\sigma_y$ away from the inner edge of the septum. Although the physical thickness of the septum is only 1 mm, an allowance is made for regions of bad field on either side (1 mm on the injected-beam side and 2 mm on the stored-beam side). Then the stored beam is kicked to within $6\sigma_y$ of the effective inner edge of the septum; incoming beam from the transport line is tangent to the stored-beam orbit at this point and clears the effective outer edge of the septum. When the stored beam bunch returns to the injection region on subsequent turns, it is already back on its DC bumped orbit; the newly injected beam is also inside the beam-stay-clear aperture of the ring and inside the septum, ready to damp and merge with the stored beam.

If due care were not taken in correcting the nonlinear chromatic functions in the rings, the beta functions at the injection point would be strongly dependent on momentum. By taking these nonlinearities into account in the chromaticity correction scheme, we have

reduced the β_y variation at the injection point by a factor of 10. The corrected phase-space diagrams for the HER and LER are shown in Fig. 6-24. We see that the emittance of the injected beam (at the 3σ contour) fits easily into the acceptance of the ring. A virtue of the vertical injection scheme is that the nonlinear dispersion (which is confined to the horizontal plane) has much less importance than it would have if injection were in the horizontal plane.

Both the kicks and the bumps will produce a small dispersion function in the vertical plane. At the injection point, this dispersion function will be very nearly equal in magnitude to the orbit displacement there. For the HER, the dispersion function due to the bumps and kickers amounts to $D_y = 0.02$ m and, for a momentum spread of $\pm 0.5\%$, results in a displacement of 0.1 mm, which is negligible. For the LER, the equivalent displacement is 0.14 mm, again a negligible amount.

Because there are magnetic elements (quadrupoles) between the elements of the kicks and bumps, there will be a small residual dispersion function leaking out of the injection straight section. We find this residual dispersion to be entirely negligible.

6.5.2 Mechanical Design

6.5.2.1 Septum Magnets. In this section, we discuss the two septa, S0 and S1, for PEP-II. S1 is a standard Lambertson septum, which bends the injected beam 11 mrad horizontally into the vertical plane of the storage ring. The maximum field required in the gap (for the HER) is 0.4 T for a magnet length of 1 m. A cross section of this septum, suitable for both the HER and the LER, is shown in Fig. 6-28. For the chosen notch angle of 22°, the maximum field anywhere in the iron yoke is 1 T.

The current-sheet septum (S0), though simple in principle, requires a more detailed discussion. Essentially, it is a current loop with an iron flux return. A review of various types of septa and some useful practical considerations can be found in Fischer [1985], and a detailed discussion of dipole septum magnets can be found in Keizer [1974].

For a current-sheet septum, the current density J (in A/mm^2) is given by

$$J = \frac{10^4}{4\pi}\frac{B}{t} \tag{6-3}$$

where B is the magnetic field of the septum (in T) and t is the septum thickness (in mm). We obtain the required total current I (in A) from

$$\begin{aligned} NI &= \frac{Bg}{\mu_0} = 796\,Bg \\ &= JA \end{aligned} \tag{6-4}$$

where N is the number of turns in the loop ($N = 1$ for a current-sheet septum), g is the magnet gap (in mm), and A is the coil cross section (in mm^2).

Using the surface resistivity of copper ($\rho = 1.7 \times 10^{-6}$ Ω·cm), we obtain a power density in the conductor, P/A, in (W/mm^2) of

$$\frac{P}{A} = J^2R = J^2\rho L = 1.7 \times 10^{-4} J^2 L \tag{6-5}$$

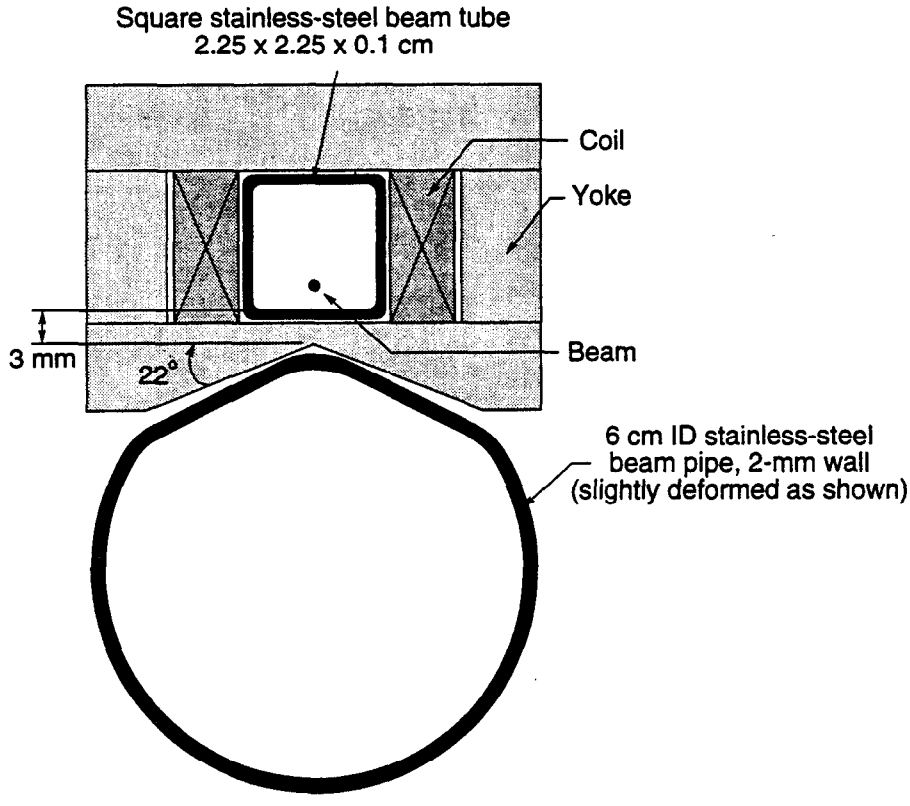

Fig. 6-28. Vacuum chambers and Lambertson septum magnet for both HER and LER.

where L is the conductor length (in cm). From this, we arrive at the total power dissipated in the conductor as

$$P = \frac{P}{A}(g \cdot t) = 1.7 \times 10^{-4} J^2 L(g \cdot t) \tag{6-6}$$

We have also estimated, in two ways, the power dissipated when 60 pulses of a 10-GeV beam with 5×10^9 e^- per pulse strike the septum. First, we ran the EGS code to examine the energy deposition from the shower generated in the initial interaction. Second, we scaled the energy deposition from the curves (also based on EGS) of Eckland and Nelson [1981]. In both cases, it was assumed that the incident beam enters perpendicular to the septum cross section, which is pessimistic in terms of the energy deposition. For the second case, we took the maximum value of $(1/E_0)\cdot(dE/dV)$ (roughly 0.1 E_0/cm^3) from the curves to make our evaluation. However, because the septum is only 1 mm thick, it intercepts just a fraction of the shower; the rest leaks away laterally. After a depth of 10 cm in copper, the radius of the shower is more than 1 cm, and the septum cross-sectional area is less than 5% of the shower area. Therefore, the volume of the septum where energy is deposited at the rate of 1 GeV/cm^3 is only about 2 cm^3. The

resulting estimates of the energy deposition per particle were 1.67 GeV (using EGS directly) or 2 GeV (using the scaled Eckland and Nelson curves).

Taking the more pessimistic value of 2 GeV, the energy deposition per particle is

$$(2 \times 10^9) \times (1.6 \times 10^{-19}) = 3.2 \times 10^{-10}\,\text{J}$$

and the power in the septum from the shower due to 60 pulses is

$$(60\ \text{s}^{-1}) \times (5 \times 10^9) \times (3.2 \times 10^{-10}\ \text{J}) = 96\ \text{W}.$$

The results of these estimates are collected in Table 6-4 for both rings. We designed both the HER and LER septum coil to safely dissipate 450 W. Figure 6-29 shows a cross section of the dipole septum and an isometric sketch of the coil. The length of the septum is 1 m. Its main features are:

- A yoke that extends beyond the septum at both ends by 5 cm, which helps to terminate the field longitudinally.
- A backleg winding to compensate for the finite permeability of the iron; with a modest number of ampere turns, the field outside the septum is reduced from 0.5 mT to less than 0.1 mT.
- Stainless-steel cooling tubes that carry a negligible fraction of the septum current. Magnetic-field maps showed that copper cooling tubes would carry a much larger portion of the current, leading to a significant distortion of the field in the gap and unacceptable leakage outside.

Cooling calculations show that the maximum rise in temperature anywhere in the septum is 3°C above the input cooling-water temperature (conservatively taken to be 30°C).

6.5.2.2 Ring Bump Magnets. Parameters for the bump magnets are summarized in Table 6-5. These magnets present no special problems since they are very weak. For diagnostic purposes, and for establishing the first-turn orbit, it is advantageous to be able to inject on-axis. To achieve this condition without increasing the kicker strength would require the strength of the bumps to increase by a factor of three. Alternatively, if the kicker strengths were doubled (as permitted by the design, see Section 6.5.2.3), then the bump magnet strengths need only be doubled to achieve on-axis injection.

Table 6-4. Parameters for the current-sheet septa at 10 and 4 GeV.

Ring	Nominal angle (mrad)	l (cm)	B (T)	J^a (A/mm^2)	Ohmic loss (W)	Beam loss (W)	Total (W)
HER	1.00	150	0.022	20.0	255	96	351
LER	1.32	150	0.012	10.0	65	96	160

[a] $t = 1$ mm, $g = 25$ mm.

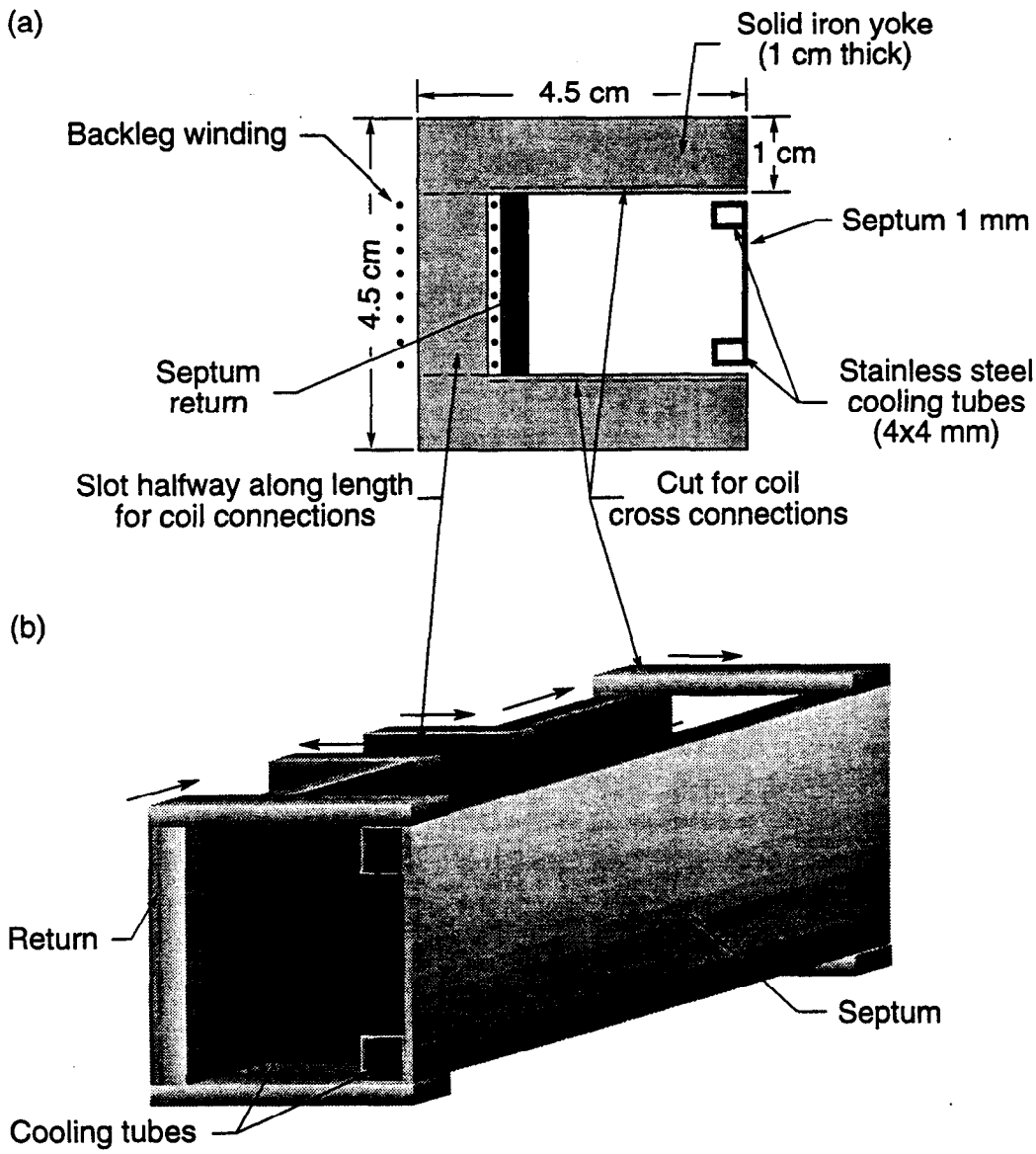

Fig. 6-29. Current-sheet septum for both HER and LER: (a) cross section, (b) isometric of coil.

6.5.2.3 Ring Kicker Magnets. We initially considered three different types of kicker:

- A current loop inside the ring vacuum
- A terminated transmission line inside the vacuum
- A ferrite magnet outside the vacuum

Details of the comparative study of these three types can be found in Bulos [1992]. Eventually, we chose the ferrite type, because it needs the lowest voltage and it avoids any penetration into the ring vacuum (as well as any additional metal surfaces inside the

Table 6-5. Bump magnet parameters at 10 and 4 GeV.

Magnet	Deflection angle (mrad)	Length (m)	Field (mT)	On-axis injection field (mT)
BM1L (HER)	–1.04	1.0	34.7	32.4
BM2L (HER)	0.61	1.0	20.4	33.4
BM1R (HER)	1.12	1.0	37.4	39.9
BM2R (HER)	–0.20	1.0	6.7	6.4
BM1L (LER)	–1.18	0.5	31.5	34.2
BM2L (LER)	0.91	0.5	24.3	44.0
BM1R (LER)	1.08	0.5	28.8	26.1
BM2R (LER)	–0.16	0.5	4.1	15.4

beam pipe, which can disturb the beam). Figure 6-30a shows a cross section of this magnet; the aperture satisfies the beam-stay-clear requirements for either the HER or the LER. The active magnetic length is 75 cm, and the ceramic beam pipe is 1 m long. The main features of this design are:

- A metallic coating on the inside of the ceramic beam pipe to carry the beam image current, as well as to shield against the electromagnetic field of the beam, while still allowing the magnetic field to penetrate the tube with minimal attenuation.
- An outside copper coating on the ceramic tube to permit external water channels to extract the ohmic heat generated by beam image currents in the coating and eddy currents from the magnetic field. The ferrite could also be cooled, if this were needed, in a similar fashion.

The calculation of the heat generated in the present design appears in Bulos [1992]; Table 6-6 lists the relevant kicker parameters.

As indicated by the simplified pulsing circuit of Fig. 6-30b, the two kickers in each ring are driven in parallel, using a common FET-switch pulser capable of delivering 6 kA at 6 kV. When the magnet is shorted at its output, it acts as an inductance, which can be turned into a pure resistance, as shown in Bulos [1992]. The magnet is fed by a cable of equal impedance and whatever length is required. This arrangement avoids any reflections.

6.5.2.4 Ring Quadrupoles. Although the ring quadrupoles in the injection straight have very modest strengths, there are a few special requirements. The two quadrupoles QDI (at the center of the straight) are required to have a large aperture, because here β_y is large and the orbit is sometimes displaced due to the injection bump. In addition, the upstream QFI quadrupole must have a small outer dimension on one side in order to provide clearance for the injection line beam pipe. Parameters for these magnets are included in Tables 5-2 and 5-5 for the HER and LER, respectively.

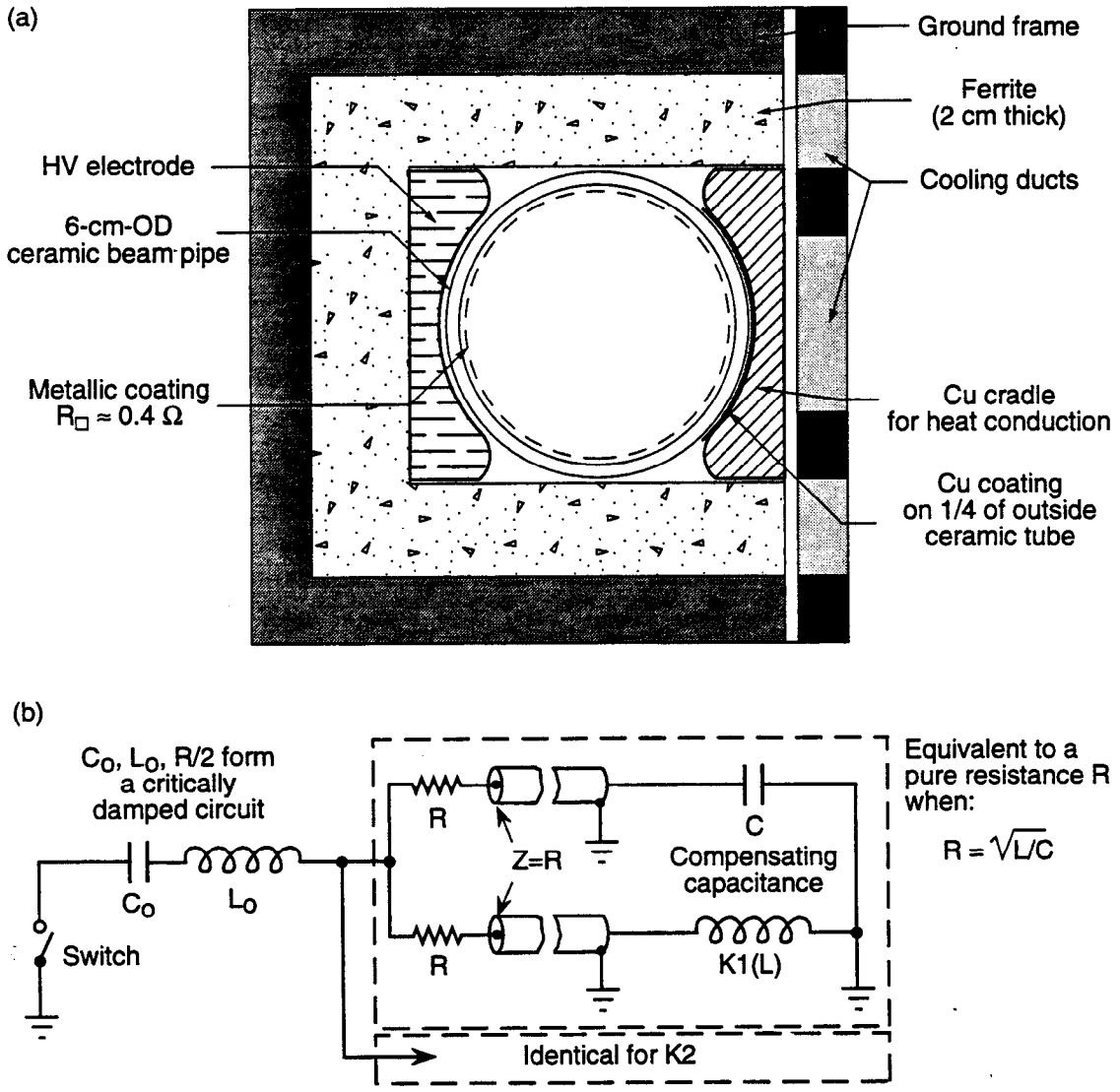

Fig. 6-30. (a) Cross section suitable for all HER and LER kickers; (b) pulsing circuit for fast kickers K1 and K2.

Table 6-6. Kicker parameters.

Ring	E_{max} (GeV)	Kick (mrad)	l (m)	B (mT)	L^a (μH)	R (Ω)	C (μF)	V (kV)	On-axis injection V (kV)
HER	10	0.13	0.75	5.8	1.0	6.6	0.023	4.0	6
LER	4	0.35	0.75	6.2	1.0	6.6	0.023	3.1	6

[a]Includes an estimate of the inductances of the leads and thyratron switch.

6.5.3 Protection of the Detector

The detector must be protected from the radiation caused both by particles lost from the stored beam and those lost due to injection inefficiencies. The relative magnitude of the problem for a high-luminosity collider may be appreciated by comparing some beam parameters of PEP-II with those of PEP and LEP (Table 6-7). Note that each time the HER and LER together lose their entire fills, 49 J/m will be deposited around the ring on average. (We refer to this circumferential average as the "fair-share" loss.) As an order-of-magnitude figure, depositing this 49 J/m into a silicon vertex detector near the beam pipe delivers about 75 rads (i.e., 0.75 J/kg). To be realistic in our estimates, we take here a 75% injection efficiency. We also assume that the 25% injection loss distributes itself around the ring evenly, so that the detector suffers its fair-share loss. In the standard injection mode, the ring will be filled roughly hourly, to bring the beam from 80% back to 100% intensity. Under these conditions, the vertex detector will receive a radiation dose of about 5 rads during each fill and an additional 15 rads associated with the beam loss between fills. Over an operating year (10^7 s), the integrated dose is thus

$$24 \text{ fills/day} \times 116 \text{ days/yr} \times 20 \text{ rad/fill} = 0.6 \times 10^5 \text{ rad/yr}$$

As 2×10^5 rads is the radiation-dose limit for the silicon vertex detector, collimators will be installed to decrease the annual dose below its fair-share amount by at least a factor of 100.

The detector must also be protected from an accident where the full injected beam is steered directly into the interaction region (IR) for any appreciable amount of time. As indicated in Table 6-7, in the case of the HER beam, the injector power (at a nominal 75% efficiency) is 650 W. Under this circumstance, the estimated radiation dose to the vertex detector would be due to 650 J/s (averaged, say, over 10 m), which corresponds to about 100 rad/s. We will deal with this possibility by installing an ionization detector (having a few-second integration time) near the IP. Exceeding a threshold of 0.1 rad/s during injection would be interlocked such that the injection rate would automatically drop from 60 to 10 pps. A manual override to 2 pps will also be possible.

Table 6-7. Comparison of stored and injected beam parameters in various machines.

	LEP	PEP	PEP-II
Charge stored in ring(s) [μC]	0.53	0.36	22.9
Energy stored in ring(s) [kJ]	24	5	108
Fair-share loss of a stored beam [J/m]	1	2	49
Injector power [W]	9	120	650[a]
Fair-share injector power [W/m]	0.003	0.05	0.3[a]

[a]HER only, assuming 1×10^{10} e^- per pulse, at 60 pps, with 75% efficiency.

As shown in Fig. 6-31, there will be three sets of IR protection collimators in each ring, located between the injection point and the detector. Details of the various collimators are summarized in Table 6-8 and discussed below. Note that a "graded-aperture" approach has been followed to protect the IR from particle losses—the aperture (in units of rms beam size) gradually increases as the IR is approached.

Collimator 1. This will be for momentum selection and beam dumping. It will consist of a pair of horizontal collimators, spaced 90° apart in betatron phase and located in a dispersive region. At the HER location shown in Fig. 6-31, $D_x = 1.2$ m and $\beta_x = 25.2$ m. A $\pm 10\sigma_x$ collimator aperture corresponds to a momentum acceptance of $\delta p/p = \pm 9 \times 10^{-3}$ for the stored HER beam.

Collimator 2. This will limit the amplitude of betatron oscillations to $10\sigma_x$ and $10\sigma_y$. Three horizontal collimators (denoted A, B, C in Fig. 6-31), spaced 60° apart in betatron phase, and three vertical collimators (A, B, C), also spaced 60° apart, are placed in a dispersion-free region. These sets of three collimators bound the 10σ beam ellipses in the two transverse planes, as shown in Fig. 6-32 (where the B and C collimators have been projected back in betatron phase to the position of the A collimator).

Collimator 3. This serves to catch any degraded particles that spray off the tips of collimator 2. It is a essentially a duplicate of the two collimator-2 sets, except that its aperture is 12σ.

As mentioned above, collimator 1 provides a momentum window that prevents a linac beam of the incorrect energy from going part way around the ring and possibly dumping near the detector. In addition, this collimator provides a place to dump the stored beam in the event of an RF trip, for example.

Due to the large stored energy (62 kJ in the HER and 46 kJ in the LER), the stored beam must be dumped in a controlled fashion. A typical ring failure might be an RF trip. The HER beam would then lose 3.6 MeV per turn and spiral into the small-aperture collimator 1 (located at a point of high dispersion) in about 20 turns. Since all other apertures are larger and are located in regions of similar or lower dispersion, the beam will be preferentially lost at collimator 1. (Even in the case of a general power failure, the magnets would maintain their fields long enough to duplicate the behavior of a simple

Table 6-8. Collimator properties.

		Horizontal collimators		Vertical collimators	
	Aperture	No.	Phase adv.	No.	Phase adv.
Injection	$12\sigma + 5$ mm	—	—	—	—
Collimator 1	10σ	2	90°	—	—
Collimator 2	10σ	3	60°	3	60°
Collimator 3	12σ	3	60°	3	60°
IR	$15\sigma + 2$ mm	—	—	—	—

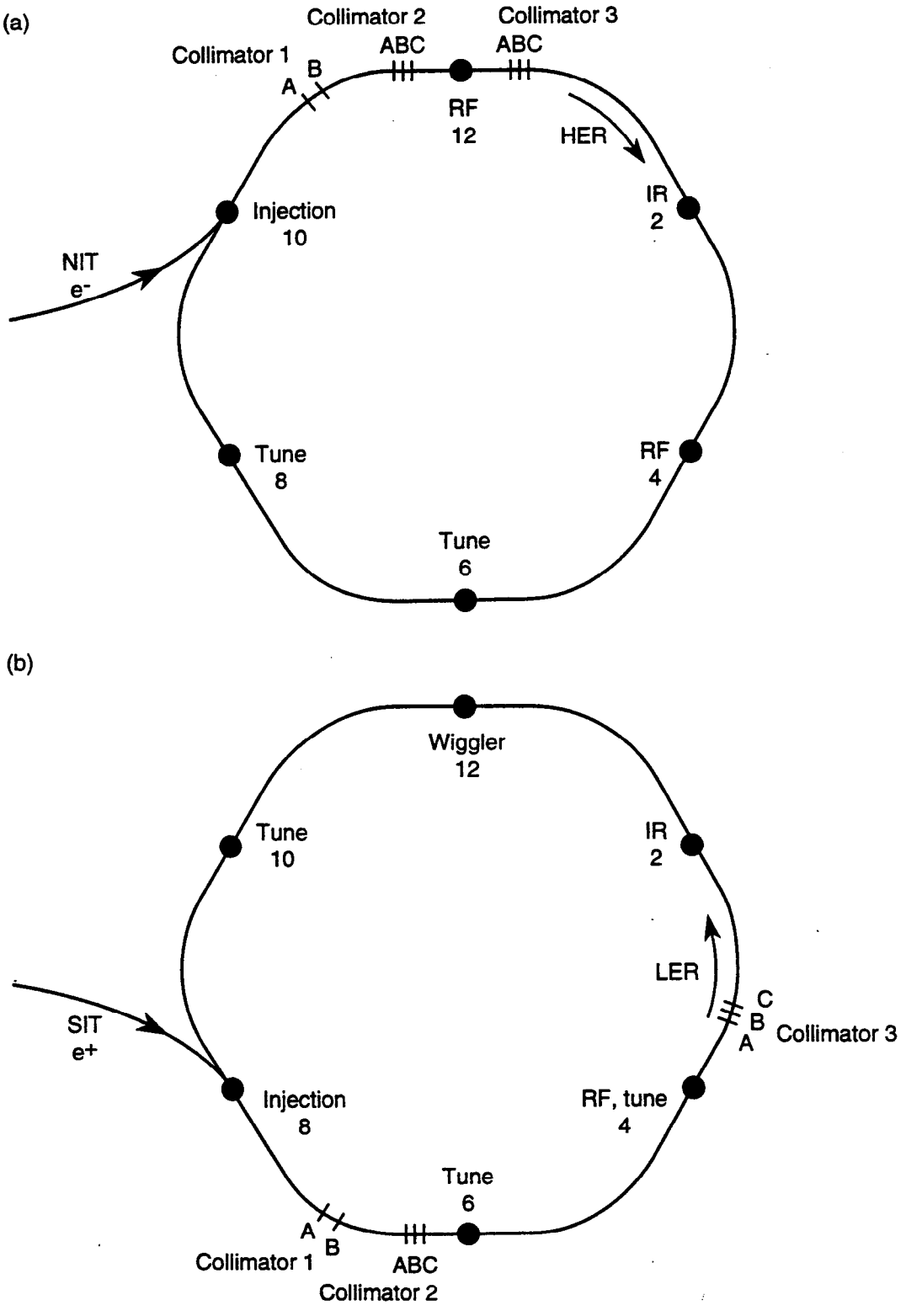

Fig. 6-31. Schematic layout of (a) the HER and (b) the LER, showing the placement of the collimator sets 1, 2, and 3.

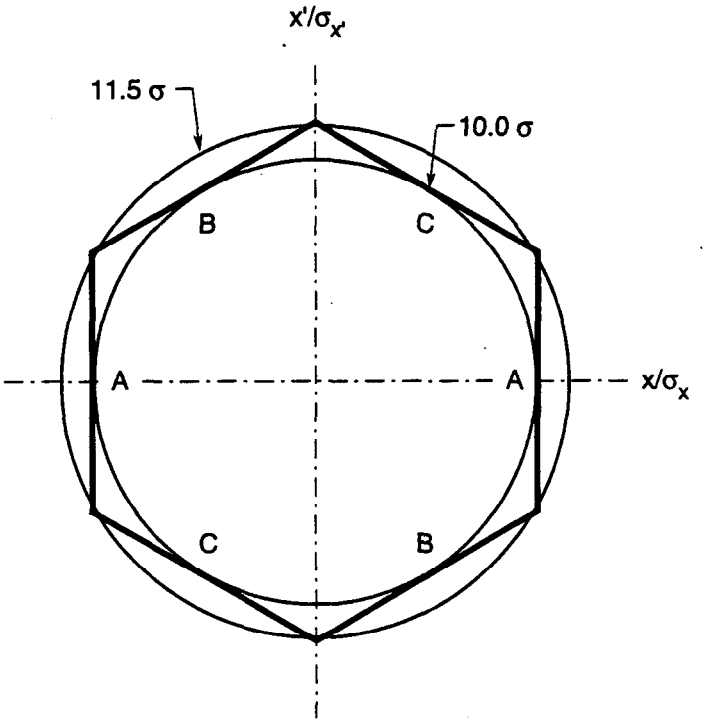

Fig. 6-32. Phase space at the location of collimator 2A. The horizontal and vertical axes have been scaled by σ and σ', respectively. The dark lines show the restrictions from collimators 2A, 2B, and 2C (the latter two projected back to the position of collimator 2A).

RF trip.) Another possible ring failure might involve one or a few steering magnets going sufficiently out of tolerance to steer the beam into something fragile. This will be protected against via the beam-loss monitors, which will detect such occurrences and purposely cause an RF trip.

To design the collimators described above, we must consider the energy deposition when the entire stored beam impinges on a single spot on the collimator (of typical beam-size dimensions) in one revolution (7.3 μs). The deposited energy will not diffuse significantly in this short time, and a very high local temperature will occur both at the surface of the struck material and more deeply inside where the shower has developed.

Figure 6-33 shows the result of an EGS calculation [Nelson, 1993] for the temperature rise of beryllium, carbon, and copper when hit by 9-GeV and 3-GeV pulses of 5×10^{10} electrons. The area of the PEP-II beam corresponds to a circular spot with $\sigma = 0.35$ mm, which is halfway between the $\sigma = 0.5$ mm and $\sigma = 0.2$ mm curves. The temperature rises shown in Fig. 6-33 must be multiplied by 900 for the HER and 1960 for the LER to scale to 4.5×10^{13} and 9.8×10^{13} particles, respectively. For the HER, Table 6-9 lists the maximum temperature reached as determined from the EGS calculation, as well as the entrance temperature due to *dE/dx* alone (that is, before the electrons have showered).

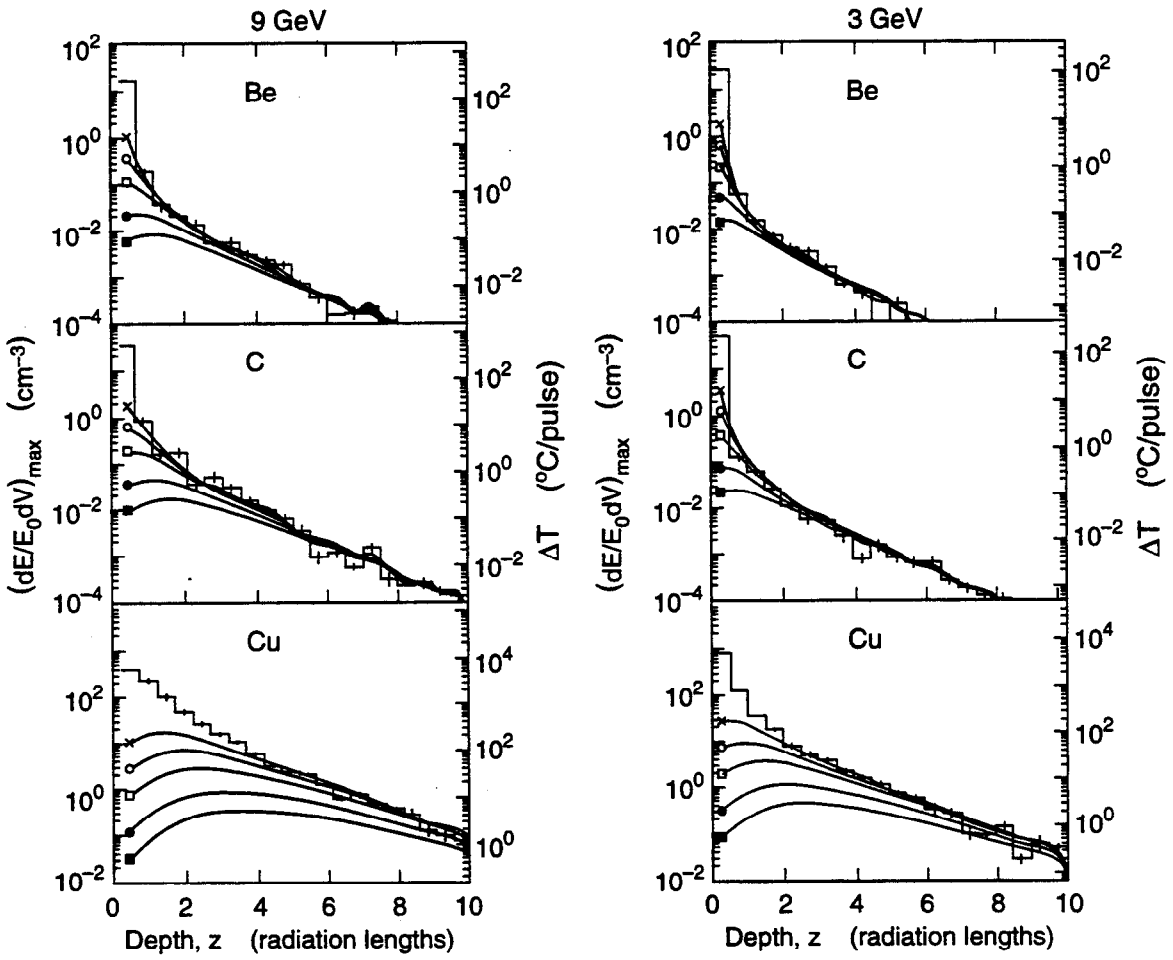

Fig. 6-33. An EGS calculation of the energy deposition and temperature rise, as a function of depth in Be, C, and Cu, for an incident pulse of 5×10^{10} electrons at 9 GeV (left column) and 3 GeV (right column). The various symbols correspond to circular bunch transverse rms size values of 0.0 (line), 0.05 (x), 0.10 (open circle), 0.20 (open box), 0.50 (filled circle), and 1.00 (filled box) mm. The area of the PEP-II beam corresponds to $\sigma = 0.35$ mm. Temperatures must be multiplied by 900 for the HER and 1960 for the LER to scale them to 4.5×10^{13} and 9.8×10^{13} stored particles, respectively.

Based on these estimates, we see that the only suitable material for the collimator (a material that will not melt in a localized dump of the ring) is carbon. A 20-radiation-length carbon collimator will be approximately 4 m long (plus some length to taper from the beam pipe diameter to the collimator hole diameter to minimize impedance and higher-order-mode losses). Movable jaws would be expensive and challenging. A simpler solution would be to have an elliptical hole through a block of carbon (machined along the length before two half-blocks were pushed together). The block could be moved out of the beam for machine physics. In the out position, the ring would be interlocked such that only a relatively small current could be stored.

Table 6-9. Predicted temperature rise from beam impact at a point. Columns 6 and 7 show the maximum temperature reached due just to dE/dx of 6.8×10^{13} electrons (9 GeV). The material begins at room temperature (27°C). Beam parameters used were $\varepsilon_x = 48$ nm·rad, $\varepsilon_y = 2$ nm·rad, $\beta_x = 8$ m, $\beta_y = 20$ m. This results in $\sigma_x = 0.6$ mm and $\sigma_y = 0.2$ mm, which is equivalent in area to a circular spot having $\sigma = 0.35$ mm. The maximum temperature reached deeper in the shower, based on an EGS calculation, is also included in column 8.

Z	A	Density (g/cm³)	dE/dx [a] (MeV·cm²/g)	dE/dx [b] (MeV·cm²/g)	Max. T [c] (°C)	Max. T [d] (°C)	Max. T [e] (°C)	Melting point (°C)
3	7	0.53	1.58	2.24	902	917	—	186
4	9	1.85	1.61	2.29	1175	1333	1100	1280
6	12	2.27	1.78	2.52	1702	2170	2200	3727
13	27	2.70	1.62	2.32	3523	3570	—	660
29	64	8.96	1.44	2.09	7468	7527	47000	1083
74	184	19.3	1.16	1.75	17946	18071	—	3410

[a]For minimum ionizing particles.
[b]Bethe-Bloch formula, $\delta = 0$.
[c]For $C_v = 6$ cal/mole-°K.
[d]For C_v from Debye theory estimate.
[e]Result from EGS calculation [Nelson, 1993].

If the decision were made to have nonadjustable collimators, then the horizontal and vertical collimators could be combined into a single cylinder, with an elliptical hole down the center. Nonadjustable collimators have the advantage of simplicity and will guarantee IR protection under all conditions—data taking, injection, accelerator physics running, and accidental beam dumps. However, there is a disadvantage in such an approach, because a decreased injection aperture will undoubtedly cause difficulties during commissioning and other nonstandard operating conditions. (This disadvantage will be partially mitigated by the enhanced capabilities of the ring BPM system, which can measure the trajectory of a single injected bunch during a single turn.)

6.5.4 Instrumentation and Control

In both the HER and LER, there will be one BPM per FODO cell (near the QD), for a total of 144 BPMs in each ring. This spacing provides roughly six orbit measurements per betatron wavelength in the HER and four per wavelength in the LER. The system

will be capable of following a single injected pulse around the ring for at least one turn. Desirable capabilities for the BPM system are:

- A particular stored or injected bunch can be followed for one turn, with each of the BPMs recording one reading
- A particular stored or injected bunch can be followed for as long as one transverse damping time (about 5000 turns); for each BPM, this requires a <7-μs ADC and a 5000-word buffer memory

To follow one particular bunch, a 4-ns analog gate or sample-and-hold circuit capable of rejecting signals from adjacent storage ring bunches is required. Because an injected pulse normally contains only 5–20% of the charge in a full bucket, the BPM and its associated electronics must be capable of measuring orbit-centroid shifts associated with currents in this range.

As shown in Figure 6-24, the injected beam must pass between the 8σ position of the septum and the 10σ aperture of the ring protection collimators. The injection line BPMs will permit the precise positioning of the injected beam in spatial coordinates and angle near the septum. The ring BPMs must be capable of determining the injected pulse position at the ring protection collimators. There is only about 1.8 mm ($2\sigma_y$, fully coupled), between the injected pulse and the collimator (at the extremes of motion). Our goal is to provide BPM sensitivity such that a single turn through a ring BPM provides a position resolution of ±0.3 mm (~1/5 of the $2\sigma_y$ injection aperture) for 5% of a full bunch charge (the minimum-size injected pulse expected). This corresponds to 0.015-mm resolution on a full ring bunch, even in the presence of adjacent bunches ±4 ns away. (If the ring BPMs were unable to accomplish this when all the bunches are approximately full, injection into the ring during top-off would be accomplished by initially filling an empty bucket in the beam gap from zero to fine-tune the injection setup.)

The dynamic range of the orbit-measuring system will be sufficient to measure from 5% of the full-bunch current (with 0.3-mm error) to twice the full-bunch current (with 0.015-mm error), or a dynamic range of 40:1. Usually, all BPM sample-and-hold circuits will be timed to look at the same bunch, but provision will be made to set the timing of individual BPMs separately so they can look at different bunches.

The horizontal position and angle at the injection point will be adjusted via the transport line optics to minimize any horizontal betatron oscillations in the ring. The vertical position and angle at the injection point will be adjusted to provide a good injection efficiency. During setup, the storage ring steering correctors will be adjusted as necessary to guide the injected beam through the center of the collimators. The ability to follow a bunch for many turns will allow an easy diagnosis of any timing mismatch between the injected bunch and the ring RF. In principle, the 144 BPMs turn the ring into a well-instrumented spectrometer that will—in conjunction with a computer model of the ring—allow the determination of the four transverse phase-space coordinates of an injected bunch.

For rapid and efficient injection, it is important that conditions for both the injected and stored beams be repeatable. Because the injection system will typically operate in top-off mode, where most of the stored beam continues to circulate in the rings, the orbits in the injection straights of the two rings can be measured and corrected back to a "golden orbit" for injection if need be. For example, the DC orbit bumps that shift the closed

orbit close to the injection septum will be adjusted to be free of residual field by automatic correction of difference orbits, in a manner similar to that used at PEP.

The lattice functions in the injection area will periodically be measured and adjusted as necessary to maintain exactly 180° of betatron phase advance between the injection kickers.

6.6 TIMING SYSTEM

For injection purposes, each ring is divided into nine "zones" of equal length. A zone has a length of about 244 m (or 815 ns) and contains 194 bunches. One of these zones in each ring will remain half empty to leave a gap for ion control. We describe here the process for filling the LER at a 60-pps rate; the HER is filled in a similar way. The transverse damping time for the HER is 37 ms. If the damping contribution of the wigglers in the LER is ignored—a worst-case situation in terms of injection—then the LER has a damping time of about 68 ms.

As shown in Fig. 6-34, the beginning of each zone is determined by the time onset of the kicker pulses. The two kickers are driven in parallel by a single pulser, consisting of a critically damped *RLC* circuit that rises and falls to practically zero within less than 1100 ns. The first bucket to be filled in zone n is located roughly 200 ns after the beginning of the kicker pulse so as to ride on the flat top, where sensitivity to time jitter is minimized. Since the rise time of the pulse is much shorter than the fall time, bunches recently stored in zone $n-1$ are unaffected. Bunches in zone $n+1$ (at least 815 ns later) are kicked slightly, but since they have been in the ring for the longest time, their orbits are almost fully damped, and, to the extent that the kickers are matched, these bumps are closed. Thus, single buckets in zones 1 through 9 are filled in succession at a 60-pps rate, and then, 150 ms later (that is, two damping times in the LER in the absence of wigglers), the next adjacent buckets (4.2 ns later) in each zone are filled, and so on. With this method, damping in the LER, even without wigglers, is quite adequate.

Compared with previous experience with PEP injection, the timing and phase jitter from the SLC damping rings will be greatly reduced by using a frequency of 476 MHz (a subharmonic of the 2856-MHz linac frequency) for the PEP-II RF systems. Timing signals from PEP-II will be completely synchronized with the SLC timing system, enabling the electron gun to fill selected S-band buckets in the linac. Our design permits the beam in the damping rings to be phase shifted on a pulse-to-pulse basis. This gives several advantages. First, it allows completely interlaced e^+ and e^- injection (using two 60-pps time slots) without loss of beam pulses during bucket transitions, and second, it minimizes the timing jitter with respect to the power line zero-crossings. Before the beam is extracted from the damping ring, it will again be phase-locked to the linac RF reference and delivered to the PEP-II ring with a pulse-to-pulse timing jitter of less than a few picoseconds. Based on past experience, the diurnal drift in the phase-lock is expected to be less than ±100 ps; studies will be made to confirm this. Should the diurnal drift prove larger, a temperature-stabilized fiber optics timing cable could be installed, which would reduce the drifts to about ±10 ps.

orbit close to the injection septum will be adjusted to be free of residual field by automatic correction of difference orbits, in a manner similar to that used at PEP.

The lattice functions in the injection area will periodically be measured and adjusted as necessary to maintain exactly 180° of betatron phase advance between the injection kickers.

6.6 TIMING SYSTEM

For injection purposes, each ring is divided into nine "zones" of equal length. A zone has a length of about 244 m (or 815 ns) and contains 194 bunches. One of these zones in each ring will remain half empty to leave a gap for ion control. We describe here the process for filling the LER at a 60-pps rate; the HER is filled in a similar way. The transverse damping time for the HER is 37 ms. If the damping contribution of the wigglers in the LER is ignored—a worst-case situation in terms of injection—then the LER has a damping time of about 68 ms.

As shown in Fig. 6-34, the beginning of each zone is determined by the time onset of the kicker pulses. The two kickers are driven in parallel by a single pulser, consisting of a critically damped *RLC* circuit that rises and falls to practically zero within less than 1100 ns. The first bucket to be filled in zone n is located roughly 200 ns after the beginning of the kicker pulse so as to ride on the flat top, where sensitivity to time jitter is minimized. Since the rise time of the pulse is much shorter than the fall time, bunches recently stored in zone $n-1$ are unaffected. Bunches in zone $n+1$ (at least 815 ns later) are kicked slightly, but since they have been in the ring for the longest time, their orbits are almost fully damped, and, to the extent that the kickers are matched, these bumps are closed. Thus, single buckets in zones 1 through 9 are filled in succession at a 60-pps rate, and then, 150 ms later (that is, two damping times in the LER in the absence of wigglers), the next adjacent buckets (4.2 ns later) in each zone are filled, and so on. With this method, damping in the LER, even without wigglers, is quite adequate.

Compared with previous experience with PEP injection, the timing and phase jitter from the SLC damping rings will be greatly reduced by using a frequency of 476 MHz (a subharmonic of the 2856-MHz linac frequency) for the PEP-II RF systems. Timing signals from PEP-II will be completely synchronized with the SLC timing system, enabling the electron gun to fill selected S-band buckets in the linac. Our design permits the beam in the damping rings to be phase shifted on a pulse-to-pulse basis. This gives several advantages. First, it allows completely interlaced e^+ and e^- injection (using two 60-pps time slots) without loss of beam pulses during bucket transitions, and second, it minimizes the timing jitter with respect to the power line zero-crossings. Before the beam is extracted from the damping ring, it will again be phase-locked to the linac RF reference and delivered to the PEP-II ring with a pulse-to-pulse timing jitter of less than a few picoseconds. Based on past experience, the diurnal drift in the phase-lock is expected to be less than ±100 ps; studies will be made to confirm this. Should the diurnal drift prove larger, a temperature-stabilized fiber optics timing cable could be installed, which would reduce the drifts to about ±10 ps.

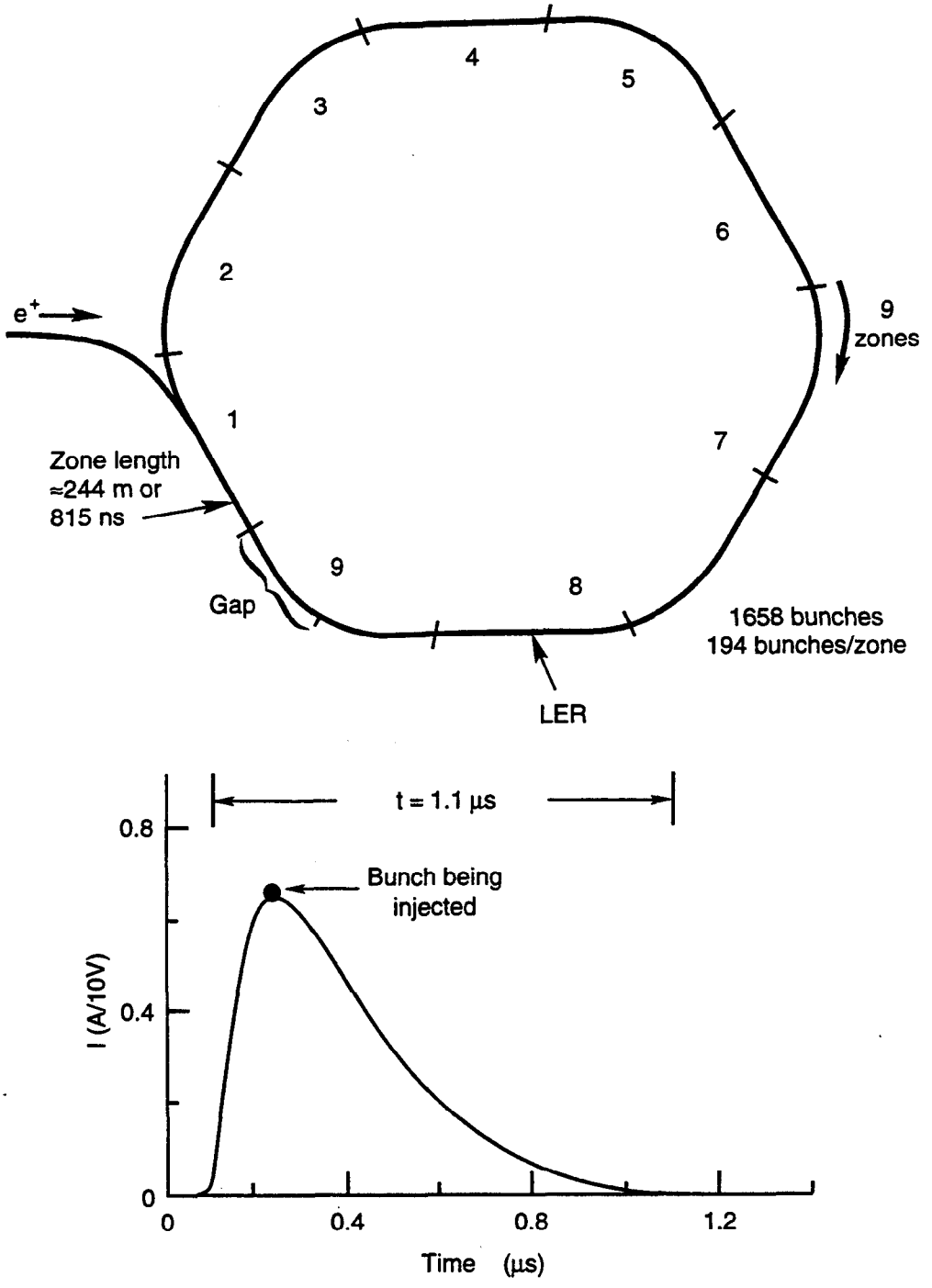

Fig. 6-34. Azimuthal zone filling sequence for the LER, showing nine zones. The kicker current pulse shown (equal for both kickers) was computed by assuming a charged, critically damped RLC circuit [$R = 2\,(L/C)^{1/2}$] in which the current reaches its maximum at $t = 2\,L/R$ after a FET-switch pulser is fired and allows the circuit to be discharged (see Fig. 6-30b).

Figure 6-35 shows schematically the layout of the injection timing system [Ronan et al., 1989]. This system transmits the linac 476-MHz reference signal from the master oscillator to the PEP-II control system, and it also sends the timing reference burst to the linac fiducial generator. Injection fiducials are transmitted to the S-band frequency dividers, the gun firing circuitry, and the damping rings. As shown in Fig. 6-36, the damping-ring phase-lock circuitry is reset by the PEP-II reference fiducial, causing a shift

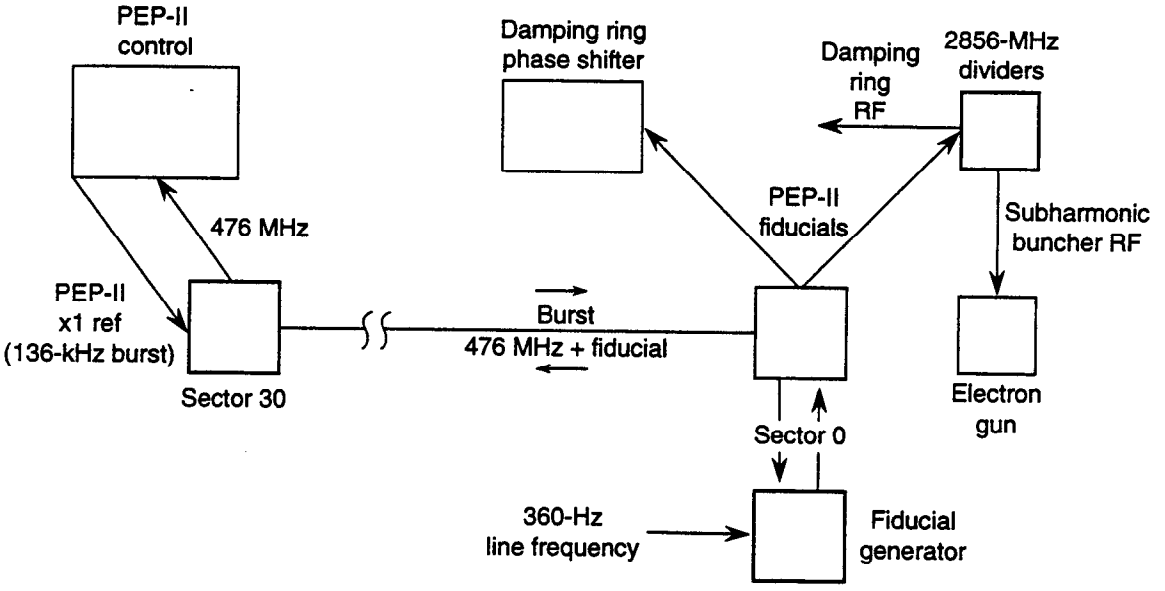

Fig. 6-35. Layout of injection timing and RF synchronization system.

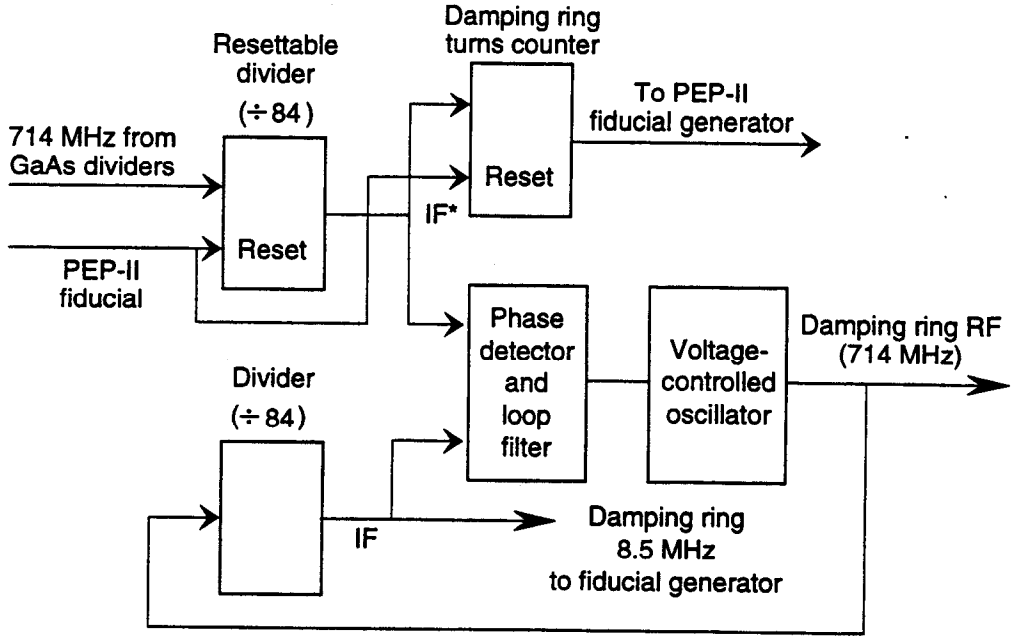

Fig. 6-36. Damping ring oscillator phase-shift circuitry.

in the revolution phase of the beam by up to half a damping-ring revolution period (or 42 damping-ring RF buckets) during an interpulse period of several milliseconds. This requires a 15-kHz shift in the damping ring frequency, which changes the orbit by only 0.1 mm—a negligible amount. The existing damping-ring phase ramp and bunch compressor maintain the phase of the extracted beam to within 0.25° at the 2856-MHz linac frequency.

The fully interlaced injection sequence is diagrammed in Fig. 6-37. When extracting $e^{\pm}$ beams from the damping rings for delivery to PEP-II, the storage ring RF bucket being filled, the bunch in the damping ring, and the damping-ring extraction kickers must all be locked to each other, as well as to the power line zero-crossing. After each delivered pulse, the PEP-II reference fiducial for the next e^+ or e^- bucket to be filled is used to reset the damping ring phase-lock circuitry, thus phasing the beam correctly for extraction on the next pulse. As the filling proceeds, e^+ and e^- bunches are continuously phase shifted for extraction and then phase-locked for delivery to the particular storage ring RF bucket being filled, thus decoupling the injection timing from the PEP-II bucket filling sequence. With this approach, the timing system places no restrictions on which bucket will be filled next, provided that the decision is made roughly 8 ms in advance. Toward the end of the filling process, the decision will be made on the basis of which buckets need more charge and on the time elapsed since they were last injected.

The entire filling sequence for the 1658 bunches will be computer controlled and automated. The selection of buckets within different zones will be done in a pattern that

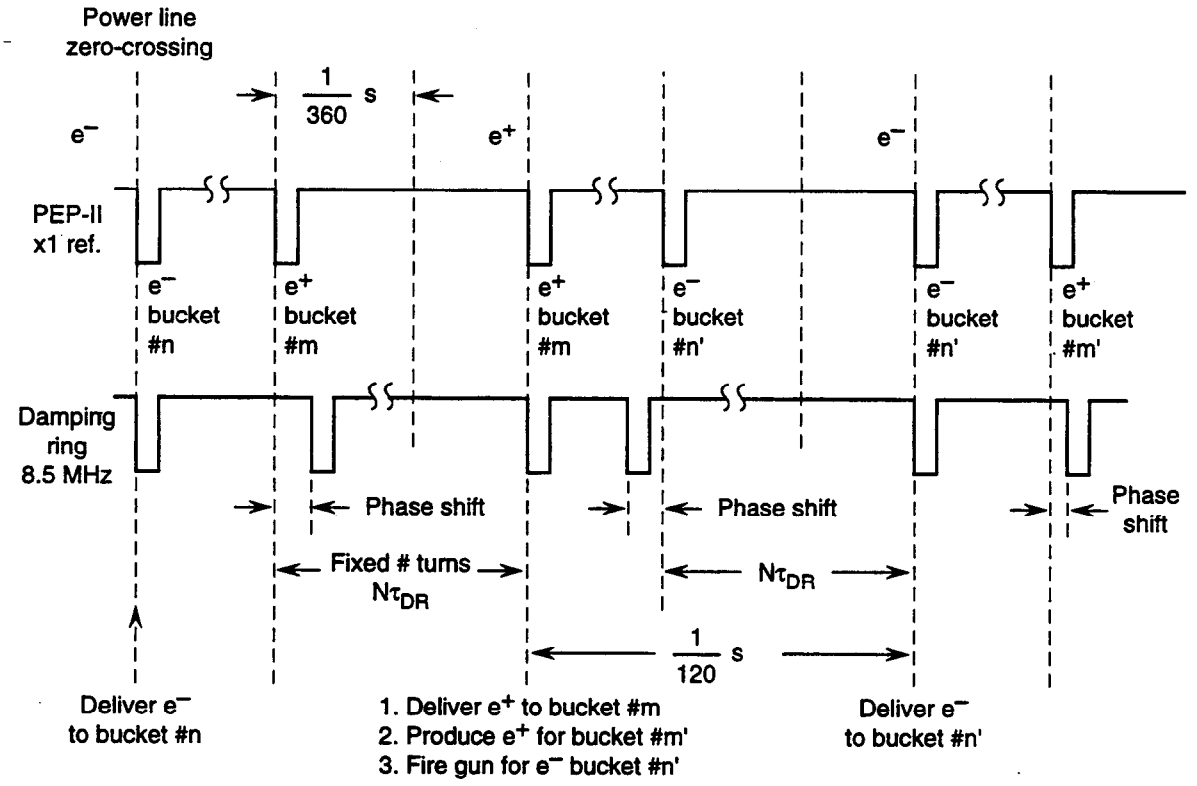

Fig. 6-37. PEP-II filling sequence.

minimizes effects due to kicker transients and allows sufficient damping time for newly injected bunches.

6.7 Optimum Time Between Fills

As part of the design for the injection system, it is useful to estimate the optimal time between injection cycles (fills). By "optimal" we mean the filling pattern that maximizes the average luminosity. Clearly, this optimal value depends on the time course of the luminosity following injection, which will be determined to some extent by the details of storage ring operation. Still, it is useful here to get a sense of the likely interval between fills. Our assumptions, stated below, are intended to err on the side of conservatism, thus yielding a worst-case estimate (smallest value) for this interval. In particular, we have taken a simple model in which the bunch sizes do not vary with time. The appropriate luminosity formula is then

$$\mathcal{L}(t) = \frac{N_{b1}(t)N_{b2}(t)n_{bi}f_i}{2\pi\sqrt{(\sigma_{x1}^{*2}+\sigma_{x2}^{*2})(\sigma_{y1}^{*2}+\sigma_{y2}^{*2})}} \tag{6-7}$$

All time-dependent terms are indicated explicitly in Eq. 6-7. The σ_{xi}^* and σ_{yi}^* are the transverse rms spot sizes at the IP. We assume here that

- Bunches are distributed such that every bunch meets an opposing bunch at the IP. Thus, $n_{b1}f_1 = n_{b2}f_2$ is the bunch collision frequency, where f_i is the revolution frequency and n_{bi} is the number of bunches for beam i.
- All bunches in a given beam have the same number of particles (N_{bi} for beam i).
- Any modifications to the above formula from beam-beam considerations, finite bunch lengths, and nonzero crossing angles are independent of time.

To the extent that the individual beams decay according to exponential decay laws, the luminosity will also decay exponentially, and the desired optimization is straightforward. However, the beams are not expected to decay in a purely exponential way. For example, in beam-gas collision processes, the loss rate is proportional to the gas pressure, which in turn depends on the beam current. For the present calculations, we make the pessimistic assumption that the pressure does not decrease as the current decreases. Then beam-gas losses yield an exponential time dependence. In addition, beam-beam scattering losses, notably $e^+e^- \rightarrow e^+e^-\gamma$ do not give an exponential luminosity dependence. However, it can be shown [Porter, 1990] that if we make the exponential approximation, with a time constant given by the exact $1/e$ decay time, then the error is at most a few percent for times of interest to us. Thus, we start with a luminosity that depends on time according to

$$\mathcal{L}(t) = \mathcal{L}_0 e^{-t/\tau} \tag{6-8}$$

The decay time τ is dominated in the present design by the bremsstrahlung and Coulomb beam-gas scattering. Including these and additional losses due to beam-beam elastic

minimizes effects due to kicker transients and allows sufficient damping time for newly injected bunches.

6.7 Optimum Time Between Fills

As part of the design for the injection system, it is useful to estimate the optimal time between injection cycles (fills). By "optimal" we mean the filling pattern that maximizes the average luminosity. Clearly, this optimal value depends on the time course of the luminosity following injection, which will be determined to some extent by the details of storage ring operation. Still, it is useful here to get a sense of the likely interval between fills. Our assumptions, stated below, are intended to err on the side of conservatism, thus yielding a worst-case estimate (smallest value) for this interval. In particular, we have taken a simple model in which the bunch sizes do not vary with time. The appropriate luminosity formula is then

$$\mathcal{L}(t) = \frac{N_{b1}(t)N_{b2}(t)n_{bi}f_i}{2\pi\sqrt{(\sigma_{x1}^{*2}+\sigma_{x2}^{*2})(\sigma_{y1}^{*2}+\sigma_{y2}^{*2})}} \tag{6-7}$$

All time-dependent terms are indicated explicitly in Eq. 6-7. The σ_{xi}^* and σ_{yi}^* are the transverse rms spot sizes at the IP. We assume here that

- Bunches are distributed such that every bunch meets an opposing bunch at the IP. Thus, $n_{b1}f_1 = n_{b2}f_2$ is the bunch collision frequency, where f_i is the revolution frequency and n_{bi} is the number of bunches for beam i.
- All bunches in a given beam have the same number of particles (N_{bi} for beam i).
- Any modifications to the above formula from beam-beam considerations, finite bunch lengths, and nonzero crossing angles are independent of time.

To the extent that the individual beams decay according to exponential decay laws, the luminosity will also decay exponentially, and the desired optimization is straightforward. However, the beams are not expected to decay in a purely exponential way. For example, in beam-gas collision processes, the loss rate is proportional to the gas pressure, which in turn depends on the beam current. For the present calculations, we make the pessimistic assumption that the pressure does not decrease as the current decreases. Then beam-gas losses yield an exponential time dependence. In addition, beam-beam scattering losses, notably $e^+e^- \rightarrow e^+e^-\gamma$ do not give an exponential luminosity dependence. However, it can be shown [Porter, 1990] that if we make the exponential approximation, with a time constant given by the exact $1/e$ decay time, then the error is at most a few percent for times of interest to us. Thus, we start with a luminosity that depends on time according to

$$\mathcal{L}(t) = \mathcal{L}_0 e^{-t/\tau} \tag{6-8}$$

The decay time τ is dominated in the present design by the bremsstrahlung and Coulomb beam-gas scattering. Including these and additional losses due to beam-beam elastic

scattering and bremsstrahlung, and those due to Touschek scattering, gives $\tau = 1.5$ hr, with the assumptions discussed above.

The scenario we envision is that a data-taking period T for the experiment is long compared with the injection time and the stored-beam time (that is, there are many such fills in a data run). In this case, it is sufficient to replace the actual distribution of injection times with a single average injection time, which we call t_I. We further assume that we take data for a fixed time interval t_c following injection, prior to beginning the next injection, and that each fill begins with the same initial luminosity ($\mathcal{L}_0$). Finally, we assume that no useful data are accumulated during injection. Given this scenario, we wish to find the optimal value for t_c.

The total integrated luminosity accumulated during our data run is given by

$$\int_0^T \mathcal{L}\, dt = n \int_0^{t_c} \mathcal{L}_0 e^{-t/\tau}\, dt \tag{6-9}$$

where $n = T/(t_c + t_I)$ is the number of injection-coast cycles in the run. The ratio of the actual integrated luminosity to that obtained if the machine were capable of running the entire time at its peak luminosity is then

$$\frac{1}{\mathcal{L}_0 T} \int_0^T \mathcal{L}\, dt = \frac{\tau}{t_c + t_I}\left(1 - e^{-t_c/\tau}\right) \tag{6-10}$$

This quantity (and hence the actual integrated luminosity) is maximized when t_c is chosen to satisfy the condition

$$\frac{t_c + t_I}{\tau} = e^{t_c/\tau} - 1 \tag{6-11}$$

Thus, the maximum average luminosity possible is

$$\langle \mathcal{L} \rangle_{\max} = \mathcal{L}_0 e^{-t_c/\tau} \tag{6-12}$$

with t_c given by Eq. 6-11.

For simplicity, we assume that the injection time required is independent of the coast time t_c. For our parameters, this is a good approximation. Thus, we assume a fixed injection time of six minutes: approximately three minutes of overhead to change both accelerator and detector states between injection and stored-beam conditions, plus about three minutes for the actual top-off.

Solving Eq. 6-11 then gives an optimal coast time between fills of about 30 minutes. This yields an average luminosity of 71% of the peak luminosity. We note that the injection conditions are nearly optimum over a rather broad range; changing the stored-beam time from its optimal value of 30 minutes to 60 minutes reduces the average luminosity by only a few percent. Increasing the average injection time to 10 minutes reduces the average luminosity to 65% of its peak value.

6.8 SUMMARY AND CONCLUSIONS

One of the main requirements to be fulfilled by a high-luminosity $e^{\pm}$ collider designed to serve as a "factory" is that its design *average* luminosity be nearly as large as its design peak luminosity. To achieve such a high average luminosity, the machine must be endowed with an $e^{\pm}$ injector that can fill it rapidly and with minimal perturbation to the experimental program. Although a number of options could be considered for the PEP-II injection system, we believe our choice is the one that makes optimum use of the unique features of the SLC linac *without taxing its capabilities*. In particular, our chosen injection system

- Exploits the low invariant vertical emittance (0.5×10^{-5} m·rad) of the single bunches from the SLC damping rings (at intensities in the range of $0.2–3 \times 10^{10}$ $e^{\pm}$) to fill both PEP-II rings, on demand, in a few minutes
- Makes electron and positron bunches at the desired energies available to any of the individual 1658 buckets in the PEP-II rings, either from zero or in top-off mode, on interleaved 60-pps time slots
- Provides a 30-GeV electron beam for high positron production rates
- Permits bunches destined for PEP-II to spend only the minimum time in the linac before being directed to separate bypass lines, thereby minimizing dilution of their six-dimensional phase space
- Requires only one bunch at a time to be stored in each damping ring, a real simplification compared with SLC operation

In addition to the benefits to PEP-II, it is important to note that the injection system described here does not preclude the SLC linac from being used for other purposes at other times, nor does it prevent the last one-third of the linac from being used simultaneously, at lower energy, for test beams or for nuclear physics experiments.

In conclusion, we believe that the proposed injection system is powerful, efficient, and flexible, that it makes cost-effective use of existing SLAC facilities, and that it meets all of the requirements of PEP-II.

7.

CONVENTIONAL FACILITIES

SINCE PEP-II will occupy the existing PEP tunnel and make use of the existing SLC linac, no conventional construction is required. Modifications will be necessary to mechanical and electrical facilities, as described below. This chapter also describes necessary removals, including the steps to be followed in disassembling and refurbishing the PEP magnets. Finally, in Section 7.2.3, the installation procedure for the new facility is given in broad outline. All conventional facilities work will conform to applicable DOE, national, and state codes and regulations, including those portions of DOE 6430.1A that pertain to PEP-II.

7.1 SITE AND UTILITIES

7.1.1 PEP Buildings and Underground Structures

The PEP conventional facilities comprise all beam housings (bored and cut-and-cover tunnels), research halls, support buildings, roads, earthwork, fencing, landscaping, AC power, mechanical utilities, sewers, and drainage facilities (see Fig. 7-1). The only changes to these facilities that will be needed to accommodate PEP-II are modifications to the cooling water system, the tunnel drainage system, and the electrical distribution system.

An Environmental Impact Statement (EIS) for PEP was issued by the Energy Research and Development Administration in 1976. Only minor modifications to the existing PEP drainage facilities will be required to comply with current regulations.

The fact that PEP lies in close proximity to known earthquake faults required a conservative seismic design. For above-ground structures, equipment, and components, the basis for seismic design was a modification of the Uniform Building Code (1976 Edition), Section 2321, such that it equals or exceeds current seismic design practices.

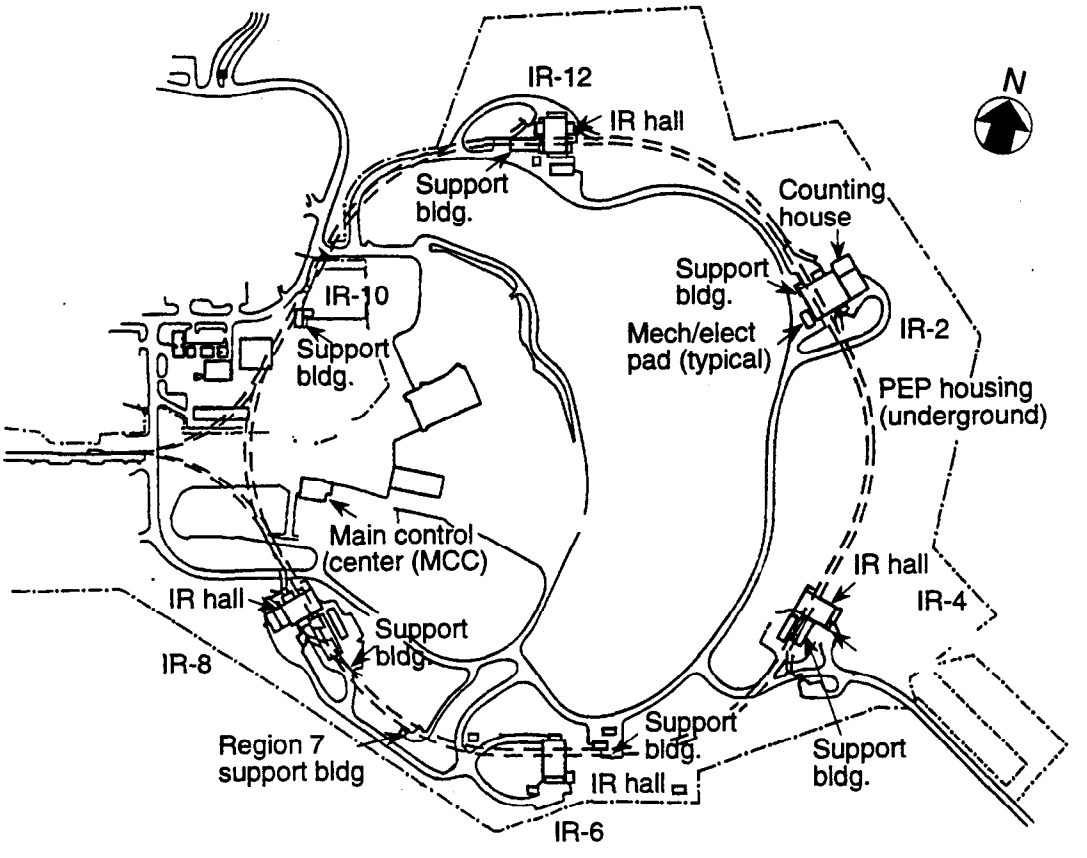

Fig. 7-1. Site map of the PEP facility.

7.1.1.1 Beam Housings. Beam housings include the PEP main ring tunnel, ring access tunnels, their junctions with the accelerator housing and the storage ring, and all penetrations into the tunnels. The underground structures were built with tunneling or cut-and-cover methods, depending on the depth underground. Beam housings are concrete lined, painted white, and have controlled ventilation. Telephone service is provided. The tunnels are protected from fire by detection and sprinkler systems. The fire-detection systems will be upgraded to current standards, as discussed in Chapter 8.

Water seepage into the PEP tunnel, primarily in regions 10 and 11, has been a problem since PEP was constructed. This water is high in mineral content, supports algae growth, and is corrosive to iron, aluminum, and some plastics. Deposits block drainage pipes, channels, and gutters. Because it was found to be uneconomical to stop the seepage, a water-management program was used consisting of equipment covers, diverting grooves, and routine maintenance of drainage systems.

A similar water-management system will be used for PEP-II. The affected areas will be thoroughly cleaned prior to installation of equipment and additional provisions for drainage will be installed where necessary. The discharge from the sumps will be routed to the sanitary sewer system to ensure long-term compliance with water-discharge regulations.

7.1.1.2 Support Buildings. Support buildings exist for instrumentation and controls (I&C) equipment at IR-2 and IR-6; for RF, I&C, and magnet power supplies at IR-4 and IR-12; and for RF, I&C, magnet power supplies, and overall operational control of the storage ring at IR-8. Additional special support buildings are located at region 7 and IR-10.

7.1.2 Mechanical Facilities

7.1.2.1 PEP Site Cooling Water. The machine components in the storage rings and the detector will be cooled by closed-loop, low-conductivity water (LCW) systems. These are, in turn, cooled by a cooling tower water (CTW) system. Existing PEP LCW water headers will be used for PEP-II; no additional headers are required.

A four-cell cooling tower is located near the Main Control Center (MCC) to provide circulating CTW to the PEP ring. The CTW is distributed to equipment pads at PEP interaction regions 2, 4, 6, 8, and 12. Each of these interaction regions has closed-loop cooling water systems including a heat exchanger to transfer the heat to the circulating CTW. Current PEP systems are designated for klystron tubes and ring magnets, RF cavities and vacuum chambers, and experimental systems.

The PEP-II heat load of 42.8 MW will need additional CTW flow, requiring all four existing pumps to operate. (This heat load is estimated assuming a conventional-collector klystron; the heat load would decrease to 37.1 MW with a depressed-collector klystron design.) One additional CTW pump will be installed to provide backup and facilitate maintenance.

The distribution of loads between the systems, both above and below ground (see Figs. 7-2 and 7-3), will be different from PEP. The heat exchangers will be replaced with suitably sized plate-type heat exchangers. The existing circulating pumps will be replaced with new appropriately sized pumps to match the PEP-II heat load distribution. The systems will be segregated such that copper and aluminum pipes are not present in the same loop.

The LCW systems will be connected to PEP-II loads as described in the following paragraphs. (The names used for the cooling systems below correspond to their current PEP functions.)

IR-2. The PEP-II detector will be installed at IR-2. The cooling water for the 3-MW detector magnet will be provided by the IR-2 experimental equipment cooling system.

IR-4. The RF-vacuum cooling system will supply cooling water to ten RF cavities, one-third of the vacuum chambers and a portion of the many magnet power supplies. The experimental equipment water systems will supply cooling to five klystron collectors. The klystron-magnet cooling system will supply cooling water to one-third of the magnets. A new closed-loop cooling system will be installed to cool the five circulators and Magic Tees.

IR-6. The experimental equipment water system will supply cooling water to one of the LER synchrotron radiation dumps.

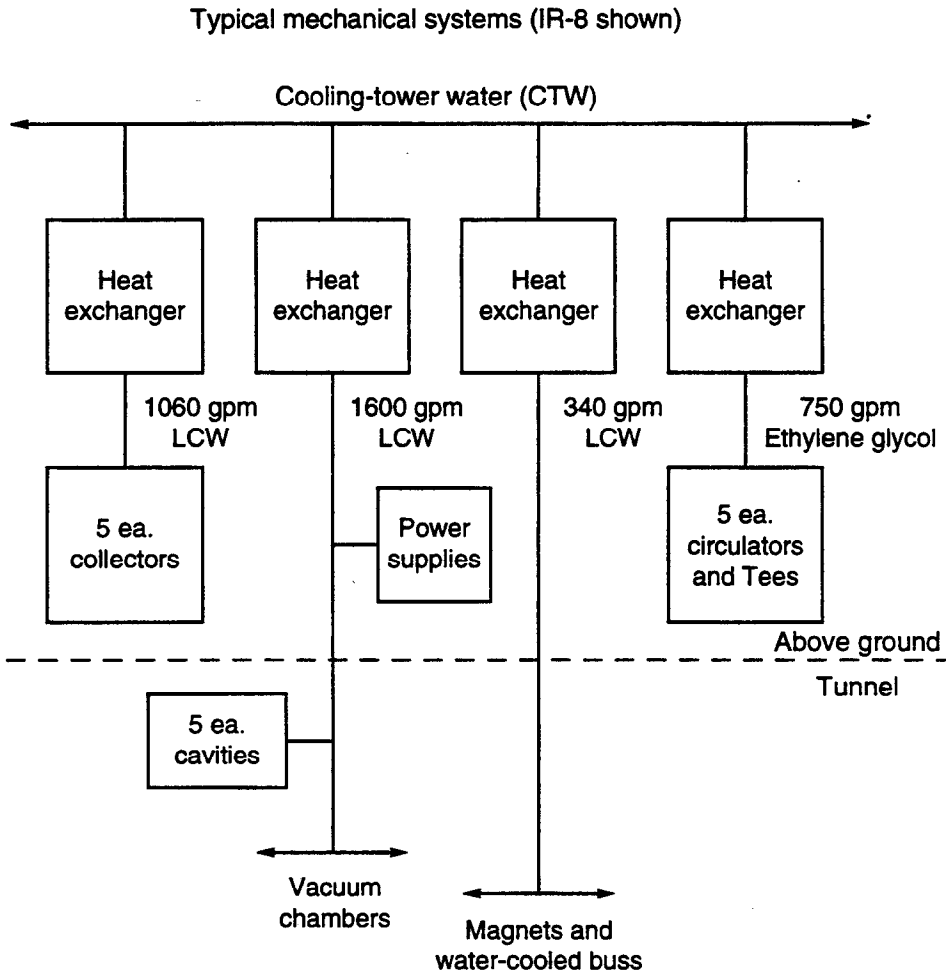

Fig. 7-2. Schematic of IR-8 cooling system.

IR-8. The RF-vacuum cooling system will supply cooling water to ten RF cavities, one-third of the vacuum chambers and some of the ring magnet power supplies. The experimental equipment water system will supply cooling to five klystron collectors. The klystron-magnet cooling system will supply cooling water to one-third of the magnets. A new closed-loop cooling system will be installed to cool the five circulators and Magic Tees.

IR-12. The RF-vacuum cooling system will supply cooling water to ten RF cavities, one-third of the vacuum chambers and the remaining ring magnet power supplies. The experimental equipment water system will supply cooling to five klystron collectors and one of the LER synchrotron radiation dumps. The klystron-magnet cooling system will supply cooling water to one-third of the magnets. A new closed-loop cooling system will be installed to cool the five circulators and Magic Tees.

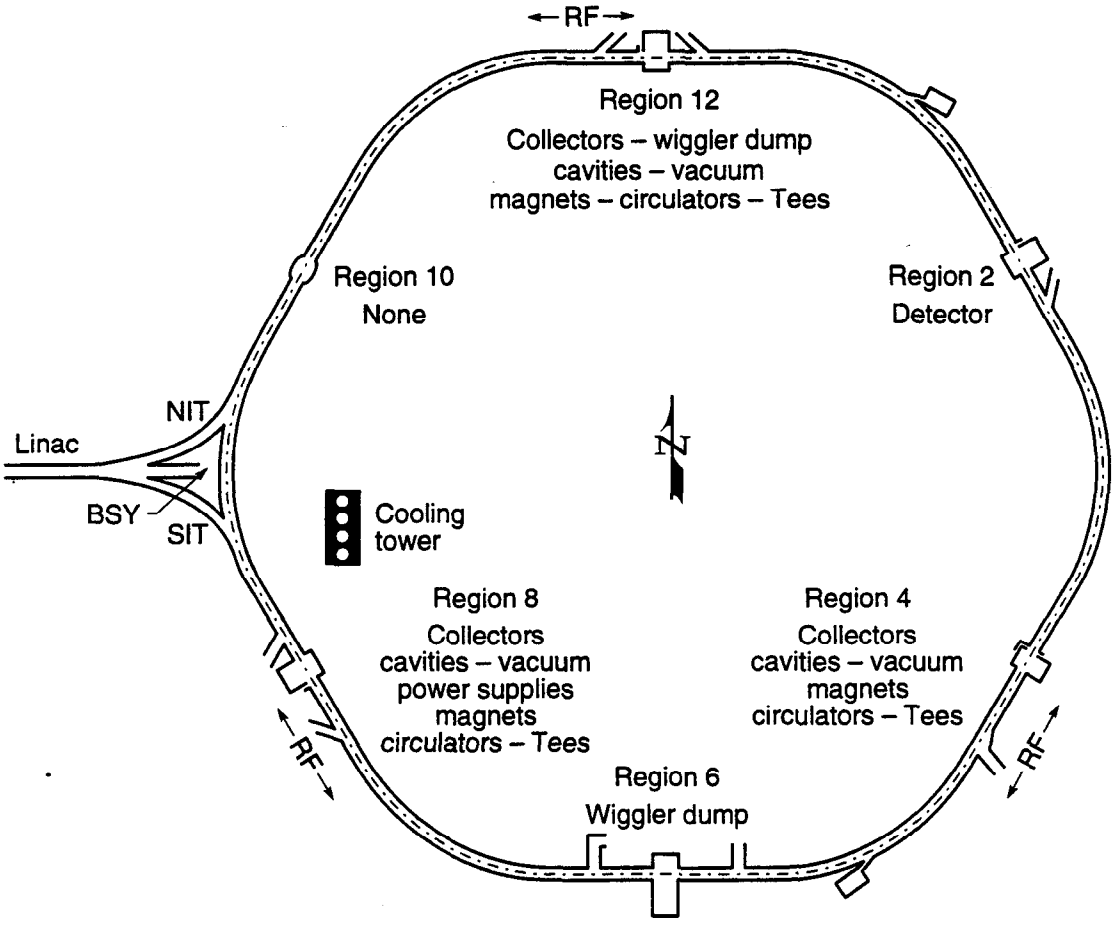

Fig. 7-3. Schematic of cooling system location.

7.1.2.2 Cooling Water for Injection System Components. The injection system magnets for PEP-II will be supplied with cooling water from existing headers in the accelerator housing and the NIT and SIT tunnels. Magnet power supplies will be located above ground and will be supplied with cooling water from existing headers.

7.1.3 Electrical Facilities

SLAC receives power from two sources: A 230-kV line with a 100-MW capacity and a standby 60-kV line with an 18-MW capacity. The two sources are asynchronous and cannot be operated in parallel. The master substation is located adjacent to Sector 30 on the south side of the linac. No expansion of the high-voltage feeders or the master substation is required for PEP-II.

The maximum electrical power demand for PEP-II will be 42.8 MW. The anticipated load is tabulated by region in Table 7-1. Electrical power to PEP-II will be distributed at 12.47 kV through the PEP duct bank to the six regional substations at regions 2, 4, 6, 8, 10, and 12.

Table 7-1. Anticipated electrical loads for PEP-II.

	Anticipated loads[a]	
Region	MW	MVA
2	4.9	6.2
4	10.9	15.2
6	1.4	1.8
8	13.3	18.0
10	0.4	0.5
12	11.9	16.5
Total	42.8	58.2

[a]Power estimated for conventional-collector klystrons. Total power would be 37.1 MW (49.2 MVA) with depressed-collector klystrons.

The PEP-II electrical power distribution system utilizes the underground duct banks of PEP. The cable capacity of this system will be increased to accommodate the higher loads of PEP-II.

7.1.4 Interaction Regions

PEP has five interaction halls designed for the assembly and operation of a large particle detector. To permit the reuse of equipment by other experimental programs, all experiments at PEP were removed. Equipment not identified for reuse has been stored for future use or salvaged in accordance with applicable ES&H guidelines. All five halls will be used for temporary storage during the disassembly of PEP and the installation of PEP-II.

Current plans are to install the detector for PEP-II in IR-2. The IR-2 experimental hall is 66 ft wide in the beam direction and 105 ft long. It is equipped with a 50-ton overhead crane. The beam height is 13.1 ft above the floor. The building can be divided into two spaces by a shielding-block wall, which makes it possible to work on a detector when it is off the beamline and beams are circulating. There is a two-story counting house on the north side of the experimental hall with 4,000 ft^2 of floor space. IR-2 has 5 MW of AC power available. The cooling water system will be expanded to handle this load by the addition of a heat exchanger.

7.2 REMOVALS AND INSTALLATIONS

7.2.1 Space Requirements

Construction of PEP-II requires that the PEP tunnel be cleared of all existing magnets and related components. Table 7-2 summarizes the components to be removed.

The covered storage and refurbishing space required for these and other components is shown in Table 7-3. The space used for PEP disassembly and HER assembly will be vacated by the time that the LER assembly space is needed. Recent tests, conducted throughout PEP, showed no residual radioactivity above background in the concrete rafts that currently support the PEP magnets. The rafts will therefore be disposed of in a conventional manner and will not require long-term covered storage. With the 40,000 ft^2 of crane-covered space already identified at SLAC (Table 7-4), no additional buildings will be required at SLAC during construction of PEP-II.

7.2.2 Disassembly and Removals

7.2.2.1 Main Tunnel. PEP disassembly will commence with the bending magnets in the water-affected area in regions 9 and 11 (see Fig. 7-1). The removal rate of these components will be two magnets or three rafts per day. At this rate, the PEP tunnel can be cleared in approximately nine months. Fixtures used for disassembly and removal will be designed to ensure that previously obtained alignment information for the bending magnet cores will be preserved.

Table 7-2. Summary of components to be removed from the PEP tunnel.

Component	Number	Weight (tons)
Bending magnets	192	1,416
Low-field bends	24	18
Quadrupoles	216	405
Insertion quadrupoles	24	207
Miscellaneous quadrupoles	48	60
Sextupoles	192	33
Concrete rafts	216	925
Miscellaneous supports	400	32
RF cavities	24	12
Vacuum chambers and components	>1,000	33
Total		3,141

Table 7-3. Space required for preinstallation, PEP disassembly, and PEP-II component assembly.

Component	Space requirement (ft^2)
PEP disassembly	
Bending magnets	10,000
Quadrupole/sextupole pairs	2,500
Miscellaneous magnets	1,500
Miscellaneous supports	2,000
Vacuum components	2,000
Miscellaneous	1,000
Total	19,000
HER assembly	
Bending magnet assembly	1,000
Quadrupole assembly	600
Quadrupole fabrication	600
Sextupole fabrication	600
Sextupole assembly	600
Support assembly	600
Mechanical measurement	1,000
Mechanical alignment	1,000
Magnetic measurement	3,000
Coil storage	1,000
Hose factory	500
Miscellaneous storage	500
Total	11,000
LER assembly	
Bending magnet assembly	1,000
Quadrupole assembly	500
Sextupole assembly	500
Support assembly	500
Mechanical measurement	500
Mechanical alignment	750
Magnetic measurement	1,000
Coil storage	500
Miscellaneous storage	250
Total	5,500

Table 7-4. Crane-covered SLAC space available for PEP-II construction activities.

Area	Space available (ft^2)
Light assembly	11,500
Heavy fabrication (center bay)	7,500
IR-2	5,200
IR-4	2,700
IR-6	4,500
IR-8	4,500
IR-12	4,100
Total	40,000

Once removed from the tunnel, the main coils, trim coils, and other ancillary equipment will be removed from the cores. The coils will be inspected for possible radiation damage and will receive an approved water-sealing coating. The cores will be inspected for damage and will be repainted. New trim coils will be wound and installed, and the magnet then reassembled. To assure the magnetic quality of these refurbished magnets, each one will be mechanically checked for twist, roll, and gap. Previous measurements at SLAC using this technique have shown that magnetic measurements are necessary only on a sample basis, provided that mechanical measurements are completed on each magnet. This procedure will be followed for the refurbished magnets.

The quadrupole-sextupole raft structure will be removed after the main bending magnets. With the bending magnets removed, the unwanted aluminum vacuum chamber will be removed. Careful attention will be given to those components that can be reused, e.g., ion pumps, vacuum gauges, and isolation valves. After the quadrupole-sextupole pairs are removed from the tunnel, they will be transported to a refurbishing area where they will be opened and the vacuum components removed. Tests will be made to determine the extent of radiation damage to the coils. If undamaged, they will be removed from the cores and resealed. The cores will then be repainted prior to reassembly.

Since the quadrupole magnets underwent magnetic measurements prior to PEP installation, it may not be necessary to remeasure each magnet. Previous data have shown that the magnetic characteristics can be duplicated, provided good mechanical measurements are taken and specific reassembly techniques are used. With the previous PEP magnetic information at hand, sample tests can be performed to ensure that the magnetic properties are preserved. The refurbished magnets can then be mounted on a new support and rough-aligned using gauges and fixtures. When the vacuum chambers and beam position monitors become available, the cores will be opened and the chamber package installed. At this time, precision mechanical alignment will be accomplished. This alignment process will be completed in a temperature-controlled area, using

precision optical alignment docks to ensure that the beam position monitors and magnet components are aligned to within a few thousands of an inch.

Generally, much of the existing PEP cable plant will be used for the HER and LER. For example, all of the vacuum system cables will remain in place and will be connected to new equipment in locations nearby. In some instances, splicing and other means may be needed to make up the required lengths. Unneeded cabling will be removed and, in some cases, stored for later reuse.

To ensure adequate documentation and control during disassembly and subsequent reassembly, bar codes will be applied and travelers will be attached to each component for tracking. A database has been set up to ensure that other information regarding these components is readily available. Data taken during PEP construction regarding mechanical and magnetic measurements can be retrieved from the database in such a way as to allow comparison of these properties.

With the tunnel housing empty, the floor will be cleared of all attachments used for PEP. New support points for PEP-II rings will be accurately placed by an alignment team. Surveys are currently under way to determine what other equipment, such as utilities, must be modified and installed once the alignment process is complete in a given section of the tunnel.

Any unneeded materials will be disposed of in accordance with applicable ES&H guidelines (see Chapter 8).

7.2.3 Installation

7.2.3.1 High-Energy Ring. Installation of the HER components (Table 7-5) will begin after alignment teams have located support points. Anchor bolts will be installed for the bending magnet supports, which will be the first components to be reinstalled for PEP-II. After the supports are grouted and aligned, the bending magnets will be installed using

Table 7-5. Inventory of HER components.

Component	Quantity	Total weight (tons)
Bending magnets	212	1,433
Quadrupoles	272	514
Sextupoles	144	26
Bending magnet supports	192	36
Quadrupole/sextupole supports	192	8
Quadrupole supports	96	6
RF cavities	20	10
Vacuum chambers	~500	72
Total		2,105

new installation fixtures. Care will be taken to ensure that all magnets are handled in an approved manner. The quadrupole-sextupole pairs on their prealigned supports will be installed in a similar way. After this, the vacuum chamber will be placed in the bending magnets and the fixed flanges made up. The final connection will be the HER flexible bellows unit. During the entire installation process, quality control measures will be undertaken to ensure that each component is installed according to written procedures. Documentation regarding the installation, fabrication, and refurbishing process of PEP-II components will also be filed in the database according to written procedures.

7.2.3.2 Low-Energy Ring. The LER components (Table 7-6) will become available after the HER is installed, owing to the fact that they must all be fabricated. Accordingly, since these magnets are installed above the HER, they will be installed on the C-frame support structure as a prealigned unit. Quality control and documentation measurements will be taken, as described for the HER.

7.2.3.3 Injector. The injector installation commences with the electron and positron extraction sections at linac Sector 4 (for positrons) and linac Sector 8 (for electrons). Short stub-lines (which connect the extraction sections to the bypass lines) are installed next, followed by the two (long) bypass lines that carry the beams to NIT and SIT. The schedule for these installation phases must mesh with the SLC downtime schedule.

The NIT and SIT lines will be reused for PEP-II. To do so, they must be joined to the bypass lines at one end and to their respective rings (HER and LER) at the other end. This final step, which can be done while the SLC is running, will complete the injector installation. Table 7-7 summarizes the components to be installed for the injection complex. Quality control and documentation measurements will be taken, as described for the HER.

Table 7-6. Inventory of LER components.

Component	Quantity	Total weight (tons)
Bending magnets	208	227
Quadrupoles	298	289
Sextupoles	144	26
Dipole/quadrupole/sextupole supports	192	77
Quadrupole supports	96	17
RF cavities	10	5
Vacuum chambers	~500	25
Total		666

Table 7-7. Inventory of injector components.

Component	Quantity	Total weight (tons)
Bending magnets	32	57
Quadrupoles	110	21
Vacuum chambers	288	11
Total		89

7.2.3.4 Cable Plant Installation. Cables will run in 4-in.-deep steel cable trays, conduits, and wireways from points of origin to terminations. Instrumentation and DC cables will extend in the air from the cable trays to the devices served; long runs will be supported. Barriers in the cable trays or separate cable trays will be used to carry conductors for different functions (for example, DC, instrumentation, AC power). All raceways will be bonded for electrical continuity.

Existing cable trays in the PEP housing will be utilized for the new cable systems. Additional cable trays will be installed to carry cables for components in the interaction region halls and in the straight sections. An additional cable tray will be installed in the PEP tunnel and new cable trays will be installed in the RF areas of the support buildings to support the RF cable plant.

Large DC Cables. Existing DC circuits in the PEP ring are capable of supplying both the HER and LER high-current magnet circuits. There are twenty-one 1-in.-OD, PVC-jacketed, water-cooled aluminum cable circuits, extending completely around the ring, with taps to power supplies and the existing magnets. Air-cooled conductors bridge the gap between the water-cooled conductors and the magnets. In addition, six air-cooled 350-MCM aluminum cables run through the same route. Existing circuits will be modified to reach the new magnet locations. Modifications will consist of jumpers in locations no longer served and taps from existing cables to new magnet locations.

Many of the existing power supplies will be reassigned or removed. Changes to the existing large DC cables will be made as appropriate.

Power supplies for HER and LER high-current magnet circuits will remain in the various IR areas. To minimize cable lengths to the magnets, power supplies for lower-current magnet circuits in the straight sections will be located in accessible areas inside the interaction halls. DC-DC converters for HER sextupole power supplies will be located in the arcs; taps from DC busses will supply these magnets.

Power supplies for the injection system magnets will be located in the RF support buildings. Cables will run in cable trays through vertical penetrations to the accelerator housing, where they will be routed to the magnets served. Additional raceways will be installed in the vertical penetrations, as needed. Cable grips will support the vertical load of cables at the entry points to raceways in the vertical penetrations.

Trim and Steering Circuits. Existing trim and steering cables will be disconnected from PEP magnets and tied back for use in the new HER circuits. For the LER trim and

steering magnets, new circuits will be run from new power supplies located at IR-2, -4, -6, -8,-10, and -12. As with the large DC cables, trim and steering cables for the injection lines will originate at power supplies in the RF support buildings.

Instrumentation and Control Cables. A wide variety of cable types will be utilized for these systems. Where practical, cables will be preassembled with connectors as complete units. In other cases, cable connectors will be installed in the field. Multiconductor instrumentation and control cables will be type TC (tray cable) and will be provided with an overall shield. Safe High-Voltage (SHV) connectors will be utilized where required. High-voltage circuits will be run separately from other circuits.

New instrumentation and control cables in the injection system will be routed through cable trays in the RF buildings to vertical penetrations, then to cable trays in the PEP-II tunnel, and thence to the instruments served.

AC Circuits. The existing AC distribution system for ring components, removed to allow the dismantling of the PEP ring, will be reinstalled in appropriate locations. Rigid steel conduits or cable trays will be used for 480-V circuits; 208Y/120-V circuits will be run in EMT or other suitable raceways. Wireways will be used for 480-V and 208Y/120-V circuits where required.

Grounding. All elements of the new rings, the IR, and the injection beamlines will be grounded to the existing SLAC ground system. Connections will be made by clamp-type connectors, for easy removal. The grounding connectors will be torqued to specifications.

8.

ENVIRONMENT, SAFETY, HEALTH, AND QUALITY ASSURANCE

SLAC has numerous environment, safety, and health (ES&H) and quality assurance (QA) programs already in place. From the ES&H and QA standpoints, PEP-II does not present any significant new challenges. All of the anticipated hazards are ones that SLAC has successfully faced during previous construction and/or experimental activities.

Installation of PEP-II in the existing PEP tunnel at SLAC will take advantage of a number of existing, mature programs, as well as proven safety features and systems. The fact that these features are already operational in the tunnel will provide an extra measure of safety during the disassembly of PEP and the installation and commissioning of PEP-II.

The SLAC programs in ES&H and QA will ensure that all aspects of the design, installation, testing, and operational phases of the project are properly managed. As appropriate, the cognizant SLAC safety committees, including the Safety Overview Committee, the Hazardous Experimental Equipment Committee, the Radiation Safety Committee, the Fire Protection Safety Committee, the Hoisting and Rigging Committee, the ALARA Committee, the Electrical Safety Committee, the Non-Ionizing Radiation Safety Committee, and the Earthquake Safety Committee [SLAC Environment and Safety Office, 1987] will review and approve various aspects of the project. All aspects of the project will conform to the applicable DOE, national, and state codes and regulations, including those aspects of DOE 6430.1A that pertain to PEP-II.

Peer and expert review have been heavily utilized to optimize the component designs and to ensure the use of best engineering practices. Ease of maintenance and reliable operation for the facility have been an integral part of the engineering design criteria.

8.1 FIRE SAFETY

The existing fire safety system in the PEP tunnel and experimental areas will remain operational throughout the installation, commissioning, and operation of PEP-II. All

The IRs in PEP were originally designed for about 20 kW of injected power at 18 GeV, though injection was always limited to 1 kW. Radiation has never been a problem at these low power levels. The PEP-II design calls for injection power levels of less than 3.2 nC/pulse × 60 pps × 10 GeV = 1.9 kW, well below the original design criterion for the IRs. (Even at the highest conceivable injection power of 8 nC/pulse × 120 pps × 10 GeV = 9.6 kW, there is a factor-of-two safety margin compared with the original PEP shielding design.) Thus, we expect little or no radiation from these areas during normal PEP-II operation.

The loss of the circulating beams in the case of the thinnest shielding (that is, a curtain wall in an IR) would result in an integrated dose-equivalent of less than 50 mrem. Since the total energy of the two circulating beams, at their maximum allowable currents of 3 A, is only 308 kJ, the potential for activating air, ground, or beamline components is very low. Operational experience with PEP and SPEAR indicates that air, ground, and beamline component activation are not significant radiological problems.

8.2.2 Personnel Protection System

The Personnel Protection System (PPS) currently in place in the PEP tunnel is designed to protect personnel from radiation, electrical, and RF hazards. This is accomplished through a system of electronically interlocked gates, lights, alarms, and operator displays and controls [Constant et al., 1977; Smith and Constant, 1981]. (See below for further discussion of electrical and RF safety considerations.) With installation of PEP-II in the tunnel, the PPS will undergo necessary upgrades and enhancements to address the new facility and operating conditions, but will remain largely the same in terms of its overall design and function. The five existing access states, as shown in Table 8-1, will be retained, as will the lighting controls and audio signals that alert personnel to a change in access state.

Because the PEP-II high- and low-energy rings (HER and LER) will be assembled within the existing PEP housing structure, and because their injection lines will occupy the existing north and south injection transport (NIT and SIT) lines, the present PPS perimeter control and interlock facility can be utilized with some modifications and upgrades. The perimeter access points into the housing tunnels from all the IR halls and the personnel and equipment tunnel access gates can be fully utilized as part of an upgraded distributed PPS system. All displays and remote control functions available in the PEP control room will be retained. In addition to interfacing with the existing hardware panels, the upgraded system will provide software-driven CRT displays and touch-panels from a dedicated distributed PPS controller system. The new upgraded system will be able to read personnel badges and grant access only to those individuals whose badges are encoded as authorized for access to the area.

The PPS stopper logic will be modified to accommodate the new HER, LER, NIT, and SIT configurations. The emergency-off button configuration will remain the same. In general, the new configurations will not impose any major new PPS logic requirements. Tone loop systems will be reconfigured to be compatible with the upgraded distributed controller logic.

areas are classified as Ordinary Hazard, Group I. The tunnel sections, interaction region (IR) halls, and support buildings are protected by automatic wet sprinkler systems and smoke detectors. The sprinkler systems are designed for a coverage of 0.15 gpm/ft^2 over 1500 ft^2. The ring is divided into twelve zones, each with its separate water supply. Six of these zones supply water to the centers of the curved (arc) sections of the tunnel. The remaining six supply water to the interaction regions. The counting houses and control room are protected by pre-action, air-supervised sprinklers activated by a smoke detection system. The support buildings in regions 4, 8, and 12 are protected by deluge sprinkler systems activated by heat-detection systems. The existing smoke detectors are of a high-voltage type that is no longer manufactured; these will be replaced with a VESDA-type detection system. This will eliminate the beam-radiation-induced false-alarm problem associated with ionization and photoelectric-type detectors. The fire alarm panels will also be replaced with improved technology.

With the exception of regions 8 through 12, each curved section of the PEP tunnel has three fans: two intake and one exhaust. Owing to the presence of above-ground structures above regions 8 through 12, the ventilation configuration there is somewhat different, with a total of five fans: two intake and three exhaust, including one double-volume exhaust fan. The fans automatically stop operating when the fire alarm sounds. The Fire Department then has the option of restarting any of the fans to provide fresh air or to exhaust smoke. The controls for this system are located on above-ground pedestals.

SLAC subcontracts with the Palo Alto Fire Department to operate an on-site fire station and to provide emergency response services. The Palo Alto Fire Department also provides ongoing fire safety inspections of SLAC facilities, as well as training of personnel.

8.2 RADIATION SAFETY

The design and operation of all facilities at SLAC are governed by the ALARA (as low as reasonably achievable) policy. Thus, SLAC has always maintained radiation dose limits below the maximum allowed by regulation.

8.2.1 Radiation Shielding

Shielding for PEP-II will conform to the Design and Control section of DOE Order 5480.11, Section 9(J) [*SLAC Radiological Control Manual*, 1993, Article 131]. The design criterion will be 1 rem/yr at 30 cm from the shield surface for normal beam losses. This assumes a 2000-hr working year and an occupancy factor of 1. In addition, SLAC internal design criteria require that (i) the boundary dose be limited to 5 mrem/yr for 7200-hr beam operation and (ii) the maximum radiation dose at 30 cm from the outer surface of the shield from an accidental beam loss not exceed 3 rem.

The PEP tunnel was originally designed for 200-GeV protons. As the shielding requirements for protons are far more stringent than those for electrons, present shielding was more than adequate for PEP operation with 18-GeV electrons and will also be adequate for PEP-II operation at its maximum values for energies and currents.

will drive fan-out distribution amplifiers in the main control room area. These, in turn, will distribute the beam-induced current signals to average-current monitors, repetition-rate monitors, and pulse-to-pulse peak-current monitors. Each current-monitoring device will generate test signals between beam pulses that will be redistributed to the beamline toroids and fed back to the processing electronics to provide a closed-loop test capability.

These beamlines will also be monitored by Protection Ion Chambers (PICs), in the same manner as is presently done in other SLAC beamlines. Other protection devices may also be needed. Protection systems will turn off beams via the existing Beam Containment System (BCS) shutoff paths.

Because the existing BCS is primarily analog in nature, it requires many careful setup adjustments to achieve the operational protection limits required by these beamlines. We are therefore exploring the possibility of upgrading the present BCS, utilizing digital-processing techniques to capture beam-pulse information and generate the necessary interlocks. The upgrade would include the use of state-of-the-art wideband preamps, flash A/Ds, serial data links, digital discrimination logic, and intelligent processors. Use of such techniques would provide rapid setup, flexibility, and improved reliability.

8.2.4 Radiation Safety Training

In accordance with SLAC's implementation plan for DOE Order 5480.11 (Radiation Protection for Occupational Workers) and the *SLAC Radiological Control Manual* [Reference Document SLAC-I-720-0A05Z-001], all SLAC employees and any persons who work at the laboratory longer than one month must receive training in radiation fundamentals through General Employee Radiological Training. In addition, those workers whose assignments make it likely that they will receive a total occupational radiation dose greater than 100 mrem in one year receive more extensive radiation safety training and are classified as Radiation Workers. Both classes of workers must be recertified every two years.

8.3 NONIONIZING RADIATION SAFETY

The RF system for PEP-II will incorporate all the safety measures that are currently in place at PEP [Allen and Karvonen, 1978]. These include the use of pressurized waveguides and strict procedures for mechanical assembly and inspection.

Each waveguide network will be pressurized with regulated 0.25-psig instrument air. Since the volumetric supply rate is limited, a leak in the waveguide will cause a drop in pressure, actuation of a pressure switch, and shutdown of the rings. After the leak is repaired, a field measurement will be made to check for RF leakage. Normal ring operation may resume when the pressure in the waveguide is restored and the RF field survey is completed.

Pressurization guards mainly against operation with a missing piece of waveguide or an improperly assembled flanged joint. Although the most likely cause of RF leakage under operating conditions is that a waveguide joint has been left open, it is possible that the system could be gas-leak-tight and not RF-leak-tight. This could occur, for example,

if the flange bolts are not tightened enough to fully compress the rubber gas seal. Thus, proper torquing of the flange bolts is necessary to prevent possible RF leakage at the flange joint.

During assembly and installation of the waveguide components, all flange bolts will be torqued and all field-assembled waveguide joints will be tested by pressurization and checked for bubbles. Joints must be free of visible bubbles. After installation, an inspector will measure the torque on a minimum of six bolts chosen at random on each flange. If the torques exceed specified levels, the inspector will then initial and date the flange joint, thus indicating that the joint is acceptable. If the joint is not acceptable, all the bolts on the flange must be retorqued and remeasured.

After the requirements for gas-leak checking and bolt torquing are satisfied, a check for RF leakage around each accessible flanged joint will be made. If the test is satisfactory, an adhesive label with the inspector's initials and the date will be applied across each joint. An intact and signed label on each waveguide joint is always a prerequisite to operational transmission of RF through a waveguide network. The coaxial connectors at the final drive amplifier and at the input to the klystron will also be surveyed for possible leakage.

When a klystron is disconnected from the waveguide between the klystron and the circulator, a cover will be bolted over the open end of the waveguide on the cavity side. The cover will be inspected and labeled, and the waveguide pressurized, before any beam can be stored in the ring. Also, a pressure switch interlock in the waveguide close to the klystron will prevent high voltage from being applied to a klystron when it is disconnected from the waveguide feeding its cavities.

PEP-II operations staff will conduct RF radiation hazard surveys periodically to ensure that the RF leakage level is less than 1 mW/cm^2.

8.4 ELECTRICAL SAFETY

It is SLAC policy that every necessary precaution is taken in the performance of work to protect all persons on the site from the risk of electrical shock and to minimize the probability of damage to property due to electrical accidents. This policy is implemented by assigning responsibility and adhering to basic safety principles, as stated in the *Environment, Safety, and Health Manual,* Chapter 8 [Reference Document SLAC-I-720-70100-100], and by complying with regulations and procedures appropriate to each operation. Appropriate electrical safety training courses are provided by the Laboratory for those workers who are likely to be exposed to high-voltage hazards.

Several PEP-II subsystems, such as the large ring power supplies, will employ high voltages. The controls and work procedures necessary to ensure safe work on these systems are well understood. The provisions for locking of these systems will utilize SLAC's established procedures for lockout and tagout. Energized equipment will be worked on only under very limited and controlled conditions, and only qualified employees will perform such work. All work will be performed in accordance with safe work practices and in accordance with OSHA 1910, Subpart S.

Special procedures are in place to permit authorized personnel to occupy areas adjacent to energized hazardous magnets. These procedures are called RASK, for

"Restricted Access Safety Key." Under these procedures, a special RASK authorization form must be filled out to obtain a key that enables the hazardous supply under test. Testing is done in accordance with written procedures. The emergency-off buttons remain active and will crash off the power supply when pushed. The RASK system will remain operational during construction of PEP-II. Thus, we will have the advantage of having this safety system in place during installation and testing of the magnets.

During the life of the PEP tunnel, there has been some damage to junction boxes and conduit due to water seepage near IR-10. Owing to the difficulty in obtaining a tight water seal in the shotcrete-lined tunnel, water flow has been managed through a series of efforts, including covering vulnerable equipment and installing drainage gutters to channel the flow of water [Weidner, 1990; see also Section 7.1.1]. No electrical accidents have occurred as a result of the water seepage. To address this continuing problem over the life of PEP-II, additional improvements to the drainage system are planned, as described in Chapter 7. Further, the entire electrical distribution system now in place will be inspected, and any elements of the system that are damaged or vulnerable to damage will be replaced and maintained in a manner that will ensure safe operation. All new electrical installations will be in accordance with current applicable codes and requirements.

8.5 CONSTRUCTION

The line organization acting through the subcontract administrator has primary responsibility for overseeing safety compliance by construction subcontractors. This responsibility includes:

- Apprising subcontractors of SLAC and DOE safety criteria prior to construction
- Conducting periodic inspections of subcontractor construction areas to evaluate the quality of the subcontractor's safety compliance program
- Receiving subcontractor accident reports and compiling information for reporting to DOE

The Quality Assurance and Compliance Department of the ES&H Division oversees the *QACD Subcontractor Oversight Program* [Reference Document SLAC-I-770-0A17A-001-R001].

8.6 EMERGENCY PREPAREDNESS

Like all experimental equipment at SLAC, PEP-II will be designed, constructed, and operated in a manner that minimizes the risk of injury to property or personnel as a result of a natural disaster or other emergency situation. In the event of any abnormal condition, the interlock system will automatically shut the machine down until the situation is diagnosed and corrected. The formal emergency planning system described in the *SLAC Emergency Preparedness Plan* [Reference Document SLAC-I-720-70000-105] will help to ensure a logical, organized, and efficient response to any emergency. It

sets forth specific steps to deal with various emergency conditions, identifies the appropriate personnel to act as resources, and provides a chain of command for responding to unplanned events.

The emergency situation most likely to arise at SLAC is an earthquake. SLAC structures are designed to withstand the effects of a major earthquake. In addition, all mechanical components of PEP-II will be secured to protect persons working nearby. This will be assured by a review of the design and installation of the experimental equipment by the SLAC Earthquake Committee, as mandated by the SLAC Safety Program. Further, as with all activities at SLAC, operation of PEP-II will be covered by the *SLAC Emergency Preparedness Plan* [1991], which outlines the procedures to be followed in the event of an earthquake severe enough to cause possible structural damage or personal injury.

8.7 ENVIRONMENTAL PROTECTION

8.7.1 Disposal of PEP Components

Disassembling PEP and making room in the tunnel for installation of PEP-II will require the removal of 925 tons of concrete rafts and hundreds of tons of other materials. The concrete rafts have been surveyed and found to be free of radioactivity other than background activity from radon (^{214}Bi, ^{214}Pb) and ^{40}K. The concrete may therefore be disposed of as nonhazardous waste. All other items will be surveyed before they are removed from the tunnel and will be handled in a manner appropriate to the level of residual radioactivity present, if any. Those materials that may be reused in PEP-II will be held in a secure area until they are reinstalled. All scrap will be disposed of in accordance with approved procedures.

8.7.2 Ongoing Environmental Protection Activities

Construction and operation of PEP-II is not expected to cause any adverse impact on the groundwater. Preservation of groundwater quality will be ensured through the implementation of the Groundwater Management Program that SLAC is currently preparing to comply with DOE Order 5400.1.

8.8 HAZARDOUS MATERIAL ISSUES

In accordance with 29 CFR 1910.1200 (the OSHA hazard communication standard), SLAC has developed a *SLAC Hazard Communication Program* [Reference Document SLAC-I-720-0A06Z-001, 1992]. Under this program, SLAC directs Department Heads and Group Leaders to conduct regular inventories of hazardous materials, to make Material Safety Data Sheets (MSDSs) available to all employees, to ensure appropriate labeling of hazardous materials, to train employees to identify and control hazards in the

workplace, and to inform users, subcontractors, and temporary employees of the hazards that may be encountered at SLAC.

8.9 DETECTOR SAFETY ISSUES

A separate Conceptual Design Report and safety evaluation will be prepared and submitted for the PEP-II detector. This discussion is intended merely to summarize the safety and environmental hazards posed by the detector and to describe the means proposed to mitigate them.

The detector for PEP-II will be similar, from a safety point of view, to particle physics detectors at many other storage rings. It is therefore possible to evaluate with some confidence potentially hazardous conditions that must be protected against. The detector systems may employ gases with a small but significant flammable component. This is also a standard situation. Safety procedures in this case involve (i) the proper venting of gases in such a way as to prevent the accumulation of explosive concentrations, (ii) the placement and proper maintenance of flammable-gas detectors on the detector itself and in the regions of gas storage and mixing, (iii) the proper siting and installation of pressure vessels, (iv) the interlocking of high voltages so as to prevent sparks that could ignite the mixture, and (v) the training of operators regarding proper safety procedures.

The final potential safety hazard is the cryogenic system associated with a superconducting solenoidal magnet if it were adopted (which presently is considered unlikely). This system must handle liquid helium to cool the magnet. Safety considerations here mainly involve prevention of spills of cryogens (liquid helium and liquid nitrogen), which could cause injury by freezing or by creating an oxygen-deprived atmosphere upon evaporation. This will be done by engineering the system such that large liquid spills can be prevented, even in the event of a major line rupture; by the installation of low-oxygen detectors; by the proper engineering of pressure vessels and attendant systems; and by extensive training of the system operators and maintenance personnel. If superconducting IR magnets were utilized for the PEP-II rings, these measures would be applied to them as well. Of course, the volume of cryogens would be much smaller for the ring magnets.

8.10 QUALITY ASSURANCE

The PEP-II project management will provide funding, staffing, thought, and time to ensure that PEP-II meets its short- and long-term performance goals. It is the responsibility of management to maintain the project's direction and to make decisions that encourage quality assurance (QA) considerations. At all levels, project management will communicate high expectations and concrete goals for the attainment of quality, and make decisions to ensure that performance objectives for both construction and operation are met. Project management will also seek out and use, as applicable, modern quality assurance, manufacturing, and reliability approaches. The project management will develop management systems that ensure that the long-term reliability, availability, and

maintainability (RAM) objectives for the entire PEP-II project (not just the individual subsystems) are attained and optimized, and that PEP-II conforms to its intended safe, functional, and environmentally-sound design. The PEP-II quality assurance strategy is described below.

Project management has used a policy of peer and expert review to monitor and guide all phases of the PEP-II design and its related R&D program. This process has been used extensively to ensure that the highest quality engineering and design practices are followed, as well as to verify that optimal technical decisions are being made. Following each review, a written report is prepared. The report is kept on file and is available for public inspection and use. Emphasis is always placed on securing the most qualified reviewers available—when local experts are not available, reviewers have been brought to SLAC from Europe and/or Japan. For example, in late 1990 four separate review teams, with experts drawn from the international community, were assembled to review the technical choices and implementation schemes for the major accelerator areas of vacuum, RF and feedback, lattice, and interaction region design. Improvements and modifications determined from the various design and R&D reviews have been incorporated, as appropriate, to optimize the PEP-II design. PEP-II management will continue this tradition of expert reviews throughout the life of the construction project.

PEP-II management is keenly aware that the "factory" nature of this project demands highly efficient operation and ease of maintenance. To ensure these goals, efficient operation and maintainability have been stressed as integral requirements for all systems. A budget for operational availability has been defined (see Section 3.4) that provides a clear target for operational efficiency for the design team.

Reporting directly to the project management, a QA manager for the PEP-II project will assist in implementing the QA effort. The QA manager will work closely with project management and subsystem managers to develop and implement the overall QA program. In accordance with the *SLAC Institutional Quality Assurance Program Plan* [Reference Document SLAC-I-770-0A17M-001] and DOE Order 5700.6C, *Quality Assurance,* the QA manager will develop a Quality Implementing Procedure (QIP) for the PEP-II project. This QIP will delineate the roles of the project management, the QA manager, the subsystem managers, and others involved in the project. The QIP will include:

- Description of the QA program (its purpose, scope, organization, and responsibilities)
- Personnel training and qualifications
- Quality improvement teams
- Documentation and records
- Work processes
- Design
- Procurement
- Inspection and testing

- Management assessments
- Independent reviews

Previous experience with other accelerators indicates that managing drawings, personnel, and administrative activities using traditional paper-based methods is slow, difficult, and labor intensive. In response to this challenge, a major effort has been under way at SLAC for over a year to develop a computerized solution. Significant progress has been made in developing a database system for managing the drawings, personnel, and administrative activities associated with the design, construction, maintenance, and operation of PEP-II. This system is very similar to a computerized approach that was successfully incorporated into the LEP project at CERN. On-line configuration control, on-line drawing availability, on-line component fabrication and operational history, and an extensive database of project personnel are all features of the application.

Although project management leads the quality assurance process and the QA manager facilitates the process, individual subsystem managers and engineers play a significant role in implementing QA objectives, including RAM objectives (see Section 3.4), for PEP-II. To foster involvement in QA of all those concerned, two types of training are planned:

(1) General QA training for the project management, subsystem managers, and engineers

(2) Specific training in quality planning, primarily for subsystem managers and engineers

The general QA training will provide an overview of modern QA principles, case studies of successfully applied techniques, and a common language to facilitate communication among all project members throughout the project's phases.

In an effort to incorporate quality assurance planning at the subsystem level, the QA program will include the use of QA milestones in project schedules. In the past, separate documents describing quality assurance issues for each subsystem have been used. The major drawback of this approach is that the documents suggest QA actions but do not provide a way for project management to verify that specified actions have been taken. The approach for PEP-II will overcome this difficulty by integrating QA milestones directly into project schedules. For example, a typical project schedule might have the following QA milestones with assigned dates and responsibilities:

- Develop drawings for the subsystem
- Review design for the subsystem
- Obtain drawing approval for the subsystem
- Submit drawings to the PEP-II database
- Develop an inspection plan
- Inspect the subsystem dimensionally
- Review dimensional inspection results

- Test the subsystem for environmental stability
- Review results of environmental stability testing
- Verify that the actual reliability of the subsystem is consistent with the reliability goals for the subsystem
- Commission the subsystem

The subsystem manager will work with project management, the QA manager, and, in some cases, other subsystem managers to develop a schedule with QA milestones. Some QA milestones, such as documentation of safety-related systems by project management, will be mandatory for all subsystems, while other QA milestones will be applicable to only a few specific subsystems. The QIP developed for PEP-II will distribute between the QA manager and subsystem managers the responsibility for determining that QA milestones have been met.

The budget presented in Chapter 9 includes the salary for the full-time QA manager, as well as funds for engineers to perform QA tasks for each subsystem. The budget includes funds for QA inspections both on site and at potential and actual vendor facilities. Detailed budgets for subsystems include funds to develop drawings, to build test fixtures, and to maintain the quality and RAM objectives of the PEP-II project.

As stated earlier, project management is committed to an ongoing process of subsystem review. Reviews will be performed by a combination of in-house and outside personnel. Reviewers will provide technical input throughout all phases of the project and ensure that best engineering practices are adhered to. Reviewers will also ensure that proper standards of not only quality but also environment, safety, and health are incorporated into designs. Since the RAM characteristics of the PEP-II project are largely a function of subsystem design, reviewers will verify that RAM-related issues have been properly considered in subsystem design.

9.

COST AND SCHEDULE

THE PEP-II project involves an upgrade of the SLAC accelerator complex. This upgrade includes construction of the PEP-II high- and low-energy rings in the existing PEP tunnel and construction of bypass lines for the electrons and positrons in the existing linac enclosure. Many PEP components will be reused in the construction of the storage rings. Although no conventional construction is required, minor modifications to the electrical and cooling-water systems are included in the project scope.

9.1 COST ESTIMATE

The PEP-II construction cost estimate was generated, and will be subsequently monitored, through a work breakdown structure (WBS), described in Section 9.3. The total construction cost in FY 1993 dollars, including contingency, is $157.4 million. This estimate is presented in Table 9-1; the associated schedule (presented in Section 9.2) assumes a "technology limited" profile, though the actual schedule may be constrained by funding limitations.

Contingency is an explicit line item that was determined after a detailed analysis of each of the major subsystems. The contingency percentage varies from system to system, depending upon the complexity of the particular system, the details of our understanding, and the status of our R&D activities. In those cases where PEP components are being duplicated, we feel justified in assigning a lower-than-average contingency. The percentage of contingency ranges from 15% (for a well-defined and well-understood magnet system) to 50% (for the less-well-defined interaction region components). The overall contingency for the project is 24%. Table 9-1 includes the individual contingency assigned to each subsystem.

9.2 CONSTRUCTION SCHEDULE

Major project milestones are listed in Table 9-2. The corresponding schedule, shown in Fig. 9-1, is based on a technology-limited funding profile. If funds are not available to

Table 9-1. Estimated cost, in FY 1993 dollars, of the PEP-II Asymmetric B Factory.

WBS code	System	Cost (FY1993 K$)	Contingency (%)	Contingency (FY1993 K$)	Total (FY1993 K$)
1	**PEP-II Asymmetric B Factory**	**127278**	**24**	**30090**	**157368**
1.1	**High-Energy Ring**	**55021**	**23**	**12690**	**67711**
1.1.1	Magnets	2705	17	459	3164
1.1.2	Power Conversion	3038	29	873	3911
1.1.3	RF	18528	28	5181	23709
1.1.4	Vacuum	18356	19	3564	21920
1.1.5	Feedback	2246	24	544	2790
1.1.6	Diagnostics	2531	20	502	3033
1.1.7	Installation	5303	23	1220	6523
1.1.8	Alignment	1072	15	161	1233
1.1.9	Supports & Stands	1242	15	186	1428
1.2	**Low-Energy Ring**	**40422**	**24**	**9837**	**50259**
1.2.1	Magnets	7084	20	1417	8501
1.2.2	Power Conversion	3017	28	854	3871
1.2.3	RF	9274	28	2594	11868
1.2.4	Vacuum	12910	25	3198	16108
1.2.5	Feedback	1336	25	331	1667
1.2.6	Diagnostics	1359	20	267	1626
1.2.7	Installation	2323	24	557	2880
1.2.8	Alignment	426	15	64	490
1.2.9	Supports & Stands	2693	21	555	3248
1.3	**Interaction Region**	**4489**	**32**	**1454**	**5943**
1.3.1	Magnets	1001	39	390	1391
1.3.2	Power Conversion	985	23	229	1214
1.3.4	Vacuum	1007	27	270	1277
1.3.6	Diagnostics	314	50	157	471
1.3.7	Installation	871	37	324	1195
1.3.9	Supports & Stands	311	27	84	395
1.4	**Injector**	**9883**	**22**	**2141**	**12024**
1.4.1	Magnets	1649	29	475	2124
1.4.2	Power Conversion	2423	17	407	2830
1.4.4	Vacuum	1301	21	272	1573
1.4.6	Diagnostics	1307	22	285	1592
1.4.7	Installation	2226	23	501	2727
1.4.8	Alignment	395	23	91	486
1.4.9	Stands and Supports	582	19	110	692

Table 9-1. Estimated cost, in FY 1993 dollars, of the PEP-II Asymmetric B Factory (continued).

WBS code	System	Cost (FY1993 K$)	Contingency (%)	Contingency (FY1993 K$)	Total (FY1993 K$)
1.5	**Control System**	**8540**	**25**	**2140**	**10680**
1.5.1	HER Controls	5150	25	1265	6415
1.5.2	LER Controls	3390	26	875	4265
1.6	**Utilities**	**4867**	**20**	**991**	**5858**
1.6.1	Electrical	2607	20	522	3129
1.6.2	Mechanical	2110	20	421	2531
1.6.3	Site Work	150	32	48	198
1.7	**Safety & Protection**	**515**	**25**	**129**	**644**
1.7.1	Accelerator	515	25	129	644
1.8	**Management**	**3540**	**20**	**708**	**4248**
1.8.1	Administration	3540	20	708	4248

maintain this schedule, the project will take longer. Note that the associated schedule for preconstruction R&D has been incorporated into the overall project schedule. That is, the schedule presented in Fig. 9-1, while based on a technology-limited scenario, takes proper account of the time required for R&D activities prior to detailed design and component fabrication.

Table 9-2. PEP-II project milestones. Q1 refers to quarter 1 of the indicated fiscal year.

Schedule	Milestone
Q1 1994	PEP-II project start
Q3 1996	Inject into first sextant - HER
Q1 1997	Inject into first sextant - LER
Q3 1997	HER complete (installed capability 1 A, 9 GeV)
Q4 1997	LER complete (installed capability 2.1 A, 3.1 GeV)
Q4 1997	Project complete
Q1 1998	Colliding-beam operation begins

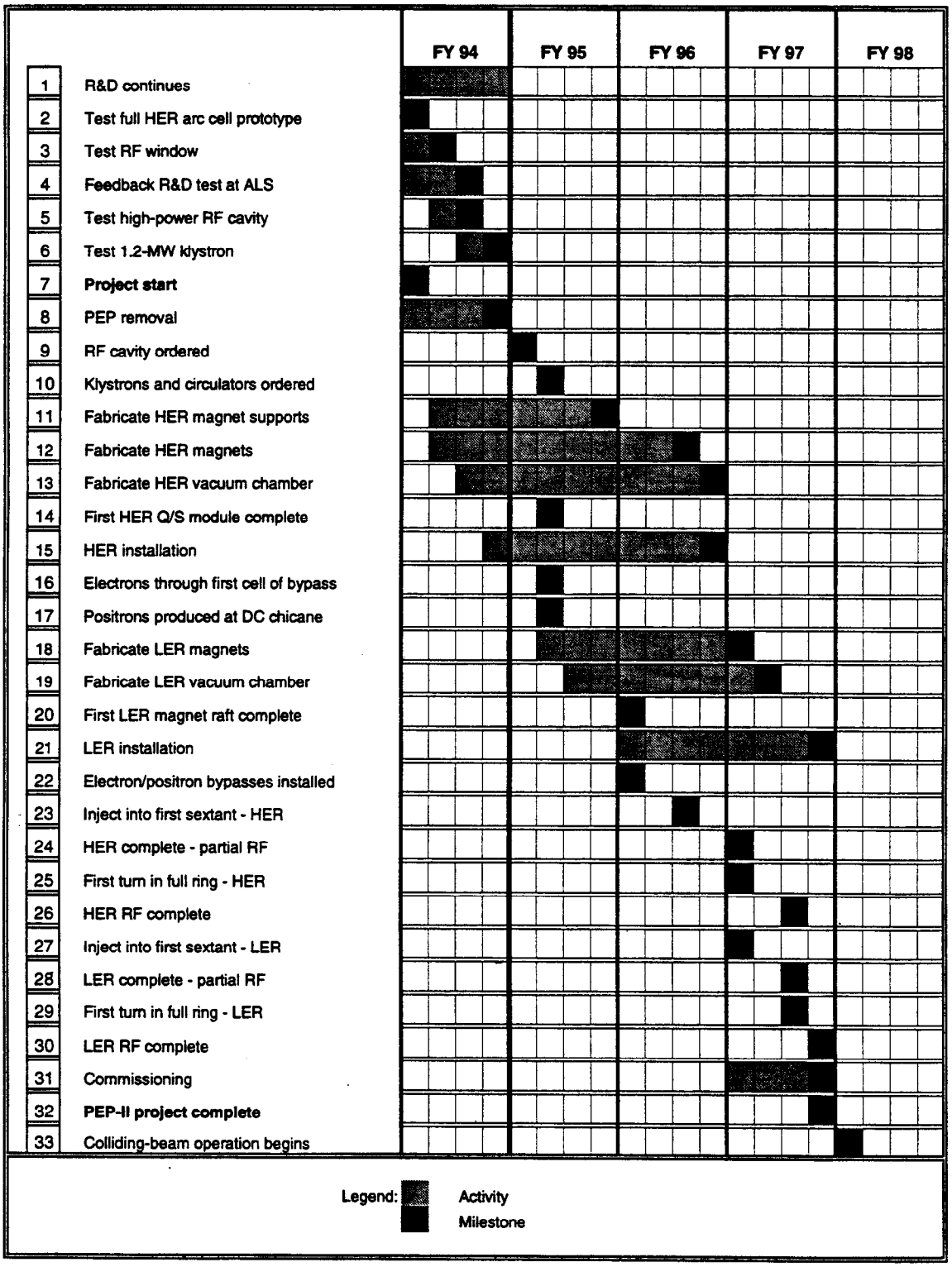

Fig. 9-1. Project schedule and construction milestones for PEP-II.

9.3 WORK BREAKDOWN STRUCTURE

The work breakdown structure was designed to be consistent with project management's need to track detailed costs of all PEP-II subsystems. It conforms to the structure used by the SLAC Accounting Office for reporting costs and commitments to PEP-II management. The levels are defined as follows:

- Level 1 = x *PEP-II*
- Level 2 = x.x *Major systems*
- Level 3 = x.x.x *Subsystems*
- Level 4 = x.x.x.x *Subsystem detail*

Definitions for levels two and three of the PEP-II WBS are given below.

1.1 High-Energy Ring (HER). PEP-II utilizes a reconfigured and refurbished PEP storage ring as the high-energy storage ring. Its nominal operating energy is 9 GeV.

1.1.1 HER Magnets. The existing PEP magnets will be refurbished and reconfigured in the PEP tunnel. Additional quadrupoles will be added to maintain the beam focusing in the long straight sections.

1.1.2 HER Power Conversion. The existing PEP large power supplies will be refurbished; additional supplies will be acquired as needed for new magnets. Monitoring systems will be constructed.

1.1.3 HER RF. New high-power, low-impedance copper cavities, driven by 1.2-MW klystrons, will be designed and fabricated or purchased. The PEP-II RF system will operate at a higher frequency (476 MHz) than the original PEP RF system (353 MHz).

1.1.4 HER Vacuum. The high circulating currents of PEP-II result in high synchrotron radiation power on the vacuum chamber wall. The existing PEP vacuum chamber will be replaced with a new copper chamber to provide the appropriate low pressure and thermal management. Costs of installation of the chamber are included here.

1.1.5 HER Feedback. To control coupled-bunch instabilities in the high-energy ring, one longitudinal and two transverse feedback systems will be employed. These will be wideband, bunch-by-bunch systems, designed and built primarily in-house but using commercially obtained power amplifiers.

1.1.6 HER Diagnostics. Beam position monitors, profile monitors, and various other beam diagnostic devices will be designed and fabricated.

1.1.7 HER Installation. The existing PEP storage ring will be disassembled, refurbished, and reassembled into its new configuration as the PEP-II HER. Mechanical, electrical, and RF installation are included here.

1.1.8 HER Alignment. The reinstallation of the PEP ring in its new configuration will require a realignment of all components.

1.1.9 HER Supports and Stands. New supports for the HER are required to lower the ring in order to accommodate the LER. These supports also incorporate the C-frame supports for the LER rafts.

1.2 Low-Energy Ring (LER). The PEP-II LER is a completely new ring having a circumference of 2200 m, to be located atop the HER in the PEP tunnel. Its nominal operating energy is 3.1 GeV.

1.2.1 LER Magnets. The LER magnet system is modeled after that of the HER, with the lengths of some of the components reduced because of the lower energy. Designs and fabrication techniques closely follow those used successfully in the construction of the PEP magnets.

1.2.2 LER Power Conversion. The bulk of the power supplies required for the LER are existing, refurbished PEP supplies.

1.2.3 LER RF. New high-power, low-impedance 476-MHz RF cavities, driven by 1.2-MW klystrons, will be fabricated or purchased for the LER. No additional penetrations or surface buildings will be required.

1.2.4 LER Vacuum. The LER vacuum system utilizes a copper beam pipe in those regions where the photon flux is high (the areas just downstream from the dipoles) and a stainless-steel beam pipe elsewhere.

1.2.5 LER Feedback. The feedback demands of the LER are comparable to those of the HER. These bunch-by-bunch feedback systems will be capable of damping both transverse and longitudinal instabilities.

1.2.6 LER Diagnostics. Beam position monitors, current monitors, profile monitors and other beam-monitoring devices and their associated electronics are included here.

1.2.7 LER Installation. The LER magnetic components will be installed on preassembled and prealigned rafts. The supports for these rafts are an extension of the HER supports. Mechanical, electrical, and RF installation are all included here.

1.2.8 LER Alignment. Conventional optical alignment tooling, already available at SLAC, will be modified to align the LER.

1.2.9 HER Supports and Stands. The magnetic elements of the LER (dipoles, quadrupoles, and sextupoles) will be prealigned on rafts in the shop.

1.3 Interaction Region (IR). PEP-II will have one interaction region, located at IR-2.

1.3.1 IR Magnets. As PEP-II consists of two separate rings, special magnets are necessary to bring the beams into collision and then to return them to their respective rings. Included here are the septum quadrupoles, as well as the permanent-magnet bending and focusing elements and their trim windings.

1.3.2 IR Power Conversion. Power supplies, as well as current-monitoring equipment are required for the septum quadrupoles, and also for some

conventional quadrupoles located in this area. Power for the permanent magnet trim windings is also included here.

1.3.4 IR Vacuum. This comprises all vacuum chamber elements in the IR, including the special thin-walled beryllium beam pipe for the detector, radial ion pumps, masks, etc.

1.3.6 IR Diagnostics. Special care must be taken to monitor the beam position and measure the luminosity in the interaction region both to maximize the luminosity and to avoid background problems.

1.3.7 IR Installation. This entry includes the costs associated with the electrical and mechanical installation of PEP-II final focusing elements, including alignment costs. The IR components will be prealigned in a support barrel to ensure proper relative alignment through the detector.

1.4 Injection System (INJ). The injector for PEP-II is the SLC linac. Separate bypass beamlines for positrons and electrons will be provided in the linac housing. These beams will be delivered to the NIT and SIT tunnels that supplied beams to PEP, and then transported to the HER and LER injection straight sections.

1.4.1 INJ Magnets. New magnets are required for the transport lines from linac Sector 4 to the SIT line (for positrons) and from linac Sector 8 to the NIT line (for electrons). Both the NIT and SIT lines will be upgraded at their entrance and exit ends.

1.4.2 INJ Power Conversion. The existing NIT and SIT line bending magnet and quadrupole power supplies will be refurbished. New trim dipole power supplies will be added, and the power supply control and monitoring equipment will be upgraded. The positron and electron bypass lines will use existing bending magnet power supplies and new quadrupole supplies. Magnet control and monitoring equipment will be all new.

1.4.4 INJ Vacuum. Roughing lines and necessary valving and piping for the bypass lines and the NIT and SIT lines are included here, as are ion pumps and their controllers.

1.4.6 INJ Diagnostics. New beam position monitors, profile monitors, and wire scanners will be installed in both the bypass lines and the NIT and SIT lines.

1.4.7 INJ Installation. Two new beam transfer lines will be installed, bypassing the linac, to transport electrons to the NIT line and positrons to the SIT line. The NIT and SIT lines will be extended and partially rebuilt to accommodate vertical injection for PEP-II.

1.4.8 INJ Alignment. The two new bypass lines must be aligned and matched to the extraction optics from the linac and the injection optics into either the NIT or the SIT line. The NIT and SIT lines require realignment, as do their injection lines into the HER and LER.

10.

SUMMARY

IN this report, we have described an updated conceptual design for the high-luminosity Asymmetric *B* Factory (PEP-II) to be built in the PEP tunnel on the SLAC site. This proposal, a collaborative effort of SLAC, LBL, and LLNL, is the culmination of more than four years of effort aimed at the design and construction of an asymmetric e^+e^- collider capable of achieving a luminosity of $\mathcal{L} = 3 \times 10^{33}\ cm^{-2}\ s^{-1}$. All aspects of the conceptual design were scrutinized in March 1991 by a DOE technical review committee chaired by Dr. L. Edward Temple. The design was deemed feasible and capable of achieving its physics goals. Furthermore, the cost estimate, schedule, and management plan for the project were fully endorsed by the committee. This updated conceptual design report captures the technical progress since the March 1991 review and reflects the lower cost estimate corresponding to the improved design. Although the PEP-II design has continued to evolve, no technical scope changes have been made that invalidate the conclusion of the DOE review.

The configuration adopted utilizes two storage rings, an electron ring operating at 9 GeV and a positron ring at 3.1 GeV, each with a circumference of 2200 m. The high-energy ring is an upgrade of the PEP storage ring at SLAC; all PEP magnets and most power supplies will be reused. The upgrade consists primarily of replacing the PEP vacuum chamber and RF system with newly designed versions optimized for the high-current environment of PEP-II. The low-energy ring will be newly constructed and will be situated atop the high-energy ring in the PEP tunnel. Utilities already installed in the PEP tunnel are largely sufficient to operate the two PEP-II storage rings.

Siting an asymmetric *B* factory at SLAC offers a number of important advantages. The existing 2200-m-circumference PEP tunnel provides sufficient space to construct the two-ring collider, and it permits a flexible design with conservative parameters. The bending radius accommodated by the arc sections, 165 m, allows the use of low-field bending magnets, thereby keeping the synchrotron radiation power density to reasonable levels (only 3.3 kW/m at the design current for the high-energy ring). The availability of six long (120-m) straight sections increases the flexibility of the design and easily accommodates the requirements for beam separation, emittance and tune control, injection, and the detector. Because the PEP tunnel was originally sized to house two rings, space is also fully adequate for the addition of the PEP-II low-energy ring. Indeed, no conventional

construction will be necessary for PEP-II, saving both cost and time in making it operational. The tunnel is adequately shielded against the additional radiation that results from high-luminosity operation, and the IR hall is sufficient to accommodate the envisioned detector and its ancillary equipment.

A unique advantage of the SLAC site is the availability of the most powerful positron injection system in the world—the SLC linac. This feature is crucial for the operation of the collider as a "factory," because maintaining a high average luminosity depends strongly on achieving rapid injection. The linac injection system is also the ideal choice in terms of the requirements of the storage ring feedback systems, because it provides a small amount of charge per injection shot, thus ensuring that the feedback systems are not overloaded by injection transients.

The design approach followed here has focused on achieving the performance goals of PEP-II in a reliable manner. This has meant designing the hardware from the outset with sufficient operating margin, as well as providing good diagnostics as part of the design. Where possible, we have adopted parameters consistent with established collider practice. For example, the required beam currents of 0.99 A and 2.14 A in the high- and low-energy rings, respectively, are split into 1658 bunches. Therefore, the single-bunch parameters (length, current, emittance, beam-beam tune shift) are all conventional and do not require any extrapolation from the operating experience of present machines.

Our choice of many low-intensity bunches, as opposed to fewer high-intensity bunches, avoids difficulties associated with single-bunch instabilities, though it does not change the need for a state-of-the-art feedback system to manage coupled-bunch instabilities. In our approach, the design challenges for PEP-II are restricted to a few selected areas. These areas, listed below, are all amenable to attack by standard engineering approaches and, though demanding, can be handled by applying and extending existing techniques in a reasonably well-understood manner.

Based on our studies, we have concentrated the design effort on those aspects where the most difficult technical challenges exist. These include

- Vacuum system
- RF system
- Multibunch feedback system
- Beam separation and detector masking system

For each of these areas, careful and systematic design work has been undertaken to identify the problems (associated mainly with the required high beam currents) and then to solve them. To ensure that our solutions are effective and appropriate, international experts in each of the above areas were brought to SLAC or LBL to review and validate our design concepts. In each case, the outcome of this process was favorable, thereby verifying the basic soundness of our design. Overall technical feasibility was subsequently confirmed by the March 1991 DOE technical review.

For the vacuum system, we have adopted a copper vacuum chamber patterned after the HERA design. Copper exhibits good thermal properties and a low rate of photon-induced gas desorption, thus ensuring a low pressure in the face of 1–2 A of beam current in each ring. Detailed estimates of photon desorption and two- and three-dimensional thermal calculations of the chamber have demonstrated that the approach is an effective one. The

required photodesorption properties of the copper adopted for fabrication have been verified at the National Synchrotron Light Source at Brookhaven National Laboratory.

The RF system is based on a standard room-temperature cavity design that includes waveguides to damp the unwanted higher-order modes of the structure. This approach has been shown (by means of three-dimensional electromagnetic calculations) to reduce the Q factors of higher-order modes to very low values that are favorable for the stabilization of coupled-bunch motions. Furthermore, experiments have been performed on a prototype PEP-II cavity that confirm the results of the calculations and demonstrate the capability of reaching, or even exceeding, the required amount of damping.

The multibunch feedback system is based on a bunch-by-bunch approach. Extensive simulations have shown that the system will perform effectively under either injection or colliding-beam conditions. The feedback system makes use of commercially available wideband power amplifiers and requires a power level of 1.5 kW for the longitudinal case and even less for the transverse case. An advantage of our approach is that the feedback system will deal with any form of bunch motion, whatever the cause. Thus, even coherent disturbances arising from the beam-beam interaction can potentially be controlled. A prototype longitudinal system has been successfully tested at both SPEAR and the ALS.

We have carefully designed a beam separation scheme to minimize detector backgrounds, and we have invested substantial effort in detailed simulations of the effects on detector background of both synchrotron radiation photons and lost electrons. This aspect is a challenge for PEP-II because we must achieve the same level of background typically found in today's colliders, but at a beam current an order of magnitude higher. Our masking design gives a factor of 84 safety margin with respect to synchrotron radiation background limitations and a factor of 20 margin with respect to lost particles. We have also shown the system to be stable against reasonable changes in our design assumptions by examining misalignments of magnets and masks.

The construction of PEP-II is an ambitious and exciting project, both as an extension of the accelerator builder's art and as a contributor to our understanding of one of the most fundamental questions in our Universe—the origin of *CP* violation. The SLAC site, with its large-circumference tunnel and the world's most powerful positron injector, is an ideal base from which to launch such a project. Moreover, the combination of the three participating laboratories, SLAC, LBL, and LLNL, offers a pool of accelerator physics, high-energy physics, and engineering expertise unmatched anywhere—a team fully capable of dealing with the challenges presented by a high-luminosity asymmetric B factory. There is, in addition, a large community of physicists worldwide who eagerly await the exceptional physics opportunities afforded by PEP-II.

The time is at hand to begin the construction of this frontier facility for high-energy physics research. Based on a four-year construction schedule, PEP-II could begin operation at the end of FY 1997. Thereafter, we envision a vigorous research effort that will last for at least 15 years and will address with unique efficacy some of the crucial problems in high-energy physics today.

ACKNOWLEDGMENTS

THIS document marks the culmination of several years of intensive R&D and design activity in support of the PEP-II project. Its technical content is a result of the high-quality work of many dedicated scientists, engineers, and designers, without whom the design of PEP-II could not have been done; computer support from the NERSC played an important role in the design work. The cooperation of the technical staff in providing the raw materials for this report did much to smooth the work of creating it. It is a great pleasure to be a member of such a team; the PEP-II Project Leader, Jonathan Dorfan from SLAC, deserves much of the credit for creating such a good working environment. Preparation of a large technical document such as this is a yeoman task in its own right and takes many people "behind the scenes." The efforts of Sylvia MacBride and Terry Anderson of the SLAC Publications Department were crucial in creating more than 300 excellent drawings. It is a pleasure to thank them for their skill and their dedication to getting the job done quickly and well. Help and advice from Vani Bustamante and Effie Clewis of the SLAC Publications Department, especially in sorting out the references, and organizational help from Bernie Lighthouse were also important. Connie Silva and Jean Wolslegel of the LBL Technical Information Department provided word-processing support for portions of the document. Their ability to quickly and accurately type difficult sections of a report is unequaled. Production of the report relied on the excellent support from members of the LBL Technical Information Department. Marilee Bailey, Alice Ramirez, and Ralph Dennis spent many hours doing the layout, and Jimmy Lovato and his crew at the LBL printing plant produced the required copies smoothly and promptly. Doug Vaughan from LBL supervised the document preparation at LBL. His editing skills and attention to detail did much to improve the contents and the presentation of the report. Coordination and transportation of the document between SLAC and LBL were cheerfully and reliably handled by Nina Adelman-Stolar and Juanita O'Malley. It is a special pleasure to thank the small "core group" of individuals, Loretta Lizama from LBL and Andrea Chan from SLAC, who together turned the many independent technical inputs into a cohesive report on the PEP-II project. Loretta organized and edited the myriad figures and spent many weeks "camped out" at SLAC to guide the document-preparation process. Her dedication and editorial prowess are noteworthy—but even more noteworthy are her good cheer and good spirit. Creating this report might well have been impossible without Loretta's help, and it certainly would have been less fun! Andrea Chan also played a crucial role, serving as production editor for the document, doing much of the technical typing, and generally making sure that the work was done promptly and properly. Her unrelenting insistence on doing things right shows up throughout the report and is one of the main reasons for its high quality. Working with people of this caliber is both an experience and an opportunity, and I would not have missed it for the world.

Michael Zisman
Berkeley, California
June 1, 1993

REFERENCES

Abrams, G., et al., 1987. Fast Energy and Energy Spectrum Feedback in the SLC Linac, in *IEEE Particle Accelerator Conference Proceedings*, Washington, D.C., p. 1258.

Albrecht, M., et al., 1987. *Physics Letters* **192B,** 245.

Alexandrov, A., A. Hutton, and P. Logatchev, 1990. *Synchrotron Radiation Power Calculations and Bending Radius Choice for the LER*, SLAC ABC-13.

Allen, M., and L. Karvonen, 1978. *Precautions against RF Radiation Leakage in PEP*, SLAC–PTM–177.

Altarelli, G., and F. Buccella, 1964. *Nuovo Cimento* **34**, 6385.

Bane, K. L., 1988. *The Calculated Longitudinal Impedance of the SLC Damping Ring*, SLAC–PUB–4618.

Bane, K. L. 1991. SLAC-PUB-5549.

Barletta, W. A., and A. Garren, 1990. *Radiation from Wigglers in the Low Energy Ring of an Asymmetric B-Factory*, SLAC-ABC NOTE 30 and LLNL Internal Report.

Barton, E., G. Eigen, D. Hitlin, and X. Liang, 1991. Private communication.

Bassetti, M., and G. A. Erskine, 1980. *Closed Expression for the Electric Field of a Two-Dimensional Gaussian Charge,* CERN–ISR–TH/80–06; see also lectures by E. Keil and G. H. Rees in *Theoretical Aspects of the Behaviour of Beams in Accelerators and Storage Rings*, CERN 77–13.

Bengtsson, T., 1992. Private communication.

Berz, M., 1989. *Particle Accelerators* **24**, 109.

Billing, M., 1993. Private communication.

Biscari, C., 1992. *Lectures at the Joint US-CERN School on Particle Accelerators*, Benalmádena, Spain, October 29–November 4, 1992.

Blinov, A. E., et al., 1988. Nuclear Instruments and Methods **A273**, 31.

Bowden, G., 1985. SLAC CN 314.

Bowden, G., 1991. *Fringe Field Representations of IP Magnets*, SLAC-ABC NOTE-46.

Bowden, G., 1993. "Permanent Magnet Quadrupole Field Errors," SLAC-PEP-II ME NOTE 4-93.

Bowden, G., and G. Putallaz, 1985. *A Positioning System for the Final Quadrupole Triplet*, Final Focus memo.

Browder, T., and M. Witherell, 1991. *Limits on Backgrounds for the B Factory Detectors*, BaBar Note-65 Rev.

Brown, K. L., et al., 1977. *TRANSPORT,* SLAC-91.

Bulos, F., 1992. PEP-II AP NOTE, 5-92.

Byrd, J. M., 1993. "Resistive Wall Instability at the PEP–II B Factory." SLAC–PEP II–AP–NOTE–9–93.

Byrd, J. M., 1993. "Study of Coupled Bunch Collective Effects in the PEP–II B Factory," SLAC–PEP II–AP–NOTE–10–93.

Carey, D. C., et al., 1982. *DECAY TURTLE,* SLAC-246.

Caspers, F., et al., 1988. *EPA Beam Vacuum Interaction and Ion Clearing System*, EPAC, Rome, Vol 2, 1324 (1988).

CERN 85-02, 1985.

CERN SL/91-29 (AP), 1991.

Chao, A. W., and J. Gareyte, 1976. *Scaling Law for Bunch Lengthening in SPEAR–II*, SLAC Note SPEAR–197, PEP–224.

Chin, Y. H., 1988. *Program MOSES, Mode-Coupling Single-Bunch Instability in Electron Storage Rings, Version 2.0,* CERN/LEP–TH/88–05.

Chin, Y. H., 1989. LBL-27665.

Chin, Y. H., 1990. "Symmetrization of the Beam-Beam Interaction," in *Beam Dynamics Issues of High Luminosity Asymmetric Collider Rings,* A. M. Sessler, ed., *AIP Conf. Proc.* **214**, 424.

Chin, Y. H., 1991a. "Parasitic Crossing at an Asymmetric B Factory, APIARY," in *IEEE Particle Accelerator Conference Proceedings*, San Francisco, CA, p. 213.

Chin, Y. H., 1991b. *Beam-Beam Dynamics During the Injection Process at the SLAC/LBL/LLNL B-Factory,* ABC-51/LBL-31434/ESG-158.

Chin, Y. H., 1992. "Effects of Parasitic Beam-Beam Interaction During the Injection Process at the PEP-II B Factory," LBL-32468, in *Proceedings of the International Conference on B Factories: The State of the Art in Accelerators, Detectors, and Physics*, Stanford, California, April 6–10, 1992, p.130.

Christenson, J., et al., 1964. *Physical Review Letters* **13,** 138.

Conciauro, G., and P. Arcioni, 1990. "A New HOM-free Accelerating Resonator," in *Proceedings of the 2nd European Particle Accelerator Conference*, Nice, France.

Constant, T. N., et al., 1977. *Operational Experience with SLAC's Beam Containment Electronics,* SLAC–1901.

Corlett, J. N., 1992. *Higher-Order Mode and Parasitic Losses to the B Factory RF Cavities,* SLAC-ABC NOTE 70.

Corlett, J. N., 1989. "Higher-Order Modes in the SRS 500 MHz Accelerating Cavities," in *Proceedings of the 1989 IEEE Particle Accelerator Conference*, Chicago, IL, p. 211.

Corlett, J. N., and S. F. Hill, 1989. *Measurement of the Damping of Higher-Order Modes in the Cavity by Waveguide Filters,* SRS/APN/89/96.

Coupal, D. P., and C. Hearty, 1990. "Detector Backgrounds from Scattered Beam Particles in the SLAC B Factory Design," in *Proceedings of the Workshop on Physics and Detector Issues for a High-Luminosity Asymmetric B Factory*, D. Hitlin, ed., SLAC-373.

de Jong, M. S., et al., 1993. *Mechanical Design Development of a 476 MHz Cavity for the PEP-II Asymmetric B Factory;* Mise au Point de La Conception Mecanique Diune Cavité A Champ de RF de 476 MHz de L'Accelerateur du Project PEP-II B Factory, AECL-10782.

Eckland, S., and G. Nelson, 1981. SLAC Collider Note CN-135 (unpublished).

Eden, J. R., and M. A. Furman, 1992a. "Assessment of the Beam-Beam Effect for Various Operating Scenarios in APIARY 6.3D," ABC-62/ESG Tech. Note 186.

Eden, J. R., and M. A. Furman, 1992b. "Further Assessment of the Beam-Beam Effect for PEP-II Designs APIARY 6.3–D and APIARY 7.5," PEP-II/AP Note 2-92/ESG Tech. Note 210.

Eden, J. R., and M. A. Furman, 1993a. "Simulation of the Beam-Beam Interaction for PEP-II with Unequal Beam-Beam Parameters," PEP-II/AP Note 6-92, ESG Tech Note 216.

Eden, J. R., and M. A. Furman, 1993b. "Simulation of the Beam-Beam Interaction with Tune Compensation," PEP-II/AP Note 4-92/ESG Tech Note 213.

Fischer, G. E., 1985. "Iron Dominated Magnets," SLAC–PUB–3726.

Fischer, G. E., 1989. *SLAC Site Geology, Ground Motion and Some Effects of the October 17, 1989 Earthquake*, SLAC–358.

Foerster, C. L., et al., 1990. *Journal of Vacuum and Science Technology A* **8**(3), 2856.

Foerster, C. L., et al., 1992. Desorption Measurements of Copper and Copper Alloys for PEP-II, in *Proceedings of the 12th International Vacuum Congress.*

Forest, E., 1993. Private communication.

Forest, E., J., Bengtsson, and M. Reusch, 1992. "DESPOT Uses n-step 'Symplectic Integrators for Thick Elements," private communication.

Forest, E., M. Berz, and J. Irwin, 1989. "Normal Form Methods for Complicated Periodic Systems: A Complete Solution Using Differential Algebra and Lie Operators," *Particle Accelerators* **24**, 91.

Funakoshi, F., et al., 1990. "Asymmetric B-Factory Project at KEK," in *Beam Dynamics Issues of High-Luminosity Asymmetric Collider Rings*, A. M. Sessler, ed., *AIP Conf. Proc.* **214,** 575.

Furman, M. A., 1991a. *The Hourglass Reduction Factor for Asymmetric Colliders*, ABC–21/ESG–161 (rev. 8/91); "Hourglass Effects for Asymmetric Colliders," in *IEEE Particle Accelerator Conference Proceedings,* San Francisco, CA, p. 422.

Furman, M. A., 1991b. *Luminosity Formulas for Asymmetric Colliders with Beam Symmetries,* ABC–25/ESG–0163.

Furman, M. A., 1993. *Beam-Beam Simulations with Displaced Beams for PEP-II*, PEP-II/AP Note 14-93/CBP Tech Note-011, revised.

Garren, A., et al., 1989. "An Asymmetric B-Meson Factory at PEP," in *Proceedings of the 1989 IEEE Particle Accelerator Conference,* Chicago, IL, p. 1847.

Glaser, W., 1956. "Electron and Ion Optics," in *Handbuch der Physik* XXXIII, S. Flügge, ed., p. 123.

Goddard, B., et al., 1992. *Measurement of Minimum Pretzel Separation as a Function of Energy*, SL-MD Note 67.

Gröbner, O., et al., 1983. *Vacuum* **33**, 397.

Halama, H. J., and Y. Guo, 1990. "Non-Evaporable Getter Investigation at the National Synchrotron Light Source," in *Proceedings of the Second Topical Conference on Vacuum Design of Synchrotron Light Sources*, Argonne National Laboratory.

Halbach, K., 1981a. *Nuclear Instruments and Methods* **187,** 107.

Halbach, K., 1981b. *Perturbation Effects in Segmented Rare-Earth Cobalt Multipole Magnets*, Lawrence Berkeley Laboratory report LBL-13221 (unpublished).

Hartill, D., 1990. "CESR B," invited talk at the International Workshop on Accelerators for Asymmetric B-Factories, KEK, October 4–6.

Hartwig, H., and J. S. Kouptsidis, 1974. "A New Approach for Computing Diode Sputter-Ion Pump Characteristics," *Journal of Vacuum and Science Technology* **11,** 1154. These design rules give satisfactory agreement with the measured performance of SLAC radial ion pumps.

Hearty, C., 1991. *OBJEGS Users' Manual*, BaBar Note 73.

Heifets, S., 1990. *Preliminary Estimate of the B Factory Impedance*, SLAC/AP–84.

Heifets, S., 1990a. *HOM Losses at the IR of the B Factory*, SLAC Note ABC-14/AP-81.

Heifets, S., 1990b. *Preliminary Estimate of B Factory Impedance*, SLAC Note ABC-21.

Heifets, S., 1991. *Broadband Impedance of the B Factory*, ABC-60.

Heins, D. et al., 1989. *Wideband Multibunch Feedback Systems for PETRA*, DESY 89-157.

Hendrickson, L., et al., 1991. *Generalized Fast Feedback System in the SLC*, SLAC-PUB-5693, presented at the International Conference on Accelerators and Large Experimental Physics Control Systems, Tsukuba, Japan.

Henke, H., and I. Wilson, 1981. *Thermal Analysis and Loss in Shunt Impedance of the LEP Accelerating Cell,* LEP Note 309.

Herb, S. W., 1985. "Field Quality and Stability of Permanent Magnet Quadrupoles," *IEEE Transactions on Nuclear Science* **NS-32,** p. 3578.

Herb, S. W., 1989. *IEEE Transactions on Nuclear Science* **NS34,** 1434.

Hermann, W., and W. Szyszko, 1989. *IEEE Transactions on Magnetics* **25,** 3278.

Hirata, K., 1990. "The Beam-Beam Interaction: Coherent Effects," in Beam Dynamics Issues of High-Luminosity Asymmetric Collider Rings, A. M. Sessler, ed., *AIP Conf. Proc.* **214,** 175.

Hitlin, D., 1989. SLAC–353/LBL PUB–5245/CALT–68–1588.

Hitlin, D., ed., 1991. *Proceedings of the Physics and Detector Issues for a High Luminosity Asymmetric B Factory Workshop* at SLAC, January–June 1990. SLAC-373/LBL PUB–30097/CALT–68–1697.

Hitlin, D., ed., 1992. *B Factories: The State of the Art in Accelerators, Detectors and Physics.*, SLAC-400.

Irwin, J., 1990. "The Application of Lie Algebra Techniques to Beam Transport Design," *Nuclear Instruments and Methods* **A298**, 460.

Irwin, J., 1992. "Simulation of Tail Distributions in Electron-Positron Circular Colliders," SLAC-PUB-5743.

Iselin, F. C., 1991. *The MAD Program (Methodical Accelerator Design) Version 8.4: User's Reference Manual*, CERN-SL-90-13-AP-REV.2, 120 (1991).

Jacob, A., G. R. Lambertson, and W. Barry, 1989. "Impedance Measurements on Button Electrodes," presented at the *IEEE Particle Accelerator Conference*, Chicago, IL, May 20–23, 1989.

Jacob, A. F., G. R. Lambertson, and W. Barry, 1990. "Higher-Order Mode Damping in an ALS Cavity," in *Proceedings of the 2nd European Particle Accelerator Conference*, Nice, France, p. 928.

Jackson, G., 1990. "Dispersive Crab Crossing: An Alternative Crossing Angle Scheme," *AIP Conf. Proc.* **214**, 327.

Jenkins, T. M., W. R. Nelson, and N. Ipe, 1990. *Synchrotron Radiation Leakage from the B-Factory Beam Pipe*, SLAC ABC Note 17.

Jurow, J., 1976. *Hot Water Bakeout Station*, PEP–Note 76-7.

Kadyk, J., 1991. *Nuclear Instruments and Methods* **A300**, 436.

Keizer, R. L., 1974. *Dipole Septum Magnet*, CERN 74-13 Laboratory I Proton Synchrotron Machine Division.

Kim, K.-J., 1986. "Angular Distribution of Undulator Power," *Nuclear Instruments and Methods* **A246**.

Ko, K., 1990. Private communication.

Krishnagopal, S., and R. H. Siemann, 1990. "A Comparison of Flat Beams with Round," in *Beam Dynamics Issues of High-Luminosity Asymmetric Collider Rings*, A. M. Sessler, ed., *AIP Conf. Proc.* **214**, 278.

Krishnagopal, S., and R. Siemann, 1990a. *Physical Review* **D41**, 2312.

Krishnagopal S., and R. Siemann, 1990b. *Physical Review* **D41**, 1741.

Krishnagopal S., and R. Siemann, 1991. *Field Calculation Algorithm for General Beam Distributions*, LBL–31094; SLAC/AP–90.

Kroll, N., and D. Yu, 1990. *Computer Determination of the External Q and Resonant Frequency of Waveguide Loaded Cavities,* SLAC–PUB–5171.

Kurennoy, S. S., 1991. *On the Coupling Impedance of a Hole or Slot,* LBL PUB-5263, SLAC-359, CALT-68-1622, March 1990.

Laslett, L. J., S. Caspi, and H. Helm, 1987. *Particle Accelerators* **22**, 1.

Laurent, J. M., 1992. Private communication.

LBL, 1986. *1-2 GeV Synchrotron Radiation Source: Conceptual Design Report,* 1986. LBL PUB–5172 Rev.

LBL, 1989. *Feasibility Study for an Asymmetric B Factory Based on PEP,* 1989. LBL PUB–5244/SLAC–352/CALT–68–1589.

LBL, 1990. *Investigation of an Asymmetric B Factory in the PEP Tunnel.* LBL PUB-5263/SLAC-359/CALT-68-1622.

Lightbody, J. W., Jr., and J. S. O'Connel, 1988. "Modeling Single-Arm Electron Scattering and Nucleon Production from Nuclei by GeV Electrons," *Computers in Physics,* May/June, p. 57.

Lisin, A., 1993. *Synchrotron Radiation Absorbers Near the IP*, PEP–II ME 3–93.

Luna, H. B., et al., 1989. *Nuclear Instruments and Methods* **A285**, 349.

Mathewson, A. G., et al., 1990. "Comparison of Synchrotron Radiation Induced Gas Desorption from Al, Stainless Steel and Cu Chambers," submitted to the Second Topical Conference on Vacuum Design of Synchrotron Light Sources, Argonne National Laboratory, November 1990.

Nelson, W. R., 1993. Unpublished results.

Nelson, W. R., G. J. Warren, and R. C. Ford, 1975. *Radiation Dose to Coil Windings and Production of Nitric Acid and Ozone from PEP Synchrotron Radiation*, PEP Note PEP–109.

Nelson, W. R., H. Hirayama, and D. W. O. Rogers, 1985. *The EGS4 Code System,* SLAC–265.

Nir, Y., et al., 1990a. *Nuclear Physics* **B345,** 301.

Nir, Y., et al., 1990b. *Nuclear Physics* **D42,** 1473.

Nir, Y., et al., 1990c. *Physics Review* **D42,** 1477.

Oddone, P. J., 1987. In Proceedings of the UCLA Workshop: Linear Collider $B\overline{B}$ Factory Conceptual Design, p. 243.

Padamsee, H., et al., 1990. "Superconducting Cavities for a B Factory—Interim Progress Report," in *Beam Dynamics Issues of High-Luminosity Asymmetric Collider Rings*, A. M. Sessler, ed., *AIP Conf. Proc.* **214**, 508.

PEP Design Handbook, 1977. Stanford Linear Accelerator Center and Lawrence Berkeley Laboratory, H. Wiedemann, ed.

Phinney, N., 1985. *Report on the SLC Control System,* SLAC-3668.

Phinney, N., and H. Shoaee, 1987. *The SLC Controls System—Status and Development,* SLAC-4215.

Porter, F., 1990. CALT–68–1611; to be published in *Nuclear Instruments and Methods A.*

Rice, D., 1989. Presentation at Third Advanced ICFA Beam Dynamics Workshop on Beam-Beam Effects in Circular Accelerators, Akademgorodok, Novosibirsk, USSR.

Rice, D., 1990. "Beam–Beam Interaction: Experimental," in *Beam Dynamics Issues of High Luminosity Asymmetric Collider Rings*, A. M. Sessler, ed., *AIP Conf. Proc.* **214**, 219.

Rivkin, L., 1987. "Collective Effects in PEP," in *Proceedings of the Workshop on PEP as a Synchrotron Radiation Source*, October 20–21, 1987, p. 139.

Rivkin, L., 1990. "B-Meson Factory in the CERN–ISR Tunnel," in *Beam Dynamics Issues of High-Luminosity Asymmetric Collider Rings*, A. M. Sessler, ed., *AIP Conf. Proc.* **214,** 536.

Rogers, D. W. O., 1984. *Health Physics* **46,** 891.

Roman, R. R., 1965. "Fabrication Techniques of Several Coils in the Zero Gradient Synchrotron Complex," in *Proceedings of the International Symposium on Magnet Technology*, Stanford, CA., p. 356.

Ronan, M. T., et al., 1989. "Timing and RF Synchronization for Filling PEP/SPEAR with the SLC Damping Rings," in *IEEE Particle Accelerator Proceedings*, Chicago, IL, p. 1577.

Rouse, F. R., et al., 1991. "A Generalized, Database Driven Fast Feedback System for the Stanford Linear Collider," in *IEEE Particle Accelerator Proceedings*, San Francisco, CA, p. 1419.

Rouse, F. R., et al., 1992. *A Database Driven Fast Feedback System for the Stanford Linear Collider*; submitted to Nuclear Instruments and Methods.

Sagan, D., R. Siemann, and S. Krishnagopal, 1990. Cornell Report CLNS 90/1001.

Sagan, D., and J. J. Welch, 1992. "The Effect of the Leakage Electrostatic Fields from the DIP on the Electron and Positron Beams," CBN 92–01.

Sands, M., 1970. *Physics of Electron Storage Rings—An Introduction*, SLAC–121.

Sands, M., 1977. *Energy Loss from Small Holes in the Vacuum Chamber*, PEP–253.

Savage, W. P., 1990. *Potential Earthquake Effect on B-Factory at PEP*, SLAC report.

Seeman, J. T., 1985. "Nonlinear Dynamics Aspects of Particle Accelerators," in *Proceedings of the Joint US–CERN School on Particle Accelerators*, Sardinia, Italy, J. M. Jowett, M. Month, and S. Turner, eds., *Springer-Verlag Lecture Notes in Physics* **247**, p. 121.

Siemann, R., 1993. unpublished results.

SLAC, 1991. *An Asymmetric B Factory Based on PEP: Conceptual Design Report*, 1991. LBL PUB–5303/SLAC-372/CALT–68-1715/UCRL–ID–106426/UC-IIRPA-91–01, (1991).

SLAC Earthquake Emergency Plan, 1987.

SLAC Emergency Preparedness Plan, 1991.

SLAC Emergency Preparedness Plan, SLAC-I-720-70000-105.

SLAC Environment and Safety Office, 1987. *SLAC Safety Program.*

SLAC Environment, Safety, and Health Manual, I-720-70100-100.

SLAC Hazard Communication Program, 1992, SLAC-I-720-0A06Z-001.

SLAC Institutional Quality Assurance Program Plan, SLAC-I-770-0A17M-001.

SLAC QACD Subcontractor Oversight Program, SLAC 1-770-0A17A-001-R001.

SLAC Radiological Control Manual, 1993. SLAC-I-720-0A05Z-001.

SLAC Radiological Control Manual, 1993. Article 131.

Smith, H., and T. Constant, 1981. *Radiation and Electrical Safety Systems for PEP,* SLAC-2675.

Spencer, J. E., 1985. SLAC-PUB 3647.

Tavares, P. F., 1992. *Transverse Distribution of Ions Trapped in an Electron Beam,* CERN-PS/92–55 (LP).

Taylor, B., 1990. Private communication.

Tennyson, J. L., 1989. "TRS," undocumented code, unpublished.

Tennyson, J. L., 1990. "The Beam-Beam Limit in Asymmetric Colliders: Optimization of the B-Factory Parameter Base," in *Beam Dynamics Issues of High Luminosity Asymmetric Collider Rings*, A. M. Sessler, ed., *AIP Conf. Proc.* **214**, 130.

Tennyson, J. L., 1991a. *Long-Range Forces in APIARY–6*, ABC Note 28.

Tennyson, J. L., 1991b. *Choosing the APIARY-6 Tunes: Luminosity Considerations*, ABC Note 29.

Ueda, S., et al., 1990. "Photodesorption from Stainless-Steel, Aluminum Alloy, and Oxygen-Free Copper Test Chambers," submitted to Proceedings of Second Topical Conference on Vacuum Design of Synchrotron Light Sources, Argonne National Laboratory.

Van Bibber, K., 1989. *Nuclear Instruments and Methods* **B40/41,** 436.

Villevald, D., 1993. *Ion Trapping in the SLAC B Factory High Energy Ring*. SLAC PEP-II AP Note 18-93.

Voelker, F., et al., 1990. "Techniques for Beam Impedance Measurements Above Cutoff," in the *Proceedings of the European Particle Accelerator Conference,* Nice, France, June 12–16, LBL-28190.

Voelker, F., G. Lambertson, and R. Rimmer, 1991. "Higher Order Mode Damping in a Pill Box Cavity," *US Particle Accelerator Physics Conference Proceedings*, San Francisco, CA, May 6–9, p. 687.

Walker, N., 1993. Private communication.

Warnock, R., and R. Ruth, 1992. "Long-term Bounds on Nonlinear Hamiltonian Motion," *Physica D* **56**, 188. See also J. Berg, R. Warnock, R. Ruth, and E. Forest, *Construction of Sympletic Maps for Nonlinear Motion of Particles in Accelerators*, SLAC–PUB–6037 and LBL–34035, 1993.

Weaver, J. N., 1981. *Measuring, Calculating and Estimating PEP's Parasitic Mode Loss Parameters*, PEP-Note-342.

Weidner, H., 1990. *Seepage into PEP Tunnel,* SLAC-ABC-10.

Winch, T.R., 1977. *Bakeout Tests for 14 m Chamber*, PEP–Note 77–3.

Zholents, A. A., 1990. "Novosibirsk B Factory," in *Beam Dynamics Issues of High-Luminosity Asymmetric Collider Rings*, A. M. Sessler, ed., *AIP Conf. Proc.* **214**, 592.

Zisman, M. S., 1990a. In *Beam Dynamics Issues of High-Luminosity Asymmetric Collider Rings*, A. M. Sessler, ed., *AIP Conf. Proc.* **214**, 81.

Zisman, M. S., 1990b. *Influence of Collective Effects on the Performance of High Luminosity Colliders*, ABC Note 8.

Zisman, M. S., et al., 1988. *Study of Collective Effects for the PEP Low-Emittance Optics*, LBL-25582, SSRL ACD Note-59.

Zisman, M. S., S. Chattopadhyay, and J. Bisognano, 1986. *ZAP User's Manual*, LBL-21270.

APPENDIX A: PARAMETERS

THIS appendix contains a summary of the PEP-II accelerator parameters. It is intended to give a self-consistent snapshot of the machine design. As such, values are often given to more precision than would ultimately be relevant (or even measurable) in an operating accelerator. We start with a few specific comments on the tables to follow:

General Machine Parameters. As is conventional, we quote the luminosity at zero bunch length, constrained by design to be 3.00×10^{33} cm^{-2} s^{-1}. If we take into account the geometric effect of a nonzero bunch length, the luminosity is reduced by about 7% to 2.80×10^{33} cm^{-2} s^{-1}.

The $1/e$ luminosity decay time is estimated under the conservative assumption that the spot sizes remain constant, i.e., that the luminosity goes like the product of the two beam currents. It includes beam loss estimates from $e^+e^- \rightarrow e^+e^-$, $e^+e^- \rightarrow e^+e^-\gamma$, beam-gas bremsstrahlung, beam-gas Coulomb scattering, and Touschek intrabeam scattering. These estimates are made for a ten-standard-deviation limiting transverse aperture (for an uncoupled beam horizontally and a fully coupled beam vertically).

Lattice Cell Parameters. There are four "standard straights" in the HER and two in the LER. These include the two phase-control straights in each ring. In addition, there is an "injection straight" and an "IR straight" in each ring, and two "wiggler straights" in the LER.

TABLES

TABLE A–1

General Machine Parameters

Parameter	Symbol	HER	LER	Units
Center-of-mass energy	$E_{\mathrm{c.m.}}$	10.580		GeV
Beam energy	E	9.000	3.109	GeV
Peak luminosity	$\mathcal{L}$	3.00×10^{33}		$\mathrm{cm}^{-2}\mathrm{s}^{-1}$
$1/e$ luminosity decay time	$\tau_{\mathcal{L}}$	1.55		hr
Number of populated bunches	k_B	1658	1658	
Number of empty bunches	$k_B(\mathrm{gap})$	88	88	
Bunch spacing	s_B	1.2596		m
Machine circumference	L	2199.318	2199.318	m
Horizontal tune	ν_x	24.570	36.570	
Vertical tune	ν_y	23.640	34.640	
Momentum compaction	α_p	.00241	.00131	
Natural energy spread	σ_E	5.51	2.51	MeV
Natural fractional energy spread	δ_E	6.1×10^{-4}	8.1×10^{-4}	
Natural bunch length	σ_ℓ	1.00	1.00	cm
Circulating current	I	0.986	2.140	A
Number of particles/bunch	N_b	2.723×10^{10}	5.911×10^{10}	
Horizontal damping time	τ_x	36.8	40.4	ms
Horizontal emittance	ϵ_x	48.24	64.32	nm·rad
Vertical emittance	ϵ_y	1.93	2.57	nm·rad
Natural chromaticity, horizontal	ξ_x	−42.640	−63.840	
Natural chromaticity, vertical	ξ_y	−45.690	−77.750	
Horizontal damping partition number	J_x	1.0031	0.9883	
Vertical damping partition number	J_y	1.0000	1.0001	
Longitudinal damping partition number	J_E	1.9969	2.0116	
Energy variation of J_x	$dJ_x/d\ln E$	−297.4	−147.6	
Energy Variation of J_y	$dJ_y/d\ln E$	0	−129.4	
Energy Variation of J_E	$dJ_E/d\ln E$	297.4	277.0	

TABLE A-2

Interaction Region Parameters

Parameter	Symbol	HER	LER	Units
Horizontal beta function at IP	β_x^*	50.00	37.50	cm
Vertical beta function at IP	β_y^*	2.00	1.50	cm
Horizontal dispersion at IP	D_x^*	0.000	0.000	m
Vertical dispersion at IP	D_y^*	0.000	0.000	m
Horizontal spot size at IP	σ_x^*	155	155	μm
Vertical spot size at IP	σ_y^*	6.2	6.2	μm
Beam cross half-angle	θ_x	0.0		mrad
Beam-beam linear tune shift	$\Delta\nu_x$	0.030	0.030	
Beam-beam linear tune shift	$\Delta\nu_y$	0.030	0.030	
$e^+e^- \rightarrow e^+e^-\gamma$ beam lifetime	τ_{Br}	14.8	34.4	hr
$e^+e^- \rightarrow e^+e^-\gamma$ luminosity lifetime	τ_{Br}	12.6		hr
Beam pipe inner radius at IP	r^*	2.50		cm
IP to first magnet distance	d_f	0.200		m
Detector solenoid field	B_{sol}	1.00		T
Detector solenoid length	L_{sol}	4.00		m

TABLE A–3

RF System Parameters

Parameter	Symbol	HER	LER	Units
Circulating current	I	0.986	2.140	A
Natural bunch length	σ_ℓ	1.00	1.00	cm
RF frequency	$f_{\rm RF}$	476.0	476.0	MHz
Harmonic number	h	3492	3492	
Synchrotron tune	ν_s	0.0516	0.0371	
Synchrotron frequency	f_s	7.0	5.1	kHz
Number of klystrons	$N_{\rm klys}$	10	5	
Power/klystron	$P_{\rm klys}$	1.10	1.10	MW
Number of cavities	$N_{\rm Cavity}$	20	10	
Shunt impedance	R_s	3.5	3.5	MΩ
Gap voltage	V_g	0.91	0.60	MV
Accelerating gradient	$\mathcal{E}$	4.09	2.70	MV/m
Wall loss/cavity	$P_{\rm Wall}$	0.122	0.050	MW
Coupling factor, no beam	β	7.5	7.5	
Unloaded Q	Q	30000	30000	
Energy loss per turn	U_0	3.57	1.14	MeV
Synchrotron radiation power	$P_{\rm SR}$	3.52	2.44	MW
HOM power (est.)	$P_{\rm HOM}$	0.15	0.45	MW
Cavity wall loss total	$P_{\rm Wall}$	2.44	0.50	MW
Total RF power	$P_{\rm RF}$	6.11	3.39	MW
Klystron power total	$P_{\rm tot\,Klys.}$	11.00	5.50	MW
RF voltage	$V_{\rm RF}$	18.29	6.03	MV
Synchronous phase angle	ϕ_s	168.2	167.0	deg
Fractional energy RF aperture	f_E(RF)	0.0105	0.0139	
Fractional energy aperture ($10\sigma_E$)	f_E	0.0061	0.0081	

TABLE A–4

Instrumentation and Feedback

Parameter	Symbol	HER	LER	Units
Number of BPMs	N_{BPM}	144	144	
Resolution (short-term repeatability)	σ_{BPM}	20	20	μm
Absolute accuracy		100	100	μm
Bunch intensity resolution		1	1	%
Bunch spacing	t_B	4.202		ns
Bunch frequency	f_B	238.0		MHz
RF frequency	f_{RF}	476.0	476.0	MHz
Luminosity	Bhabha scattering monitor			
Longitudinal feedback system				
Beam pickup central frequency		2856	2856	MHz
Down-sampling factor		4	4	
Linear phase range correction		$\pm$15.0	$\pm$15.0	deg
Phase detector resolution		0.50	0.50	deg
Bunch-to-bunch signal isolation		$-$30	$-$30	dB
Kicker structure operating frequency	f_{kick}	1012	1012	MHz
Number of kicker units	N_{kick}	3	3	
Kicker length	L_{kick}	0.32	0.32	m
Kicker bandpass		241	241	MHz
Driver bandwidth		357	357	MHz
Kicker shunt impedance	Z_{kick}	1600	1600	Ω
Installed power/unit		500	500	W
Power for 1 kV/unit		313	313	W
Maximum voltage/turn		3	3	kV

TABLE A–4 (continued)

Instrumentation and Feedback

Parameter	Symbol	HER	LER	Units
Transverse feedback system				
Detection central frequency		1428	1428	MHz
Detection bandwidth		250	250	MHz
Kicker length	L_{kick}	0.63	0.63	m
Impedance at 10 kHz (vertical)		57.9	57.9	kΩ
Impedance at 10 kHz (horizontal)		38.3	38.3	kΩ
Impedance at 119 kHz (vertical)		23.5	23.5	kΩ
Impedance at 119 kHz (horizontal)		15.5	15.5	kΩ
Voltage kick/turn (vertical)		2.34	5.01	kV
Voltage kick/turn (horizontal)		1.55	3.32	kV
Power required (vertical)		47.3	217	W
Power required (horizontal)		31.4	144	W
Beta function at kicker	$\beta_{\perp}$	20	20	m

TABLE A–5

Vacuum Parameters

Parameter	Symbol	HER	LER	Units
Vacuum (3A design goal, N_2 equivalent):				
Arcs		≤ 10		nTorr
Straights		3		nTorr
IR straight		1		nTorr
Wigglers			10	nTorr
Value assumed for lifetime		5	6	nTorr
Horizontal chamber aperture	a_x	± 4.5	± 4.5	cm
Vertical chamber aperture	a_y	± 2.5	± 2.5	cm
Dipole critical energy	$\epsilon_{\rm crit}$	9.8	4.8	keV
Beam-gas brems. cross section	$\sigma_{eZ\gamma}$	7.42×10^{-32}	6.96×10^{-32}	cm^2
Beam-gas brems. lifetime	$\tau_{\rm BGbrem}$	7.8	6.9	hr
Average horizontal beta	$\langle\beta_x\rangle$	24.8	18.5	m
Average vertical beta	$\langle\beta_y\rangle$	20.2	17.5	m
Horiz. angular aperture	$\theta_{\min x}$	0.4498	0.6015	mrad
Vert. angular aperture	$\theta_{\min y}$	0.3526	0.4374	mrad
Beam-gas Coul. cross section	σ_{eZ}	2.05×10^{-32}	1.06×10^{-31}	cm^2
Beam-gas Coulomb lifetime	$\tau_{\rm BGcoul}$	28.2	4.6	hr
Nominal desorption for Cu	$\eta_{\rm Cu}$	2×10^{-6}		$\frac{\text{molecules}}{\text{photon}}$
Pumping speed in arc cell		2000 130	780 50	L/s L/s/m
Pumping speed in straight section cell		540 35	440 29	L/s L/s/m

TABLE A–6

Lattice Cell Summary

Parameter	Symbol	HER	LER	Units
Standard arc cells				
Cell Layout		QF-B-QD-B		
Cell length	L_{cell}	15.200	15.191	m
Phase advance	ϕ_c	60.0	90.0	deg
Dipole magnetic length	L_B	5.400	0.450	m
Dipole field at E_{des}	B_B	0.1819	0.7540	T
Bend radius	ρ	165.012	13.751	m
Dispersion suppressor cells				
Cell Layout		QF-B-QD-B		
Cell length	L_{cell}	15.200	15.191	m
Phase advance	ϕ_c	~ 90	~ 90	deg
Dipole magnetic length	L_B	5.400	0.450	m
Dipole field at E_{des}	B_B	0.1819	0.7540	T
Bend radius	ρ	165.012	13.751	m
Standard straight cells				
Cell Layout		QF-O-QD-O		
Cell length	L_{cell}	15.419	16.030, 14.608	m
Phase advance	ϕ_c	~ 60	~ 90	deg

TABLE A–7

Conventional Dipole Physical Parameters

Designation	Number	L_{magnetic} (in., m)	Pole width (in., cm)	Gap height (in., cm)
2C24	2	23.62, 0.600	8, 20.3	2, 5.08
2.8C212	192	212.60, 5.400	8.425, 21.4	2.787, 7.08
2H24	6	23.62, 0.600	8, 20.3	1.0, 2.54
2H60	7	59.06, 1.500	8, 20.3	1.0, 2.54
2H80	1	78.74, 2.000	8, 20.3	1.0, 2.54
2.8H12	2	11.81, 0.300	8, 20.3	2.8, 7.11
2.8H17	4	17.72, 0.450	7.5, 19.1	2.787, 7.08
2.8H18	192	17.72, 0.450	8, 20.3	2.87, 7.29
2.8H24	4	23.62, 0.600	8, 20.3	2.8, 7.11
2.8H29	4	29.53, 0.750	8, 20.3	2.8, 7.11
2.8H49	2	49.21, 1.250	8, 20.3	2.8, 7.11
2.8H59	2	59.06, 1.500	8, 20.3	2.8, 7.11
2.8H80	4	78.74, 2.000	8, 20.3	2.8, 7.11
2.8H98	2	98.43, 2.500	8, 20.3	2.8, 7.11
5.8H80	8	78.56, 1.995	5.9, 15.0	5.875, 14.92
5.8H85	8	84.96, 2.158	5.9, 15.0	5.875, 14.92
BMH (HER bump)	4	39.37, 1.000		
BML (LER bump)	4	19.69, 0.500		

TABLE A–8

Conventional Dipole Operating Parameters at E_{design}

Transport	Designation	Number	B (T)	$\int B d\ell$ (T-m)	Bend angle (deg)
HER (E_{design} = 9 GeV)					
B	2.8C212	192	0.1819	0.9824	1.875
Injection bump					
BM1L	BMH	1	0.031	0.0312	0.060
BM2L	BMH	1	0.018	0.0183	0.035
BM1R	BMH	1	0.034	0.0336	0.064
BM2R	BMH	1	0.006	0.0060	0.011
IR bends					
B2	5.8H80	8	0.0216	0.0431	0.082
B3	5.8H85	8	0.0216	0.0466	0.089
B4	2.8H17	4	0.0904	0.0407	0.078
LER (E_{design} = 3.109 GeV)					
B	2.8H15	192	0.754	0.339	1.875
Wiggler chicane					
BD+,BD–	2.8H80	4	0.226	0.452	2.50
Injection bump					
BM1L	BML	1	0.024	0.0122	0.068
BM2L	BML	1	0.017	0.0085	0.047
BM1R	BML	1	0.023	0.0114	0.063
BM2R	BML	1	0.004	0.0019	0.010
IR vertical bends					
B4	2.8H23	2	0.400	0.240	1.329
B7	2.8H23	2	0.451	0.271	1.5
B8	2.8H12	2	0.100	0.030	0.166
B9	2.8H60	2	1.209	1.814	10.048
IR horizontal bends					
B3	2.8H30	4	0.481	0.361	2.0
B5	2.8H100	2	0.500	1.250	6.925
B6	2.8H50	2	0.718	0.898	4.973

TABLE A–8 (continued)

Conventional Dipole Operating Parameters at E_{design}

Transport	Designation	Number	B (T)	$\int B d\ell$ (T-m)	Bend angle (deg)
Positron extraction					
Bs	2H24	1	0.752	0.451	2.5
Bch	2C24	2	0.752	0.451	2.5
BRec	2H24	1	0.752	0.451	2.5
B1	2H24	2	0.752	0.451	2.5
B2	2H24	2	0.338	0.203	1.122
BH1	2H60	2	0.019	0.029	0.162
BVup	2H80	1	0.074	0.149	0.842
B02	2H60	2	0.449	0.674	3.731
B01	2H60	2	0.078	0.117	0.646
BH1	2H60	1	0.019	0.029	0.162

TABLE A–9

Conventional Quadrupole Physical Parameters

Designation	Number	L_{magnetic} (in., cm)	Inscribed diameter (in., cm)
Injector			
1Q4	94	4.17, 10.6	1.015, 2.58
1Q6	14	6.61, 16.8	1.015, 2.58
1Q10	1	9.84, 25.0	1.015, 2.58
1Q20	12	20.35, 51.69	1.015, 2.58
2Q9	9	9.84, 25.0	2.030, 5.16
2Q10	23	9.84, 25.0	2.030, 5.16
Rings			
4Q17	282	16.93, 43.0	3.936, 10.0
4Q18	70	17.72, 45.0	3.936, 10.0
4Q22	94	21.65, 55.0	3.936, 10.0
4Q29	82	28.74, 73.0	3.936, 10.0
4Q40	36	39.37, 100.0	3.936, 10.0

TABLE A–10

HER Conventional Quadrupole Operating Parameters at 9 GeV

Lattice	Designation	Number	Gradient (T/m)	$B_{poletip}$ (T)	$\int G d\ell$ (T)	$k = G/B\rho$ (m^{-2})
QD	4Q22	54	7.33	0.366	4.03	0.244
QF	4Q29	60	5.48	0.274	4.00	0.183
Dispersion suppressor						
QFS11	4Q22	1	9.48	0.474	5.22	0.316
QFS12	4Q22	1	9.48	0.474	5.22	0.316
QFS1L	4Q22	1	9.76	0.488	5.37	0.325
QFS1R	4Q22	1	9.80	0.490	5.39	0.326
QFS21	4Q18	1	11.77	0.588	5.30	0.392
QFS22	4Q18	1	11.75	0.588	5.29	0.391
QFS2L	4Q18	1	11.68	0.584	5.26	0.389
QFS2R	4Q18	1	11.74	0.587	5.28	0.391
QFS31	4Q29	1	5.61	0.280	4.10	0.187
QFS32	4Q29	1	5.62	0.281	4.10	0.187
QFS3L	4Q29	1	5.61	0.281	4.10	0.187
QFS3R	4Q29	1	5.62	0.281	4.10	0.187
QDSOL	4Q18	1	8.61	0.430	3.87	0.287
QDSOR	4Q18	1	8.61	0.430	3.87	0.287
QDSO1	4Q29	1	5.33	0.266	3.89	0.178
QDSO2	4Q29	1	5.35	0.267	5.35	0.178
QDS11	4Q18	1	8.61	0.430	3.87	0.287
QDS12	4Q18	1	9.79	0.489	4.41	0.326
QDS1L	4Q22	1	7.98	0.399	4.39	0.266
QDS1R	4Q22	1	8.01	0.400	4.41	0.267
QDS21	4Q22	1	7.19	0.359	3.95	0.239
QDS22	4Q22	1	7.17	0.358	3.94	0.239
QDS2L	4Q18	1	8.68	0.434	3.90	0.289
QDS2R	4Q18	1	8.76	0.438	3.94	0.292

TABLE A–10 (continued)

HER Conventional Quadrupole Operating Parameters at 9 GeV

Transport	Designation	Number	Gradient (T/m)	B_{poletip} (T)	$\int G d\ell$ (T)	$k = G/B\rho$ (m^{-2})
Dispersion suppressor (continued)						
QDS31	4Q22	1	7.33	0.366	4.03	0.244
QDS32	4Q22	1	7.33	0.366	4.03	0.244
QDS3L	4Q22	1	7.33	0.366	4.03	0.244
QDS3R	4Q22	1	7.33	0.366	4.03	0.244
QFS11E	4Q22	4	8.06	0.403	4.43	0.268
QFS12E	4Q22	4	8.08	0.404	4.44	0.269
QFS21E	4Q18	4	10.55	0.527	4.75	0.351
QFS22E	4Q18	4	10.53	0.526	4.74	0.351
QFS31E	4Q29	4	6.16	0.308	4.49	0.205
QFS32E	4Q29	4	6.16	0.308	4.50	0.205
QDSO1E	4Q29	4	5.62	0.281	4.10	0.187
QDSO2E	4Q29	4	5.66	0.283	4.13	0.189
QDS11E	4Q18	4	9.37	0.468	4.22	0.312
QDS12E	4Q18	4	9.41	0.470	4.24	0.313
QDS21E	4Q22	4	7.72	0.386	4.25	0.257
QDS22E	4Q22	4	7.71	0.385	4.24	0.257
QDS31E	4Q22	4	7.33	0.366	4.03	0.244
QDS32E	4Q22	4	7.33	0.366	4.03	0.244

TABLE A–10 (continued)

HER Conventional Quadrupole Operating Parameters at 9 GeV

Transport	Designation	Number	Gradient (T/m)	B_{poletip} (T)	$\int G d\ell$ (T)	$k = G/B\rho$ (m^{-2})
Straight section						
QFO	4Q18	16	8.83	0.441	3.97	0.294
QDO	4Q18	14	8.83	0.441	3.97	0.294
Phase trombone						
QDP1	4Q40	2	4.06	0.203	4.06	0.135
QFP2	4Q40	4	4.29	0.214	4.29	0.143
QDP3R6	4Q40	2	4.02	0.201	4.02	0.134
QDP3R8	4Q18	2	8.94	0.447	4.02	0.298
QFP4	4Q18	4	9.46	0.473	4.26	0.315
QDP5R6	4Q40	2	4.00	0.200	4.00	0.133
QDP5R8	4Q18	2	8.89	0.444	4.00	0.296
QFP6	4Q22	4	7.61	0.380	4.19	0.253
QDP7R6	4Q40	2	3.99	0.199	3.99	0.133
QDP7R8	4Q18	2	8.88	0.444	3.99	0.296
QFP8	4Q18	4	9.22	0.461	4.15	0.307
Injection						
QFOI	4Q40	2	4.08	0.204	4.08	0.136
QDOI	4Q40	2	2.98	0.149	2.98	0.099
QFI	4Q40	2	1.92	0.096	1.92	0.064
QDI	4Q40	2	1.95	0.097	1.95	0.065
IR						
QD6	4Q40	2	7.89	0.394	7.89	0.263
QF7	4Q40	2	5.96	0.298	5.96	0.199

TABLE A–11

LER Conventional Quadrupole Operating Parameters at 3.1 GeV

Transport	Designation	Number	Gradient (T/m)	$B_{poletip}$ (T)	$\int G d\ell$ (T)	$k = G/B\rho$ (m^{-2})
QD	4Q17	80	4.50	0.226	1.93	0.434
QF	4Q17	74	4.55	0.227	1.96	0.439
Dispersion suppressor, IR						
QF1	4Q17	2	7.07	0.354	3.04	0.682
QD2	4Q17	2	6.33	0.316	2.72	0.610
QF3	4Q17	2	5.18	0.259	2.23	0.499
QD4	4Q17	2	3.46	0.173	1.49	0.334
QF5	4Q17	2	4.55	0.227	1.98	0.439
Dispersion suppressor, tune regions 3,5,9,11						
QF1,QF1A	4Q17	4	4.16	0.208	1.79	0.401
QD1,QD1A	4Q17	4	5.58	0.279	2.40	0.538
QF2,QF2A	4Q17	4	4.38	0.219	1.88	0.422
QD2,QD2A	4Q17	4	4.95	0.247	2.13	0.477
QF3,QF3A	4Q17	4	4.84	0.242	2.08	0.467
QD3,QD3A	4Q17	4	4.12	0.206	1.77	0.397
QF4,QF4A	4Q17	4	4.77	0.239	2.05	0.460
QD4,QD4A	4Q17	4	4.55	0.227	1.96	0.439
RF/Tune straights						
QDT4,QDT4A	4Q17	2	1.88	0.094	0.81	0.181
QFT4,QFT4A	4Q17	4	3.29	0.165	1.42	0.317
QDT3,QDT3A	4Q17	4	3.57	0.179	1.53	0.344
QFT3,QFT3A	4Q17	4	4.14	0.207	1.78	0.399
QDT2,QDT2A	4Q17	4	3.48	0.174	1.50	0.336
QFT2,QFT2A	4Q17	4	4.83	0.242	2.08	0.466
QDT1,QDT1A	4Q17	4	4.04	0.202	1.74	0.390
QFT1,QFT1A	4Q17	4	4.90	0.245	2.11	0.472

TABLE A–11 (continued)

LER Conventional Quadrupole Operating Parameters at 3.1 GeV

Transport	Designation	Number	Gradient (T/m)	$B_{poletip}$ (T)	$\int G d\ell$ (T)	$k = G/B\rho$ (m^{-2})
Injection straight						
QDI	4Q17	2	0.66	0.033	0.28	0.064
QFI	4Q17	2	1.47	0.074	0.63	0.142
QDOI	4Q17	2	2.34	0.117	1.01	0.226
QFOI	4Q17	2	4.17	0.208	1.79	0.402
Wiggler straight section						
QFW1,QFW1A	4Q17	4	2.52	0.126	1.08	0.243
QDW2,QDW2A	4Q17	4	1.64	0.082	0.70	0.158
QFW3,QFW3A	4Q17	4	3.92	0.196	1.69	0.378
QFW4,QFW4A	4Q17	4	0.28	0.014	0.12	0.027
QDW5,QDW5A	4Q17	4	2.02	0.101	0.87	0.195
QFW6,QFW6A	4Q17	4	3.58	0.179	1.54	0.345
IR straight						
IQF1	4Q17	2	7.12	0.356	3.06	0.687
IQD2	4Q40	2	5.04	0.252	5.04	0.486
IQF3	4Q40	2	4.53	0.226	4.529	0.437
IQD4	4Q40	2	5.05	0.253	5.05	0.487
IQF5	4Q17	2	10.35	0.517	4.45	0.998
IQF6	4Q40	2	5.20	0.260	5.20	0.501
IQD7	4Q40	2	5.98	0.299	5.98	0.577
IQF8	4Q40	2	9.80	0.490	9.80	0.945
IQD10	4Q17	4	7.12	0.366	3.06	0.687
IQF11	4Q17	4	11.76	0.587	5.05	1.134
IQD12	4Q17	2	10.46	0.523	4.50	1.009
IQD13	4Q17	2	7.04	0.352	3.03	0.679
IQF14	4Q40	2	8.25	0.413	8.25	0.795
IQD15	4Q17	2	5.87	0.293	2.52	0.566
IQF16	4Q17	2	19.21	0.960	8.26	1.852
IQD17	4Q17	2	10.54	0.527	4.53	1.016
IQF18	4Q17	2	8.89	0.444	3.82	0.857

TABLE A–12

Injector Conventional Quadrupole Operating Parameters at E_{design}

Transport	Designation	Number	Gradient (T/m)	B_{poletip} (T)	$\int G d\ell$ (T)	$k = G/B\rho$ (m^{-2})
e^- (9 GeV)						
QD ext	2Q9	1	13.193	0.340	3.30	0.439
QF1 ext	2Q9	1	13.988	0.361	3.50	0.466
QD2 ext	2Q9	1	13.252	0.342	3.31	0.441
QF3 ext	2Q9	1	13.156	0.339	3.29	0.438
QD4 ext	2Q9	1	13.304	0.343	3.33	0.443
QF1 ext	2Q9	1	12.396	0.320	3.10	0.413
QD2 ext	2Q9	1	13.132	0.339	3.28	0.437
QF3 ext	2Q9	1	13.228	0.341	3.31	0.441
QD4 ext	2Q9	1	13.080	0.337	3.27	0.436
QF ext	1Q6	1	19.631	0.253	3.30	0.654
QAlf	1Q6	1	21.798	0.281	3.66	0.726
QDM	1Q6	3	5.648	0.073	1.41	0.188
QFm ext	1Q6	2	5.648	0.073	1.41	0.188
QDyB ext	1Q6	1	7.888	0.102	1.97	0.263
QFB1 ext	1Q6	1	12.232	0.158	2.06	0.407
QDSL match	1Q6	2	11.862	0.153	1.99	0.395
QFSL match	1Q6	2	11.862	0.153	1.99	0.395
QA2 match	1Q6	1	80.437	1.037	13.51	2.679
QFM match	1Q10	1	105.215	1.356	26.30	3.505
DEF match	1Q20	5	4.852	0.063	2.51	0.162
QED match	1Q20	5	4.852	0.063	2.51	0.162
QD match	1Q20	1	4.852	0.063	2.51	0.162
Q1 match	1Q20	1	5.391	0.069	2.79	0.180

TABLE A–12 (continued)

Injector Conventional Quadrupole Operating Parameters at E_{design}

Transport	Designation	Number	Gradient (T/m)	B_{poletip} (T)	$\int G d\ell$ (T)	$k = G/B\rho$ (m^{-2})
e^+ (3.1 GeV)						
Extraction	2Q10	18	9.008	0.232	2.25	0.869
Extraction	2Q10	4	4.041	0.104	1.01	0.390
Extraction	2Q10	1	2.370	0.061	0.59	0.229
Bypass	1Q4	43	2.387	0.031	0.25	0.230
30 match	1Q4	5	5.585	0.072	0.59	0.539
30 match	1Q4	1	4.115	0.053	0.44	0.397
30 match	1Q4	4	8.182	0.105	0.87	0.789
30 match	1Q4	9	0.818	0.011	0.09	0.079

TABLE A–13

Sextupole Physical Parameters

Parameter	Value	Units
Magnet designation	4.5S10	
Number in HER	144	
Number in LER	152	
Inscribed radius	2.362, 5.999	in., cm
Core length	8.071, 20.500	in., cm
Magnetic length	10.041, 25.504	in., cm

TABLE A–14

Sextupole Operating Parameters at E_{design}

Transport	Number	Gradient (T/m^2)	B_{poletip} (T)	Integrated strength (T/m)
HER ($E_{\text{design}} = 9$ GeV)				
SD	48	79.654	0.143	10.40
SF	48	42.029	0.076	4.49
SD1	2	104.863	0.189	13.70
SF1	2	5.674	0.010	0.74
SD1A	2	130.921	0.236	17.10
SF1A	2	17.952	0.032	2.34
SD2,SD4	4	105.073	0.189	13.72
SF2	2	78.654	0.142	10.27
SD2A,SD4A,SD6A	6	150.104	0.270	19.60
SF2A	2	86.190	0.155	11.28
SD3,SD3A,SD5,SD5A	8	60.042	0.108	7.84
SF3	2	90.272	0.162	11.79
SF3A	2	90.062	0.162	11.76
SF4	2	11.618	0.021	1.52
SF4A	2	13.659	0.025	1.78
SF5	2	54.908	0.099	7.17
SF5A	2	107.835	0.194	14.08
SD6	2	61.903	0.111	8.08
SF6	2	96.006	0.173	12.54
SF6A	2	75.742	0.136	9.89
LER ($E_{\text{design}} = 3.109$ GeV)				
SF	72	25.62	0.046	7.53
SD	72	45.60	0.082	13.40
SX	4	113.75	0.205	33.43
SY	4	186.13	0.335	54.70

TABLE A–15

IR Permanent-Magnet Parameters

Parameter	Symbol	Value	Units
Magnetic material	Sm_2Co_{17} – R26HS		
Remanent field	B_r	1.050	T
Temperature dependence	$\frac{dB_r}{dT}$	−0.03	%/°C
Curie point	T_C	1093	K
Density	ρ	8.4	g/cm^3

Parameter	Symbol	HER	LER	Units
B1: First separation dipole				
Nominal field	B_{B1}	0.675		T
Integrated field	$\int B d\ell$	0.3375		T-m
Bend angle at E_{des}		0.64	1.86	deg
Length	L_{B1}	0.500		m
Inner diameter	ID_{B1}	7.5–12.0		cm
Outer diameter	OD_{B1}	10.2–25.1		cm
Magnet weight	W_{B1}	220		lb
Trim range (air core coil)		±3		%
QD1: IR quadrupole				
Gradient	G_Q	10.64		T/m
Pole tip field	B_Q	0.890		T
Length	L_Q	1.200		m
Inner diameter	ID_Q	0.0875		m
Outer diameter	OD_Q	0.166		m
Magnet weight	W_Q	1393		lb
Trim range (air core coil)		±3		%
BH1: Steering for background (HER)				
Field	B	0.15		T
Integrated field	$\int B d\ell$	0.060		T-m
Bend angle at E_{des}		0.11		deg
Length	L_B	0.40		m

TABLE A–16

IR Septum Quadrupoles

Parameter	Symbol	Value	Units
Q2: First septum quadrupole (LER)			
Technology	conventional warm iron		
Number of magnets	N_{Q2}	2	
Distance from IP	d_{Q2}	2.800	m
Beam-beam spearation at d_{Q2}		8.69	cm
Beam-beam stay clear separation at d_{Q2}		3.00	cm
Magnetic length	L_{Q2}	0.50	m
Gradient	G_{Q2}	11.5	T/m
Pole tip bore radius		4.23	cm
Q4: First septum quadrupole (HER)			
Technology	conventional warm iron		
Number of magnets	N_{Q4}	2	
Distance from IP	d_{Q4}	3.7	m
Beam-beam spearation at d_{Q4}		13.7	cm
Beam-beam stay clear separation at d_{Q4}		6.7	cm
Magnetic length	L_{Q4}	1.5	m
Gradient	G_{Q4}	−7.74	T/m
Aperture		13.8	cm
Q5: Second septum quadrupole (HER)			
Technology	conventional warm iron		
Number of magnets	N_{Q5}	2	
Distance from IP	d_{Q5}	5.95	m
Beam-beam spearation at d_{Q5}		25.2	cm
Beam-beam stay clear separation at d_{Q5}		14.5	cm
Magnetic length	L_{Q5}	1.5	m
Gradient	G_{Q5}	7.27	T/m
Aperture		19.8	cm

TABLE A–17

Injection Septum Dipoles

Parameter	Symbol	HER	LER	Units
Technology		Current sheet		
Designation		S0	S0	
Number		1	1	
Magnetic length	L_{mag}	1.5	1.5	m
Field at E_{design}	B	0.018	0.008	T
Bend angle		1.0	1.3	mrad
Technology		Lambertson		
Designation		S1	S1	
Number		1	1	
Magnetic length	L_{mag}	1.0	1.0	m
Field at E_{design}	B	0.30	0.10	T
Bend angle		11	11	mrad
Aperture		2.25×2.25	2.25×2.25	cm^2

TABLE A–18

Injection Kickers

Parameter	Symbol	HER	LER	Units
Number		2	2	
Technology		Ferrite		
Length	L_k	0.75		m
Aperture		6×6		cm^2
Kick angle		0.13	0.43	mrad
Field at E_{design}	B	5.2	4.8	mT
Voltage at E_{design}	V	3.6	2.4	kV
Inductance	L	1		μH
Stability at peak		2		%
Beam pipe				
Material		Ceramic		
Coating resistance	$R_\square$	0.4		Ω/sq
Length	L_{pipe}	1.0		m
Thickness	t_{pipe}	2.5		mm
Outside diameter	OD_{pipe}	6		cm

TABLE A–19

Wiggler Parameters (Low-energy ring)

Parameter	Symbol	Value	Units
Number of wiggler arrays	N_W	2	
Wiggle plane	Horizontal		
Total length of wigglers	L_W	32	m
Total magnetic length		19.2	m
Energy loss/turn at E_{design}	$U_{0,W}$	0.43	MeV
Wiggler segments per array	N_S	4	
Segment length	L_S	4	m
Periods/segment		6	
Dipole length		0.20	m
Drift space		0.133	m
Fill factor		60	%
Wiggler period		0.666	m
Dipole field at E_{design}	B_W	1.35	T
Critical energy at E_{design}	E_{crit}	8.7	keV

TABLE A–20

Injection Parameters

Parameter	Symbol	HER	LER	Units
Injection energy	E	9.000	3.109	GeV
Injection energy range		8–10	2.8–4	GeV
Number of populated bunches	k_B	1658	1658	
Number of empty bunches	k_B(gap)	88	88	
Bunch spacing	t_B	4.202		ns
Revolution frequency	f_0	136.312	136.312	kHz
Circulating current	I	0.986	2.140	A
Number of particles/bunch	N_b	2.723×10^{10}	5.911×10^{10}	
Horizontal emittance	ϵ_x	48.24	64.32	nm·rad
Vertical emittance	ϵ_y	1.93	2.57	nm·rad
Vertical damping time	τ_y	37.0	39.9	ms
Linac repetition rate		60		s^{-1}
Linac current ($e^{\pm}$/bunch/pulse)		$(0.1 - 3) \times 10^{10}$		
Linac invariant emittance (horiz.)	$\epsilon_{N\,\mathrm{linac}}$	4.0×10^{-5}		m·rad
Linac invariant emittance (vert.)		0.5×10^{-5}		m·rad
Ring kicker pulse length	t_{kick}	≤ 300		ns
Injection top-off time from 80%		3.0		min
Injection time from zero		6.0		min
Fractional energy spread		0.007	0.005	FWHM
Fractional energy jitter	$\delta E/E$	0.001		

TABLE A–21

Parameters Relevant to Experiment Design

Parameter	Symbol	HER	LER	Units
Horizontal spot size at IP	σ_x^*	155	155	μm
Vertical spot size at IP	σ_y^*	6.2	6.2	μm
Natural bunch length	σ_ℓ	1.00	1.00	cm
Beam cross half-angle	θ_x	0.0		mrad
Natural energy spread	σ_E	5.51	2.51	MeV
Natural C.M. energy spread	$\sigma_{E_{\rm c.m.}}$	5.36		MeV
Beam pipe inner radius at IP	r^*	2.50		cm
Beam pipe outer radius at IP	$r^*_{\rm out}$	2.82		cm
IP to first magnet distance	d_f	0.200		m
Detector solenoid field	$B_{\rm sol}$	1.00		T
Detector solenoid length	$L_{\rm sol}$	4.00		m
Beam pipe thickness	$X_{0;\rm pipe}$	0.0053		X_0
Support tube ID	$\rm ID_{tube}$	39.00		cm
Support tube OD	$\rm OD_{tube}$	43.00		cm
Support tube thickness at IP	$X_{0;\rm tube}$	0.0047		X_0
Support tube length	$\rm L_{tube}$	4.20		m
Minimum acceptance angle	$\theta_{\rm min}$	0.300	0.300	rad
cos(min. acceptance angle in C.M.)	$\cos\theta^*_{\rm min}$	0.876	0.984	